

Cholinergic and Metabolic Consequences of Streptozotocin-induced Brain Injury

Dissertation
zur Erlangung des Doktorgrades
der Naturwissenschaften

vorgelegt beim Fachbereich 14
der Johann Wolfgang Goethe-Universität
in Frankfurt am Main

von
Tri Yuliani
aus Yogyakarta (Indonesia)

Frankfurt 2020
(D30)

vom Fachbereich 14 der Johann Wolfgang Goethe-Universität als Dissertation angenommen.

Dekan:

Prof. Dr. Clemens Glaubitz

Gutachter:

Prof. Dr. Jochen Klein

Prof. Dr. Dr. Achim Schmidtke

Datum der Disputation

Gedruckt mit Unterstützung des
Indonesia Endowment Fund for Education (LPDP)
Ministry of Finance, the Republic of Indonesia

Printed with the support of the
Indonesia Endowment Fund for Education (LPDP)
Ministry of Finance, the Republic of Indonesia

For my family

©2020 – Tri Yuliani
all rights reserved.

Summary

Introduction:

Alzheimer's disease (AD) is the major cause of dementia. It is characterized by the accumulation of abnormal proteins (amyloid- β plaque and neurofibrillary tangles) leading to loss of synapses, dendrites, neurons, memory and cognition. Sporadic late-onset AD is the major type of AD characterized by unclear etiology and a lack of disease-modifying therapy. To understand this disease, an alternative AD hypothesis has been proposed: AD may resemble diabetes in the brain or "diabetes type 3". This hypothesis is supported by the fact that (1) brain glucose hypometabolism precedes AD clinical symptoms and (2) diabetes increases the risk of AD.

To test this hypothesis, wild-type rats receiving intracerebroventricular administration of streptozotocin (icv-STZ) were used as a model. Streptozotocin (STZ) is a glucosamine-nitrosourea compound commonly used to induce experimental diabetes by peripheral administration. A similar pathological mechanism to peripheral STZ is then proposed to explain icv-STZ toxicity: insulin receptor signaling impairment results in glucose hypometabolism leading to cognitive deficits.

Objective:

Icv-STZ model seems promising as a toxin-induced, non-transgenic AD model with the possibility to connect AD and diabetes mellitus (DM), one of the risk factors for AD. However, the mechanisms of how icv-STZ induced AD-like symptoms are unclear. Therefore, using microdialysis as the main technique, we tested 2 AD hypotheses in this model: (1) the glucose hypometabolism as an alternative AD hypothesis and (2) the cholinergic deficit as an important characteristic of AD pathology. Hippocampus was chosen because cholinergic function in this region is severely affected in AD. In comparison, the striatum was chosen because it contains cholinergic interneurons and is less affected in AD.

Methods:

In this study, we used male Wistar rats of 190-220 g body weight (5 weeks of age). The rats were injected intracerebrally with STZ at a dose of 3 mg/kg (2x1.5 mg/kg; „high dose“) and 0.6 mg/kg („low dose“) with saline as control. After 21 days, samples were collected to investigate cholinergic and metabolic changes using histology, biochemistry, and neurochemistry. Brain injury was confirmed using GFAP staining and Fluoro jade staining in the hippocampus. Mitochondrial toxicity was investigated by measurement of mitochondrial

respiratory function in both hippocampus and striatum. Cholinergic markers such as acetylcholinesterase (AChE) activity, choline acetyltransferase (ChAT) activity, and choline transporter (CHT-1) activity, commonly known as high-affinity choline uptake (HACU), were measured in both hippocampus and striatum using a spectrophotometer and a scintillator.

Microdialysis is the main technique in our study. It was done in awake animals under behavioral or pharmacological stimulation. We used a self-built probe with a semi-permeable membrane (pore size of 30 kDa) that was implanted in either hippocampus or striatum. The probes were then perfused with artificial cerebrospinal fluid (aCSF) supplemented with 0.1 μ M neostigmine for extracellular acetylcholine level measurement. During the perfusion, small hydrophilic compounds from brain extracellular space diffuse into the dialysates. Dialysates of 15 minutes intervals were collected for 90 minutes and used for analysis. After collection of dialysates for the first 90 minutes (basal data), rats were moved to an open field box (35x32x20 cm) for behavioral stimulation. After collection of the second 90 minute dialysates, the rats were transferred back to the microdialysis cage and dialysates were collected for another 90 minutes. On day 2, after collection of dialysates under basal conditions, 1 μ M scopolamine was added to the perfusion solution for stimulation of acetylcholine release. The dialysates were also collected for 90 min followed by another 90 min of dialysis without scopolamine. The microdialysate samples were then analyzed as follows. ACh level was measured by HPLC-ECD. Glucose metabolites (glucose, lactate, pyruvate) were measured by a CMA-600 microanalyzer. An alternative energy metabolite (beta-hydroxybutyrate/BHB) was measured by GC-MS. Choline and glycerol as membrane breakdown markers were also measured by HPLC-ECD and CMA-600 microanalyzer, respectively. Markers of oxidative stress (isoprostanes) were measured using a commercially available ELISA kit.

Results and findings:

Sign of toxicities:

Icv-STZ toxicity was clearly observed on day 7 in only high-dose group based on reduced body weight gain. Although recovery was observed after day 10, the body weight in the high dose group was still less than control at the end of the experiment (21 days; -17%). The histological study also shows astrogliosis in the dorsal and ventral hippocampus and neurodegeneration in the CA1 region of the hippocampus of the high-dose group.

Microdialysis study also shows some *in vivo*-signs of toxicities. Extracellular choline levels were increased dose-dependently in the hippocampus but only after high-dose STZ in the

striatum. Extracellular glycerol levels were also increased dose-dependently in the striatum. Both choline and glycerol are well-known markers of membrane damage. On the other hand, isoprostane, an oxidative stress marker, was unchanged in striatal microdialysates.

Signs of mitochondrial impairment were also observed in the hippocampus. All of the mitochondrial respiration complexes were decreased in the hippocampus (ca. 14%; normalized by citrate synthase (CS) activity); the changes were significant on complexes II and IV. These decreases occur in the presence of increased CS activities indicating changes in mitochondrial biogenesis. By contrast, these changes were not observed in striatum.

Metabolic changes

Interestingly, our microdialysis study does not support “diabetes in the brain“ hypothesis. Extracellular glucose levels remained relatively unchanged both during basal condition and under the challenges in both the hippocampus and striatum. Small, insignificant increases of extracellular glucose might be caused by cell death such as observed in the CA1 region. Extracellular BHB, an alternative energy metabolite, was also unchanged. The extracellular lactate level after both doses in the hippocampus was slightly decreased but responded well to the behavioral challenges. By contrast, extracellular lactate and pyruvate levels were increased dose-dependently in the striatum.

A bioinformatics study (collaboration with S. Lobentanzer) indicates a different mechanism of icv-STZ when compared to peripheral-STZ. It is more likely that cellular uptake of STZ in the brain is mediated by GLUT-1 and GLUT-3 transporters. Both GLUT-1 and GLUT-3 transporters are highly expressed in the brain whereas GLUT-2 and GLUT-4 transporters that mediate peripheral STZ toxicities are expressed in a very low amount in the brain. Therefore, the non-specific cell death such as in the CA-1 region of the hippocampus and astrocyte activation may explain the decrease of mitochondrial respiratory function and consequently, of glucose uptake in the hippocampus.

Cholinergic changes

Similar to other studies, some changes in cholinergic markers were observed in our study. ChAT activity was decreased significantly (-30%) in the hippocampus after icv-STZ but was unchanged in the striatum. AChE activity was decreased significantly in the hippocampus (-30%) but was increased in the striatum (+7%). HACU was unchanged in the hippocampus but was increased significantly in the striatum after high-dose icv-STZ (+30%).

Interestingly, the microdialysis study revealed a preserved cholinergic function after icv-STZ. The extracellular ACh levels in both hippocampus and striatum were unchanged, as well as the response to the behavioral and cholinergic stimulations.

We found that the extracellular ACh levels correlate well with HACU activities. In the hippocampus, both ACh and HACU were unchanged. On the other hand, HACU was increased in the striatum which indicates increased cholinergic firing leading to a slight increase of ACh level in the striatal microdialysates sample. Many previous studies on this model assumed a cholinergic deficit by measuring ChAT and AChE activities which, however, poorly correlate with extracellular ACh. Of note, bioinformatics data shows that AChE is not exclusively cholinergic whereas ChAT and CHT-1 (SLC5A7) are highly co-expressed in cholinergic neurons. Furthermore, GLUT3 has a significant correlation with cholinergic genes while GLUT2 and 4 do not.

The hippocampus seems more prone to icv-STZ toxicity than the striatum. Our hippocampal data shows decreased cholinergic markers (ChAT and AChE) and decreased mitochondrial respiration despite normal availability of extracellular glucose and choline. However, this condition did not change acetylcholine release as the remaining cholinergic nerve endings were able to fire normally as shown by intact HACU after icv-STZ. Since the hippocampus receives cholinergic innervation from the septum, decreased hippocampal ChAT activity might be caused by axonal and nerve terminal damage. We suggest that the damage was mediated by GLUT-3 because of its higher correlation to cholinergic neurons than other GLUTs. In comparison, short projecting cholinergic interneurons in the striatum were relatively spared from STZ toxicity. In our striatal study, icv-STZ only results in increased cholinergic neuronal firing and increased ACh degradation leading to preserved extracellular ACh level. Furthermore, striatal lactate release and mitochondrial respiration were also preserved. This condition might be caused by limited diffusion of STZ to cholinergic neurons in the striatum or (more likely) less sensitivity of cholinergic interneurons towards STZ. Taken together, our data indicate that the cholinergic deficit reported in this AD model is either not present (striatum) or at least incomplete (hippocampus). Since GABAergic interneurons and GABAergic terminals predominate in the CA1 of the hippocampus and striatum, respectively, we speculate that GABAergic neuronal damage followed by a reduction of inhibitory neurotransmission may indirectly influence cholinergic transmission.

Conclusion:

STZ does not induce diabetes in the brain. It induces only unspecific toxicities such as reduced body weight gain, hippocampal astrogliosis and neurodegeneration, and some impairment of energy metabolism. By contrast, the cholinergic transmission seemed to be well preserved in both hippocampus and striatum but with a different profile in some biomarkers. Cholinergic neurons in the striatum seemed to be well preserved from STZ toxicity whereas minor damage to the hippocampal cholinergic terminals occurs. Overall, the icv-STZ model fails to mimic cholinergic dysfunction, an important part of AD pathology. This model is more suitable for an animal model of hippocampal gliosis with CA1 region injury.

Contents

| | | |
|---------|--|----|
| 1 | Introduction | 1 |
| 1.1 | Dementia | 1 |
| 1.2 | Alzheimer's disease | 1 |
| 1.2.1 | Alzheimer's disease drug therapy | 2 |
| 1.3 | Alzheimer's disease hypothesis | 3 |
| 1.3.1 | Cholinergic deficit hypothesis | 3 |
| 1.3.2 | Glucose hypometabolism hypothesis | 8 |
| 1.3.3 | Impaired brain insulin signaling hypothesis | 9 |
| 1.3.4 | Inflammation, disturbance of insulin signaling, and AD | 9 |
| 1.3.5 | Mitochondrial dysfunction | 9 |
| 1.4 | Animal models of Alzheimer's disease | 11 |
| 1.4.1 | Transgenic model | 11 |
| 1.4.2 | Non-transgenic model | 12 |
| 1.4.2.1 | A β infusion | 13 |
| 1.4.2.2 | 192 IgG Saporin | 13 |
| 1.4.2.3 | Excitotoxin | 14 |
| 1.5 | Streptozotocin (STZ) | 14 |
| 1.5.1 | Peripheral streptozotocin cytotoxic mechanism | 14 |
| 1.5.2 | Peripheral streptozotocin DM model | 15 |
| 1.6 | Central administration of STZ | 16 |
| 1.6.1 | Memory impairment | 17 |
| 1.6.2 | Glucose hypometabolism | 17 |
| 1.6.3 | Mitochondrial dysfunction | 18 |
| 1.6.4 | Increased oxidative stress markers | 18 |
| 1.6.5 | Cholinergic deficits | 18 |
| 1.6.6 | A β peptide and p-Tau | 19 |
| 1.6.7 | Insulin receptor signaling impairment | 19 |
| 1.6.8 | Comparison of icv-STZ model and 3xTg mice | 20 |
| 1.7 | Objectives of the study | 21 |

| | | |
|---------|--|----|
| 2 | Materials and Methods | 24 |
| 2.1 | Materials | 24 |
| 2.2 | Buffers and solutions | 29 |
| 2.3 | Experimental animals | 31 |
| 2.4 | Sample collection | 33 |
| 2.5 | Histology study | 34 |
| 2.5.1 | Fluoro-Jade staining | 34 |
| 2.5.2 | Immunohistochemistry of glial fibrillary acidic protein (GFAP) | 34 |
| 2.5.3 | Microscopic evaluation | 35 |
| 2.6 | Mitochondrial respiration study | 35 |
| 2.6.1 | Isolation of mitochondria from hippocampus and striatum | 35 |
| 2.6.2 | Mitochondrial respiratory measurement | 36 |
| 2.6.3 | Citrate synthase activity | 37 |
| 2.7 | Cholinergic marker study | 38 |
| 2.7.1 | Protein level determination | 38 |
| 2.7.2 | Acetylcholinesterase activity | 38 |
| 2.7.3 | High-affinity choline uptake (HACU) | 39 |
| 2.7.4 | Choline acetyltransferase activity | 40 |
| 2.8 | Microdialysis study | 41 |
| 2.8.1 | Construction of microdialysis probe | 42 |
| 2.8.2 | In vitro recovery | 42 |
| 2.8.3 | Microdialysis probe implantation | 44 |
| 2.8.4 | Microdialysis experiment | 46 |
| 2.8.5 | Analysis of microdialysates | 47 |
| 2.8.5.1 | Choline and acetylcholine | 48 |
| 2.8.5.2 | Glucose, lactate, pyruvate, and glycerol | 49 |
| 2.8.5.3 | Beta-hydroxybutyrate (BHB) | 50 |
| 2.8.5.4 | Isoprostane | 51 |
| 2.9 | Statistical analysis | 52 |
| 3 | Results | 53 |

| | | |
|---------|---|----|
| 3.1 | Confirmatory study for icv-STZ local toxicity | 53 |
| 3.1.1 | Icv-STZ decreased both body weight and hippocampal weight | 53 |
| 3.1.2 | Icv-STZ induced gliosis and neurodegeneration in hippocampus | 54 |
| 3.2 | Hippocampus | 55 |
| 3.2.1 | High dose of icv-STZ reduced mitochondrial respiration especially on complex II and IV in hippocampus | 55 |
| 3.2.2 | Cholinergic marker study in hippocampus | 57 |
| 3.2.3 | Microdialysis study: Effect of icv-STZ on metabolic and cholinergic profile in hippocampus during cholinergic challenge | 57 |
| 3.3 | Striatum | 61 |
| 3.3.1 | Preserved mitochondrial respiratory function after high dose of icv-STZ in striatum | 61 |
| 3.3.2 | Cholinergic marker study in striatum | 62 |
| 3.3.3 | Microdialysis study: Effect of icv-STZ on metabolic and cholinergic profile in striatum during cholinergic challenge | 62 |
| 3.4 | In vitro recovery | 66 |
| 4 | Discussion | 67 |
| 4.1 | Introduction: Alzheimer's disease and diabetes in the brain | 67 |
| 4.2 | Methodical considerations: the microdialysis technique | 68 |
| 4.3 | Methodical considerations: experimental set-up | 69 |
| 4.4 | Icv-STZ distribution and cellular damage | 70 |
| 4.5 | Early icv-STZ toxicity | 70 |
| 4.6 | Icv-STZ toxicity after 3 weeks | 71 |
| 4.6.1 | Inflammation and neuronal degeneration after icv-STZ | 72 |
| 4.6.2 | Mitochondrial dysfunction | 73 |
| 4.6.3 | Oxidative stress following icv-STZ | 75 |
| 4.6.4 | ATP level and mitochondrial membrane potential | 76 |
| 4.6.5 | Energy metabolites | 76 |
| 4.6.5.1 | Glucose | 77 |
| 4.6.5.2 | Lactate | 77 |
| 4.6.5.3 | β -hydroxybutyrate (BHB) | 78 |
| 4.6.6 | STZ mechanism of toxicity | 79 |

| | | |
|---------|--|-----|
| 4.6.7 | Cholinergic parameters | 80 |
| 4.6.7.1 | ChAT activity | 80 |
| 4.6.7.2 | AChE activity | 80 |
| 4.6.7.3 | HACU (high affinity of choline uptake) | 81 |
| 4.6.7.4 | Acetylcholine | 82 |
| 4.6.8 | Summary of cholinergic changes and its relation to bioinformatics data | 82 |
| 4.6.9 | Brain region specificity | 84 |
| 4.6.10 | Role of other neurotransmitters | 84 |
| 4.7 | Conclusion | 85 |
| 5 | References | 86 |
| 6 | List of figures | 97 |
| 7 | List of tables | 98 |
| 8 | Required Documents | 99 |
| 8.1 | Declarations | 99 |
| 8.2 | Summary in German Language | 100 |
| 8.3 | Curriculum vitae | 105 |
| 8.4 | Publications | 106 |

“And God is the best of the Planners.” Quran 8:30.

Acknowledgments

I would like to thank my family for their supports. My husband, Daddy, who is currently finishing his Ph.D. in Mechanical Engineering at TU Dresden and my daughter, Maheswari, who is currently adapting to a 5th grader life in Gymnasium Riedberg. I also want to thank my mother for her endless praying, my father in the Hereafter, and my big sisters, Mbak Septi and Mbak Dwi, for taking care of our mother.

I would like to thank Indonesia Endowment Fund for Education, Ministry of Finance, Republic of Indonesia (LPDP) for a 4 years 3 months-financial support and my homeland Institute (Research Center for Chemistry, Indonesian Institute of Sciences) for my study leave.

I would like to express my sincerest admiration and gratitude to Prof. Dr. Jochen Klein as my first advisor in and outside the lab. I am also grateful to Prof. Dr. Dr. Achim Schmidtko as my second advisor for granting me unlimited access to his labs and antibody collections. Many thanks go to Ms. Helene Lau for her contribution to cholinergic parameters data and knowledge sharing of both technical skills and social skills. Many thanks also go to all my former colleagues of AK Klein especially Magdalena König for being a really great mentor, Anna Thinner and her team (Franziska Wirth and Mara Westenberger) for the help and kindness, and Sebastian Lobentanzer for utmost cooperation on bioinformatics data and manuscript writing. I also would like to thank all the current colleagues of AK Klein Christian Viel, Alina Lehto, and Marius Fuchs for the wonderful cooperation. I am particularly appreciative of Constantin Kondak for always being there when needed. He translated the summary of this thesis into the German language. Many thanks also go to almost all of my colleagues of AK Schmidtko, particularly to Jonas Petersen and Cyntia Schäfer.

August 2020

Tri Yuliani

List of abbreviations

Acetyl-CoA Acetyl Coenzyme A
ACh acetylcholine
AChE acetylcholinesterase
aCSF artificial cerebrospinal fluid
AD Alzheimer's dementia
AF64ethylcholine aziridinium
AP anterior / posterior
ApoE apolipoprotein E
APP amyloid precursor protein
APP amyloid precursor protein
AQP4 aquaporin-4
ATC acetylthiocholine
ATP adenosine triphosphate
AUC area under the curve
A β amyloid- β
A β o amyloid- β oligomers
BBB blood-brain barrier
BChE butyrylcholinesterase
BPSD behavioral and psychological symptoms of dementia
BSA bovine serum albumine
CA cornu Ammonis
CBF cerebral blood flow
Ch choline
ChAT choline acetyltransferase
ChI Cholinergic interneuron
CHT-1 high-affinity choline transporter 1
CNS central nervous system
CS Citrate synthase
CS citrate synthase
CSF cerebrospinal fluid
Cyt C cytochrome C
DAG diacylglycerol

DCFDA 2',7'-dichlorofluorescein diacetate
DG dentate gyrus
DLP1 dynamin-like protein 1 protein
Enk enkephalin-positive MSNs
eoAD early-onset AD
ETC electron transport chain
ETC electron transport chain
fAD familial AD
FITC Fluorescein isothiocyanate
FJ Fluoro-Jade C
GABA gamma-aminobutyric acid
GABAergic gamma-aminobutyric acidergic
GFAP glial fibrillary acidic protein
GLUT glucose transporter
GPe globus pallidus externus
GPi globus pallidus internus
GSK3 β glycogen synthase kinase-3 beta
HACU high affinity choline transporter
HEPES Hydroxyethylpiperazine Ethanesulfonic Acid
HPC hippocampus
HPLC high performance liquid chromatography
i.p. intraperitoneally
icv intracerebroventricular
IDE insulin degrading enzyme
IHC immunohistochemistry
IP3 inositol trisphosphate
IR insulin receptor
IRS-1 insulin receptor substrate-1
KGDHC α -ketoglutarate dehydrogenase
L lateral
LACU low affinity choline transport
LRP1 lipoprotein receptor related protein 1
mAChR muscarinic acetylcholine receptor

MAP mitogen-activated protein
MCT monocarboxylat-transporter
MDA malondialdehyde
Mfn1 mitofusin 1
MMP matrix metalloproteinase
MNU methyl nitrosourea
MSN medium spiny neurons
mt-DNA mitochondrial DNA
nbm nucleus basalis magnocellularis
NEP neprilysin
NFT neurofibrillary tangles
NGF neurotrophic growth factor
NMDA N-methyl-D-aspartate
NRFs nuclear respiratory factors
OXPHOS oxidative phosphorylation
PARP poly(ADP-ribose) polymerase
PBS phosphate-buffered saline
PDHC pyruvate dehydrogenase
PFA, paraformaldehyde
PGC-1 α PPAR γ coactivator-1 α
PINK1 PTEN-induced kinase 1
PKC protein kinase C
PSEN1 presenilin1
PSEN2 presenilin2
PV parvalbumin-positive interneurons
ROS reactive oxygen species
rpm revolutions per minute (rounds per minute)
sAD sporadic AD
sAPP α soluble APP α
SD standard deviation
SEM standard error (standard error of the mean)
SNc substantia nigra pars compacta
SNr substantia nigra pars reticulata

SP substance P–positive MSNs

STN subthalamic nucleus

STR striatum

STZ Streptozotocin

T1DM type 1 diabetes mellitus

T2DM type 2 diabetes mellitus

TBA thiobarbituric acid

TCA tricarboxylic acid

TDP thiamine diphosphate

TNF- α tumor necrosis factor- α

TRITC Tetramethylrhodamine isothiocyanate

VACht vesicular acetylcholine transporter

VMAT vesicular monoamine transporter

1 Introduction

1.1 Dementia

More than 50 million people in the world suffer from dementia in 2019 and the number is increasing along with increased life span (Balsinha et al., 2019). Dementia is a central nervous system (CNS) disorder characterized by progressive cognitive decline such as memory, learning, orientation, language, and problem-solving. In a later stage of the disease, another syndrome appears known as behavioral and psychological symptoms of dementia (BPSD) that is frustrating for the carers. The behavioral changes include agitation, aggression, calling out, sleep disturbance, wandering, and apathy. The psychological changes include anxiety, depression, delusions, and hallucinations (Prince and Jackson 2009).

1.2 Alzheimer's disease

Alzheimer's disease (AD) is the major brain pathology in dementia which affects mostly the cerebral cortex and hippocampus (Francis et al., 1999). It is characterized by the accumulation of abnormal protein leading to loss of synapses, dendrites, and neurons (Fig. 1.1). Those proteins are extracellular amyloid- β ($A\beta$) plaque which is derived from mis-metabolism of amyloid precursor protein and intracellular neurofibrillary tangles (NFT) which contain hyperphosphorylated tau microtubule proteins.

AD is classified into early-onset and late-onset. Early-onset AD (eoAD) affects people less than 65 years old and contributes to only 1% of AD cases. It is commonly known as familial AD (fAD) and linked to gene mutations on $A\beta$ peptide metabolism leading to $A\beta$ plaque disposition. The mutations occur on the precursor (amyloid precursor protein (APP)) and the metabolizing enzymes (presenilin1 (PSEN1) or presenilin2 (PSEN2) (Masters et al., 2015)).

On the other hand, late-onset AD affects older people (>65 years old) and contributes to 95% of AD. It is also known as sporadic AD (sAD) because of multiple etiologic factors such as glucose hypometabolism, neuroinflammation and genetic polymorphism (the apolipoprotein E (apoE) gene $\epsilon 4$ allele), leading to failure on $A\beta$ clearance and NFT disposition (Hoyer 1996) (Chen et al., 2013) (Prince and Jackson 2009). APOE, together with microglia and macrophage, has been thought to be involved in $A\beta$ clearance despite unclear mechanisms (Masters et al., 2015).

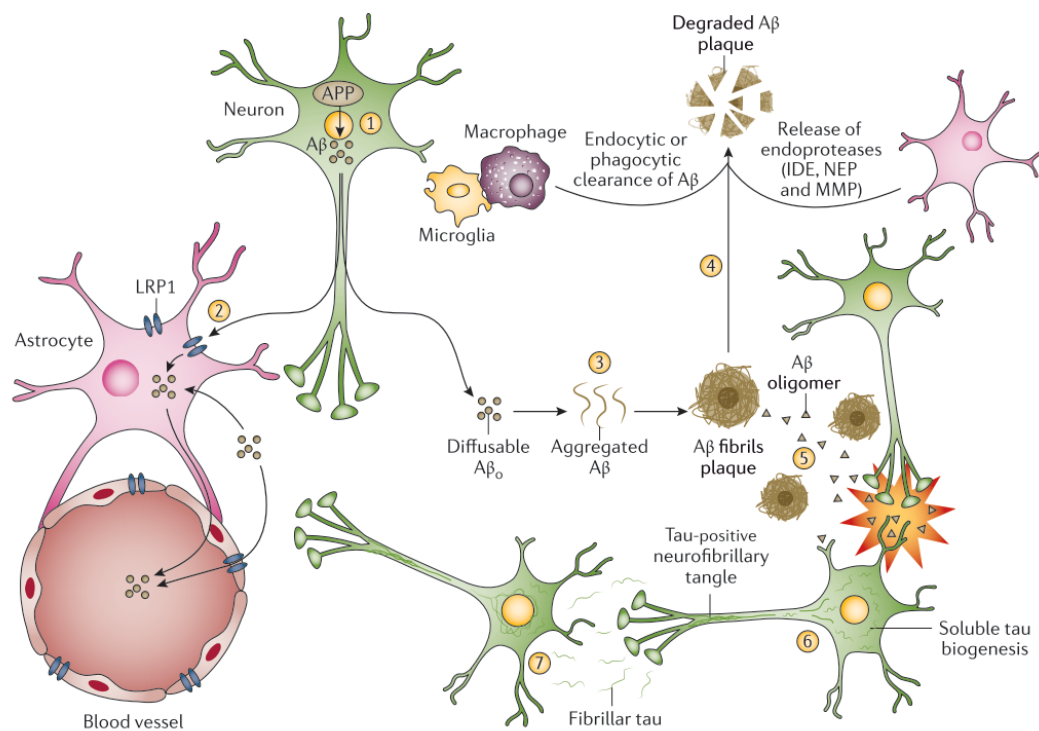


Figure 1. 1. Proposed pathways leading to A β plaques and NFT formation. APP metabolism results in A β peptide production which is then released into the extracellular space as diffusible oligomers (A β _o). A β _o clearance involves APOE or astrocytes via low-density lipoprotein receptor-related protein 1 (LRP1; step 2). Otherwise, A β _o may aggregate leading to A β plaque formation (step 3). A β plaque clearance involves endocytic or phagocytic clearance by macrophages and microglia, or endoproteases from astrocytes (such as insulin-degrading enzyme (IDE), neprilysin (NEP) and matrix metalloproteinase (MMP); step 4). However, certain A β oligomers may not be cleared and are toxic to adjacent synapses (step 5) leading to NFT production (step 6) by unknown mechanisms. Fibrillar tau may be released and taken up by healthy neurons leading to NFT production in the uptaking cell (step 7) (Masters et al., 2015).

1.2.1 Alzheimer's disease drug therapy

Although numerous drug candidates have been investigated in clinical and preclinical studies, no new AD drugs have been approved since 2003 by the United States Food and Drug Administration. To date, only 4 drugs have been approved to reduce dementia symptoms: donepezil, rivastigmine, galantamine, and memantine. The first three are acetylcholinesterase (AChE) inhibitors which increase ACh level and the last one is an N-methyl-D-aspartate (NMDA) receptor blocker (Wood and Cummings 2004).

Although disease modification is difficult to achieve with these drugs (Masters et al., 2015), some studies indicated that AChE inhibitors may play a role on APP metabolism leading to A β plaque reduction, e.g. by direct effect on the machinery involved in APP synthesis or by increasing non-toxic soluble APP α (sAPP α) release through activation of protein kinase C

(PKC) and/or mitogen-activated protein (MAP) kinase pathways independent or dependent on muscarinic ACh receptor (mAChR) activation (Racchi et al., 2004). Besides, other studies indicated that AChE may play a role in A β disposition through interaction with toxic A β . Therefore, inhibition of AChE may reduce A β disposition (Rees et al., 2003).

1.3 Alzheimer's disease hypothesis

The underlying mechanism of AD pathology remains elusive despite increased understanding of the disease (Wang et al., 2020). Several AD hypotheses related to our recent study are briefly discussed in this section.

1.3.1 Cholinergic deficit hypothesis

Cholinergic deficit plays an important role in AD pathology as it is the current target of therapy and correlates well with clinical signs of dementia. This hypothesis emerges after the discoveries of ACh's role in memory and cholinergic deficit in a selective brain region of AD patients, such as reductions of basal forebrain cholinergic neurons, choline acetyltransferase (ChAT), choline uptake, and ACh release (Francis et al., 1999).

The majority of basal forebrain neurons are cholinergic (50-75%). Medial septal nuclei and the vertical limb of the diagonal band, part of the basal forebrain, project their cholinergic neurons to the hippocampus (Ballinger et al., 2016). Because as much as 75% cholinergic neuronal degeneration in basal forebrain may occur in AD, a large decrease of cholinergic transmission in the hippocampus may occur (Pepeu and Giovannini 2017) followed by postsynaptic neurodegeneration (Hampel et al., 2018).

The medial septal cholinergic neuron is responsible for 60% of hippocampal CA1 region innervation. This innervation modulates pyramidal glutamatergic neurons, the second major interneuron in the CA1 region of hippocampus. The CA1 region of the hippocampus contains 20% glutamatergic interneuron and 70% is gamma-aminobutyric acidergic (GABAergic) interneuron (Müller and Remy 2018). Therefore, loss of cholinergic function in the hippocampus results in a reduction of glutamatergic neuronal activation (Francis et al., 1999).

Basal forebrain cholinergic neurons, including the hippocampus, are a part of an uninterrupted band of core limbic area. This region, somehow, is vulnerable to NFT disposition and cell death caused by aging and AD. In contrast, cholinergic interneurons in the striatum remain relatively intact in AD brain (Mesulam 2004).

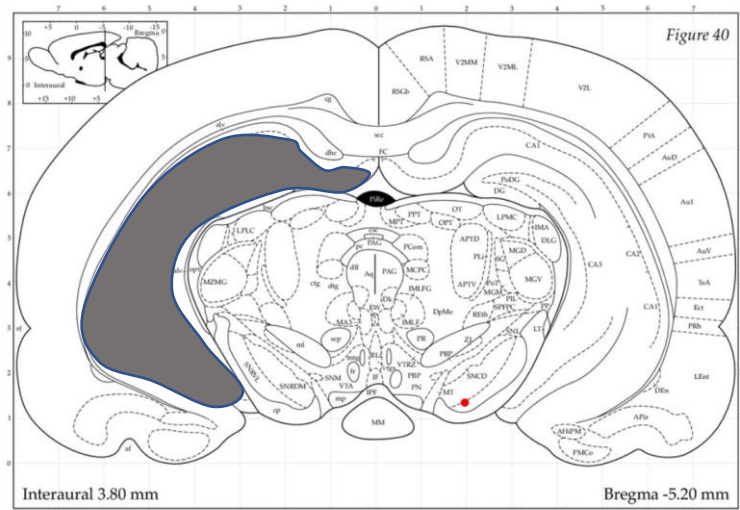
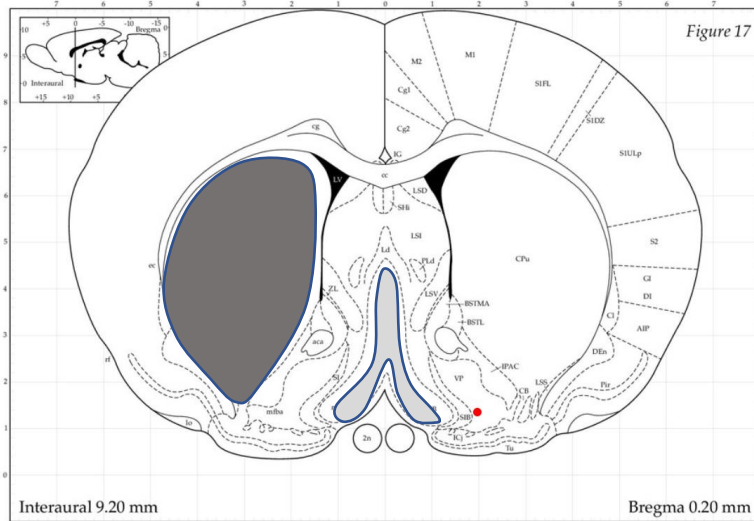


Figure 1. 2. Coronal section of a rat brain on striatum and hippocampus. A. It shows striatum (grey) and medial septum (light grey) at 0.20 mm anterior to bregma. B. It shows hippocampus (grey) at 5.20 mm posterior to bregma. Black shows the ventricle. (<http://labs.gaidi.ca/>).

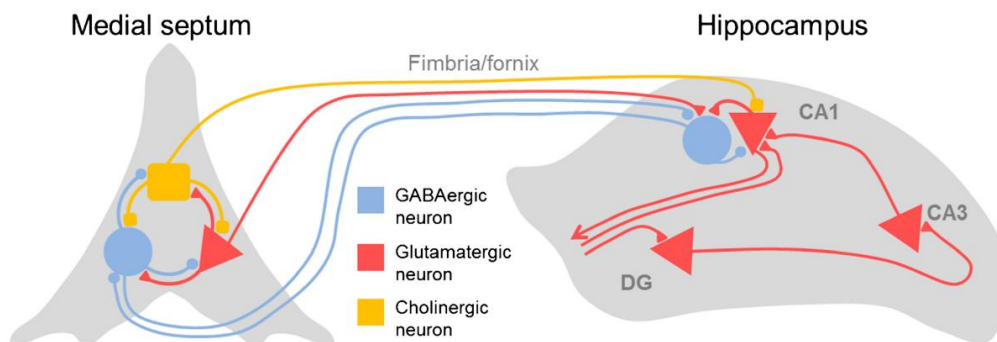


Figure 1. 3. Illustration of septohippocampal connection. It focuses on medial septal connections to CA1 (Müller and Remy 2018).

The striatum is a brain region with the highest concentration of cholinergic markers and ACh. In rodents, striatum contains 95% GABAergic projecting neurons and 5% interneurons of which 1% are cholinergic interneurons (ChI). Striatal ChI is proposed to receive mainly GABAergic terminals (60%; from globus pallidus) and only 20% glutamatergic terminals (from cortex and thalamus) (Gonzales and Smith 2015). The connection of the cholinergic interneuron in striatum is illustrated in Fig 1.4.

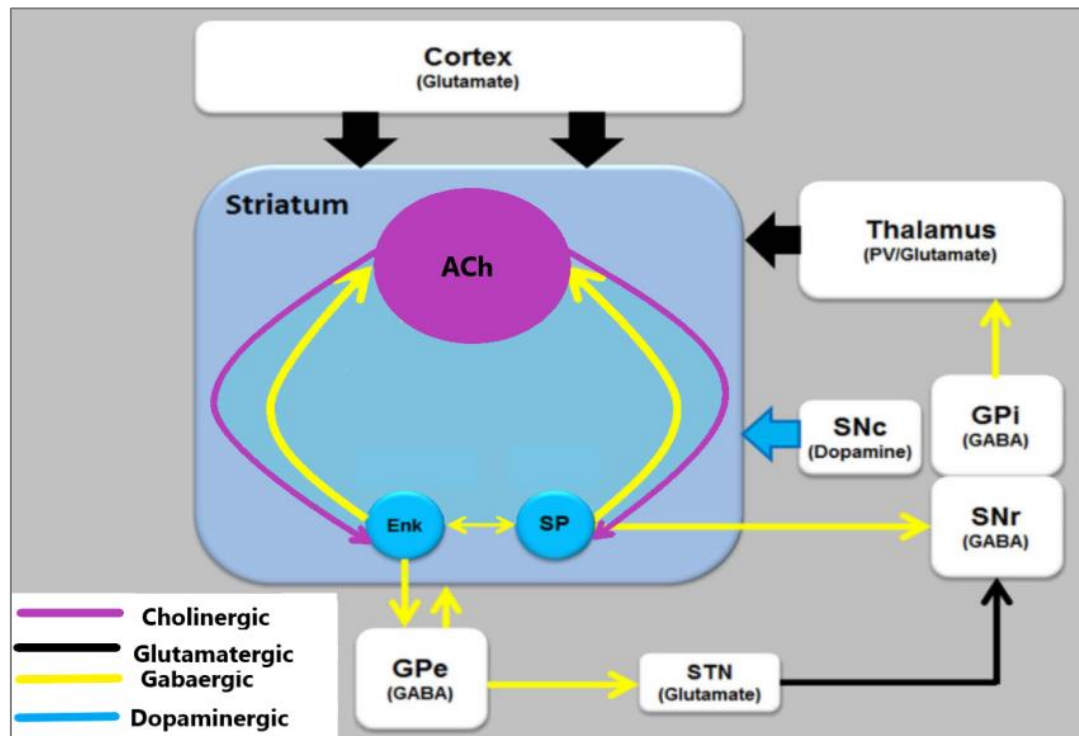


Figure 1. 4. Synaptic inputs to striatal cholinergic interneurons. Thalamus, cerebral cortex, GPe, and SNc innervates striatum and modulates ChIs. Abbreviations: SNc (substantia nigra pars compacta), SNr (substantia nigra pars reticulata), STN (subthalamic nucleus), GPe (globus pallidus externus), GPi (globus pallidus internus), Enk, enkephalin-positive MSNs; SP, substance P–positive MSNs; MSN (medium spiny neurons), PV, parvalbumin-positive interneurons (Gonzales and Smith 2015).

It is worth noting, however, that selective cholinergic lesions in basal forebrain do not always lead to memory impairment in either animal studies or human AD (Hampel et al., 2018). In other words, the cholinergic lesion almost certainly contributes to the severity of memory impairment, however, it is very unlikely that it serves as the only contributor of clinical symptom and neuropathological changes (Mesulam 2004).

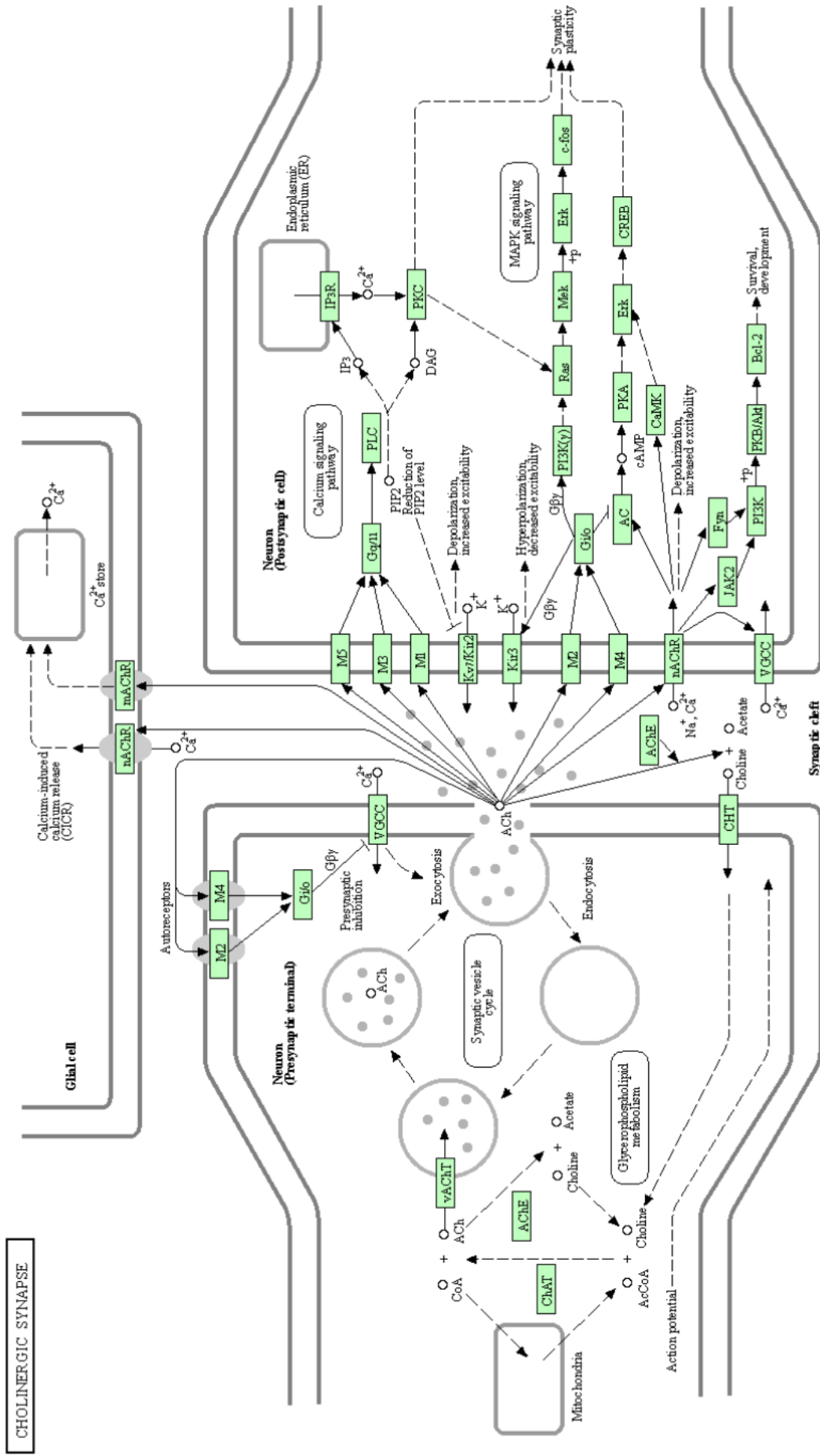


Figure 1. 5. Cholinergic synapse. See next page for description.

A cholinergic synapse is illustrated in Fig. 1.5 and its main characteristics and targets of cholinergic drugs are illustrated in Fig. 1.6. In cholinergic presynaptic neurons, ChAT catalyzes the synthesis of acetylcholine (ACh) from acetyl-coenzyme A (acetyl-CoA) produced by mitochondria and choline from the cytosol. ACh is then stored in vesicles by the vesicular ACh transporter (VACHT). Following presynaptic depolarization, ACh is released into the synaptic cleft and binds to its presynaptic and postsynaptic receptors. Both G protein-coupled receptors (“muscarinic” receptors) and ligand-gated ion channels (“nicotinic receptors”) may be present. Gi-linked muscarinic receptors elicit mainly inhibitory response, e.g. presynaptic M2/4 receptor activation regulates ACh release via negative feedback response. Gq-linked M1, M3, and M5 muscarinic receptors are excitatory and activate an intracellular signaling pathway involving diacylglycerol (DAG), inositol trisphosphate (IP3), and a Ca²⁺-dependent protein kinase (PKC). In the synaptic cleft, acetylcholinesterase (AChE) rapidly hydrolyzes ACh to acetate and choline. Choline transporters, such as high-affinity choline transporter (CHT-1), then take up choline into the presynaptic cholinergic neuron (Fig. 1.5 was obtained from Kyoto Encyclopedia of Genes and Genome <https://www.genome.jp/>).

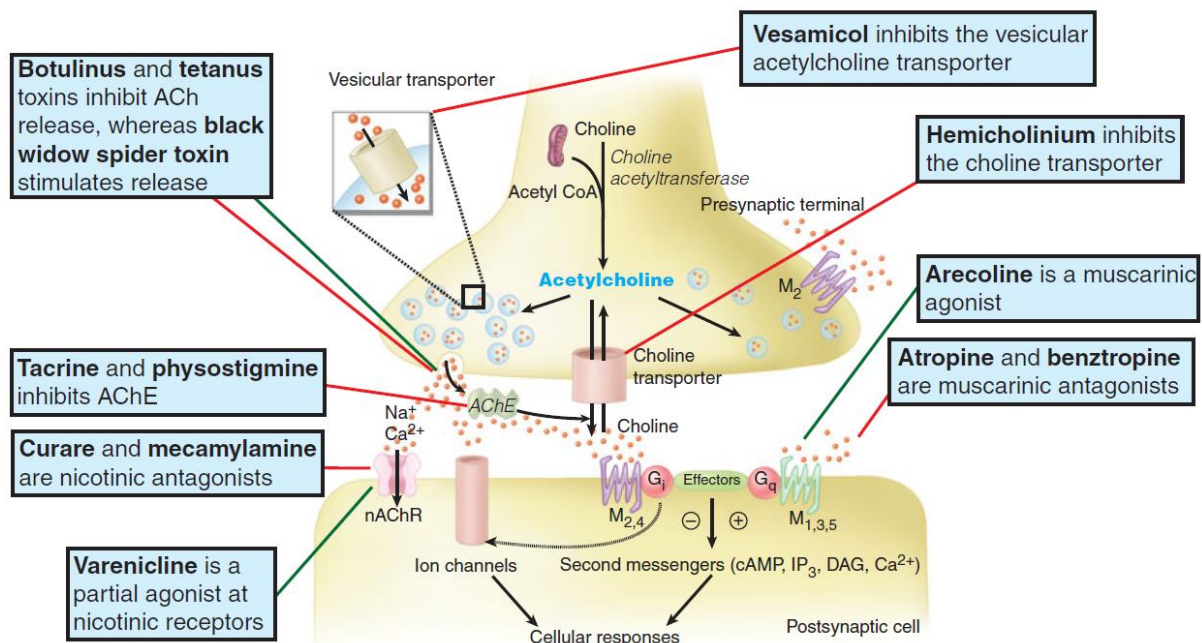


Figure 1. 6. Interesting features of cholinergic synapse. (1) Mitochondria are needed to supply acetyl-CoA for ACh synthesis. (2) Choline membrane transporter (CHT-1) transports choline for ACh synthesis. (3) The transporter (VACHT) is distinct from the vesicular monoamine transporter (VMAT). (4) Both G protein-coupled receptor (M1-M5) and ligand-gated ion channel (nAChR) may be present (5) ACh action is terminated by AChE, a highly active enzyme. (Mc Graw Hill, 2015).

1.3.2 Glucose hypometabolism hypothesis

Glucose hypometabolism was proposed as the cause of AD after a significant decrease of glucose utilization (-40%) in the presence of slightly decreased oxygen utilization (-20%) was discovered in the early stage of brain AD. It indicates that substrates other than glucose may be oxidized or dying neurons consume less oxygen (Hoyer 1991). Notably, glucose hypometabolism correlates poorly with A β disposition in both fAD and sAD despite preceding clinical signs of dementia by decades. In fAD where glucose hypometabolism is secondary to A β disposition, the regional distribution of A β disposition is not associated with regional glucose hypometabolism in one patient. In sAD, glucose hypometabolism was found in APOE4 carriers without A β disposition suggesting glucose hypometabolism as the primary cause of AD (Wang et al., 2020).

In the human AD brain, the reduction of enzymes involved in glycolysis, tricarboxylic acid (TCA) cycles, and mitochondrial oxidative phosphorylation (OXPHOS) has been reported. Hexokinase activity was reduced in nucleus basalis of Meynert in AD brain (Hoyer, 1991). The first half of TCA enzyme activities were reduced (pyruvate dehydrogenase (PDHC), isocitrate dehydrogenase, and α -ketoglutarate dehydrogenase (KGDHC)) but the later half were increased (succinate dehydrogenase and malate dehydrogenase) (Bubber et al., 2005). These reductions were associated with reduced blood thiamine diphosphate (TDP) levels, a critical coenzyme of PDHC and KGDHC in the TCA cycle and transketolase in the pentose phosphate pathway (Sang et al., 2018). Deficits in mitochondrial electron transport chain (ETC) have also been reported, especially in complex IV (Perez et al., 2018) (Maurer et al., 2000).

The glucose hypometabolism hypothesis was tested in a non-transgenic AD model induced by intracerebroventricular injection of a diabetogenic compound: streptozotocin (icv-STZ model; will be discussed later in 1.6). Supported by some preclinical and clinical studies, the mechanism behind glucose hypometabolism in this model is proposed as a disturbance of brain insulin receptor (IR) signaling through the PI3K/AKT pathway, leading to AD-like symptoms (Frölich et al., 2015). Slowly, the hypothesis has been expanded to the impaired brain insulin signaling pathway as the cause of AD. These two hypotheses have been used to connect diabetes mellitus (DM) and AD.

1.3.3 Impaired brain insulin signaling hypothesis

Impaired brain insulin signaling or insulin-resistant brain state has been proposed as the cause of both fAD and sAD. In fAD, A β peptide inhibits insulin receptor (IR) activation at the extracellular α subunit, while in sAD, the age-related increases of both cortisol and noradrenaline may inhibit IR activation at the intracellular β subunit (Hoyer 2004). Furthermore, two pathological hallmarks of AD, A β and NFT disposition, have been suggested to be caused by a decrease of insulin-degrading enzyme (IDE) responsible for A β clearance and decrease of PI3K/AKT pathway resulting in glycogen synthase kinase-3 beta (GSK3 β) activation which leads to tau hyperphosphorylation (Salas and De Strooper 2019). Several clinical trials with the purpose of enhancing brain insulin signaling pathways are being conducted despite the unclear mechanism (Cummings et al., 2019).

Similar to other AD hypotheses, brain insulin resistance is not an AD specific event because it was also found in other neurodegenerative diseases, such as Parkinson's disease and tauopathies, and even in non-demented aging (Arnold et al., 2018). Therefore, brain pathology other than a disturbance of insulin signaling is required to connect between DM and AD and between icv-STZ and AD-like symptoms.

1.3.4 Inflammation, disturbance of insulin signaling, and AD

DM-induced peripheral inflammation may also spread to the brain leading to AD because inflammatory markers, such as tumor necrosis factor- α (TNF- α), are found in both diseases. Following brain injury (trauma, abnormal protein aggregation), astrocytes and microglia are activated leading to inflammatory cytokine release. The cytokines then activate stress kinases, such as JNK and IKK, which result in abnormal phosphorylation of insulin receptor substrate-1 (IRS-1) leading to diminished intracellular insulin action (Ferreira et al., 2014).

1.3.5 Mitochondrial dysfunction

Mitochondrial dysfunction has also been proposed to connect glucose hypometabolism and AD because a normal mitochondrial function is needed by neurons for a significant amount of ATP production, neurotransmitter synthesis, and intracellular calcium regulation. Dysfunction of mitochondria may lead to impaired cellular bioenergetic status, increased reactive oxygen species (ROS) and damage to mitochondrial DNA (mt-DNA) (Wang et al., 2020).

Regarding ATP production, as discussed before, reduced activity of (OXPHOS), especially on complex IV, and the first half of the TCA cycle enzymes have been reported in AD (Maurer et

al., 2000). Despite some variation between studies, a certain threshold reduction of complexes I, II, and IV is needed to alter ATP production (Wang et al., 2020). It is noteworthy that cell-specific alterations of gene expression of mitochondrial complexes may occur as decreased nuclear gene expression was found in pyramidal neurons but an increase was found in hippocampal homogenate (Rice et al., 2015).

Mitochondria have been proposed to be responsible for 90% of cellular ROS generation due to electron leak from complex I and III during OXPHOS. While ROS damage a wide range of biomolecules (protein, sugar, lipid, and nucleic acid), mitochondrial DNA (mtDNA) itself is prone to oxidative damage and DNA alkylation due to lack of DNA-protective histones and inefficient DNA repair mechanisms (Oliver and Reddy, 2019).

To maintain a healthy pool of mitochondria, they undergo dynamic cycles of fusion and fission. Mitochondrial fission is regulated by fission proteins such as dynamin-like protein 1 protein (DLP1 or Drp1) while mitochondrial fusion is regulated by fusion proteins such as mitofusin 1 (Mfn1). Several insults during AD, such as A β peptide formation, may induce DLP1 translocation to mitochondria resulting in increased mitochondrial fission which is associated with AD pathology (Hroudová et al. 2014). A DLP1 inhibitor has been reported to alleviate AD symptoms in transgenic mice (Baek et al. 2017).

Coordination between nuclear DNA and mt DNA expression is crucial for mitochondrial biogenesis as both DNA are involved in mitochondrial protein expression. A master regulator of mitochondrial biogenesis, PPAR γ coactivator-1 α (PGC-1 α), interacts with nuclear respiratory factors (NRFs) leading to mitochondrial protein expression involved in both mtDNA replication and transcription (Oliver and Reddy 2019). Indeed, the reduction of PGC-1 α expression has been reported in AD patients and in AD animal models. Furthermore, enhancing PGC-1 α function has been reported to be beneficial in both A β and tau models in mice (Wang et al., 2020).

Finally, damaged mitochondria are degraded by mitophagy. Impaired mitochondrial membrane potential activates PTEN-induced kinase 1 (PINK1) at the outer mitochondrial membrane which results in parkin recruitment leading to mitophagy (Oliver and Reddy 2019). In the AD brain, mitophagy is interrupted as shown by the accumulation of PINK1 and parkin labeling in damaged mitochondria. Furthermore, enhancing mitophagy has been reported to be beneficial in APP transgenic mice (Wang et al., 2020).

1.4 Animal models of Alzheimer's disease

In addition to clinical studies, preclinical studies using an animal model have been used for decades to understand the pathology and to evaluate potential therapies of AD (Drummond and Wisniewski 2017). AD models, despite few similarities to human AD, may be useful to reveal different pathways involved in AD pathology leading to the discovery of new therapeutic approaches (Van Dam and De Deyn 2006).

It should be noted, however, that behavioral studies for cognitive function cannot easily distinguish learning, memory, attention, and motivation (Toledano and Álvarez 2004). Besides, no obvious relation between brain pathologies and dementia syndrome has been described. For example, two pathological hallmarks of AD, extracellular amyloid- β ($A\beta$) plaques and intracellular neurofibrillary tangles (NFTs), are also present in normal aging brain (Cavanaugh et al., 2014).

Aging animals were suggested as AD models, however, although they mimic human aging the most, senile animals showed high variability in brain glucose metabolism and behavioral study even in the same test group (Gage et al., 1984). Inducing AD with a toxin in senile animals may be more complicated as the age-associated changes can modify neuronal adaptive responses involved in initial recovery from damage (Toledano and Álvarez 2004). Apart from that, it is difficult to control age-associated changes such as deficits in neurotransmission, growth factors, hormones, gliosis, neuronal death, blood flow, and metabolism (Toledano and Álvarez 2004).

1.4.1 Transgenic model

Transgenic animals have been considered as the gold standard to model AD leading to underutilization of non-transgenic models. Transgenic animals, however, have several limitations. High expression of human genes may induce unpredictable responses or defense mechanisms. It is also possible that the pathology is due to abnormal development of transgenic animals which is not associated with AD. Regarding the $A\beta$ plaques, different post-translational modifications between human and murine cells lead to different properties of $A\beta$ plaques. For example, despite a similar immunohistochemical picture, $A\beta$ plaques in murine cells are soluble, but not in humans (Cavanaugh et al., 2014). Regarding neurofibrillary tangles (NFT), only one transgenic animal develops NFT similar to humans, namely TgF344-AD rat. However, the NFT was expressed by mutant human APP^{sw} and PSEN 1 genes which corresponds more to the fAD type (Cohen et al., 2013).

To sum up, the poor similarity of the transgenic AD model to human AD may be the cause for unsuccessful clinical trials on hundreds of drug candidates previously proven to be effective in the transgenic AD model. Therefore, the utilization of a non-transgenic model may offer a hope for AD research (Grieb 2016).

1.4.2 Non-transgenic model

Several non-transgenic animal models of AD have been developed by toxin injection into a specific brain region or brain ventricle (intracerebroventricular or icv). It should be noted that several factors may affect toxin distribution, such as dose and particle size. In the case of ethylcholine aziridinium (AF64) toxin, a choline analog, for example, icv injection of a high dose (>2 nmol) is followed by histological damage of cholinergic neurons in most brain regions such as the septum, nucleus basalis magnocellularis (nbm), hippocampus, and neocortex. On the other hand, a low dose of AF64 (1-2 nmol) affects only nearby regions of the ventricle with long projecting cholinergic neurons such as the septum, nbm, and hippocampus. Striatal cholinergic interneurons are relatively spared (Toledano and Álvarez 2004).

Local injection of excitotoxin has been used to model AD. Injection in nucleus basalis magnocellularis (nbm) of basal forebrain induces cortical cholinergic hypofunction, while injection in septum induces cholinergic hypofunction in the hippocampus. However, a complete cortical cholinergic deficit is difficult to achieve due to the presence of cortical cholinergic interneurons and innervation from other cholinergic centers leading to hyperactivation of the remaining cholinergic neurons (Pavia et al., 2000). It should be noted that injection in one hemisphere may lead to only minimal changes in the contralateral part (Toledano and Álvarez 2004) (will be discussed in 1.4.2.3).

Icv injection has been considered to resemble human AD more because of wider distribution than local injection into specific brain regions (Gluscock et al., 2011). However, a recent study shows that following icv injection, both small and large molecule (759 Da and 2kDa) minimally enter brain parenchyma and distribute only to the surrounding ventricle as observed using *in vivo* two-photon imaging of small fluorescent tracers. It is unclear why, in this study, injection into cisterna magna results in a rapid distribution of molecules to brain parenchyma with the large molecule confined to the paravascular space surrounding arteries and the small molecule going farther, reaching the interstitial space which was then cleared along paravenous drainage. The authors suggest that aquaporin-4 (AQP4) in astrocytes plays an important role in this system (Ilf et al., 2012).

1.4.2.1 A β infusion

Continuous infusion of A β 1-40 for 2 weeks (300 pmol/day) leads to spatial memory impairment, A β disposition in the ventricle wall surrounding hippocampus, and decreased ChAT activity (-20%) in the hippocampus but not in striatum (Nitta et al., 1994). However, the hippocampal ACh level was unchanged even during high-potassium stimulation (Itoh et al., 1996). Two weeks after icv A β peptide, cholinergic hyperactivity in nbm and cortex occurs in the presence of muscarinic receptor downregulation. Notably, the animals recovered following A β peptide clearance (Toledano and Álvarez 2004). Besides, the concentration of A β used to induce AD-like symptoms was much higher than the concentration founded in human AD. However, this model may be useful for understanding A β toxicity and for investigating A β -targeting drug candidates despite several limitations (Van Dam and De Deyn 2006).

1.4.2.2 192 IgG Saporin

The long projecting neurons, such as basalocortical cholinergic neurons, are highly dependent on neurotrophic growth factor (NGF) and the low-affinity NGF receptor (p745GFr). Immunotoxin, such as IgG saporin, binds on this receptor and delivers saporin (a ribosome-inactivating protein) which results in selective damage of the neurons leading to a cholinergic deficit and AD-like pathology (Toledano and Álvarez 2004).

After 7 days, icv IgG saporin decreased ACh level in microdialysates (-70% until -80%), ChAT activity (-80%), AChE activity (-40%), and HACU (-30%) in the hippocampus (Waite and Chen 2001) (Garcia-Alloza et al., 2006). An almost similar reduction of cholinergic function was also observed in the frontal cortex indicating deafferentation both in the hippocampus and cortex (Garcia-Alloza et al., 2006). During potassium stimulation, an increase of ACh level in microdialysates following lesion was reduced by 50% compared to control (Garcia-Alloza et al., 2006). 15 weeks later, both ChAT and ACh were still decreased. Acute behavioral changes (lack of grooming) were observed 1 week after injection but were recovered over time (Waite and Chen 2001).

This model, however, showed some limitations. (1) Purkinje cells in the cerebellum also express p75NGFr resulting in unspecific toxicity towards saporin which may interfere during the behavioral test. (2) In a long-term study (11 months) unspecific toxicity appears as shown by excessive tissue loss at the site of the lesion. (3) Notably, no significant cognitive deficit was observed during both short and long term studies (Toledano and Álvarez 2004).

1.4.2.3 Excitotoxin

Several toxins work on the glutamatergic receptor, such as quinolic acid, kainic acid, NMDA, ibotenic acid, and quisqualic acid, have been used to induce AD-like symptoms, mainly by local injection into nbm. The mechanism is by increasing Ca^{2+} influx into neurons leading to cholinergic neuronal death (Toledano and Álvarez 2004).

However, the cognitive effects are inconsistent and mainly related to unspecific cell damage dependent on different receptor subtypes. The damage may affect neighboring cells rather than cholinergic neurons, such as nbm interneuron or nbm non-cholinergic projecting neuron leading, for example, to reduced GABAergic function. Other inconsistency includes cholinergic impairment with behavioral recovery and biochemical cholinergic recovery with or without histochemical recovery. Glucose hypometabolism has been reported to recover but not ChAT activity (Toledano and Álvarez 2004).

It should be noted that despite decreased cholinergic neuronal count, the surviving neurons are hyperactive and hypertrophic leading to normal cortical cholinergic function or even an increased cholinergic neuronal count. Three months following lesion, increased cholinergic neuronal count (ChAT label; 2x) may be caused by cholinergic neurons which previously were under detection limit (Toledano and Álvarez 2004).

1.5 Streptozotocin (STZ)

The next AD model which will be discussed in detail is the icv-STZ model. In this model, STZ is injected into the lateral ventricle of the brain. However, peripheral administration of STZ is widely used to induce diabetes, and peripheral STZ administration will be discussed first because (1) mechanism of toxicity of peripheral STZ is well described, in contrast to peripheral STZ model (2) the icv-STZ has been developed to mimic peripheral STZ action in the brain.

1.5.1 Peripheral streptozotocin cytotoxic mechanism

Streptozotocin (STZ), a glucose analog bound to nitrosourea moiety, is an antibiotic produced by *Streptomyces achromogenes* (Fig. 1.7). Following cell uptake through glucose transporter 2 (GLUT2), STZ is split to glucose and lipophilic methyl nitrosourea (MNU) moiety. The main mechanism of STZ toxicity is DNA alkylation followed by DNA fragmentation (Lenzen 2008). Excessive DNA strand breaks hyperactivates poly(ADP-ribose) polymerase (PARP), a DNA repair enzyme, and results in NAD^+ and ATP depletion leading to cellular death. This

mechanism has been revealed in PARP-knock out mice which showed preserved blood glucose and beta-cell structure and function despite increased DNA strand breaks (Pieper et al., 1999). Additional toxicities include other biomolecule methylation, glycosylation, or nitric oxide liberation (Lenzen 2008). It should be noted that female mice are less sensitive to STZ toxicity than males (Furman 2015).

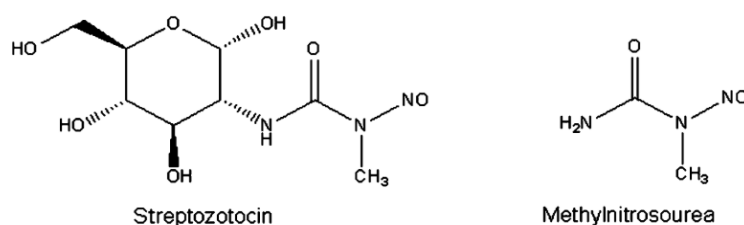


Figure 1. 7. STZ structure (Lenzen 2008).

DNA alkylation has been found in GLUT2 expressing organs such as the pancreas, kidney, and liver. In the pancreas, following i.p or i.v administration, STZ is concentrated in GLUT2 expressing beta-cells resulting in beta-cell necrosis leading to type 1 diabetes mellitus (T1DM)-like symptoms such as insulin deficiency, hyperglycemia, polydipsia, and polyuria (Lenzen 2008) (Furman 2015).

STZ's diabetogenic action is characterized by a triphasic blood glucose response: hyperglycemia, hypoglycemia, and permanent hyperglycemia. In the first hour, uptake of STZ by beta cells results in reduced insulin secretion leading to 2 hours of hyperglycemia. Four hours after STZ injection, beta-cell damage results in massive insulin release leading to several hours of hypoglycemia. Finally, persistent hyperglycemia occurs as soon as 12 hours after STZ injection (Lenzen 2008). Therefore, the central effect following peripheral STZ is likely caused by hyperglycemia (Grieb 2016).

1.5.2 Peripheral streptozotocin DM model

Both single high dose (mice: 200 mg/kg; rat 40-70 mg/kg) or multiple low doses (mice: 40 mg/kg; 5x in 5 days) of STZ are used to induce T1DM. The latter is considered to resemble T1DM as pancreatic islet inflammation involves mild hyperglycemia (fasting blood glucose 150 mg/dL), while a single high dose rapidly induces pancreatic beta-cell death and severe hyperglycemia (fasting blood glucose 500 mg/dL) within 2 days. Beta-cell necrosis following STZ administration results in hyperinsulinemia leading to hypoglycemia. Therefore, 10% sucrose is supplemented to drinking water after STZ administration until hyperglycemia occurs (day 2 for single-dose; day 6 for multiple doses). After 1-2 weeks of hyperglycemia, the

experiments are usually started. Severe hyperglycemia usually occurs after 3 weeks and persists for several weeks. For a chronic study, the second round of STZ injection is needed at week 7 to maintain a diabetic state (Furman 2015).

In human DM, insulin fails to activate its resistant receptor resulting in impaired glucose uptake leading to hyperglycemia. Following hyperglycemia, more insulin is released resulting in either normal glucose level (hyperinsulinemic euglycemia) or maximum insulin release without increased glucose uptake (hyperinsulinemic hyperglycemia) (Banks 2014).

To induce insulin resistance, the animals are exposed to a high-fat diet (60% fat diet for 3 weeks) before STZ administration resulting in normoglycemia and hyperinsulinemia (insulin resistance). Next, to induce hyperglycemia (T2DM), partial damage of beta cells (-60%) are induced by STZ combined with administration of nicotinamide 15 minutes before STZ administration. Nicotinamide is an NAD⁺ precursor and, therefore, reduces NAD⁺ depletion and STZ toxicity. The majority of animals show moderate non-fasting hyperglycemia (non-fasting glucose >200 mg/dl) while some animals may show normoglycemia with impaired oral glucose tolerance tests (Furman 2015).

1.6 Central administration of STZ

Central administration of STZ has been used widely to induce AD-like symptoms. This model was developed after (1) glucose hypometabolism was reported in both sAD and fAD patients and (2) a role of insulin on brain glucose metabolism was shown by increased glycolytic enzymes activities following icv insulin (Nitsch et al., 1989) (Hoyer et al., 1991) (Hoyer et al., 1993). In this model, STZ is directly injected into the brain ventricle (Fig. 1.8) because it poorly penetrates the blood-brain barrier (Bennett and Pegg, 1981). Therefore, it is called intracerebroventricular injection of STZ or icv-STZ. Several AD-like symptoms have been reported, normally 3 weeks after injection, such as memory impairment, reduced cholinergic markers, glucose hypometabolism, increased oxidative stress, neuroinflammation, and neurodegeneration (Salkovic-Petrisic et al., 2013). More detailed information of its toxicities will be presented in chapter IV.

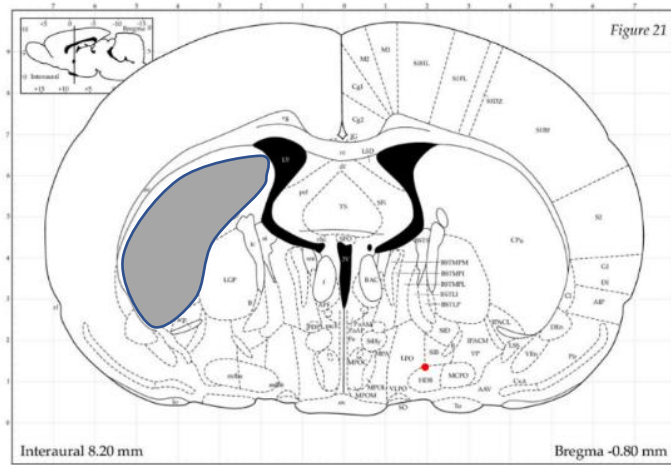


Figure 1. 8. A coronal section of a rat brain at 0.80 posterior to bregma. It shows large part of lateral ventricle (black) and striatum (grey). (<http://labs.gaidi.ca/>).

1.6.1 Memory impairment

The icv-STZ model shows persistent memory impairment following lesion, unlike other toxin models. For example, in basal forebrain lesion model, the memory was recovered despite persistent cholinergic deficit (Mayer et al., 1989). Memory impairments were observed 3 weeks after icv-STZ and persisted until 6 months; this was mostly tested by Morris water maze test for spatial learning (Knezovic et al., 2015) (Knezovic et al., 2018) (Saxena et al., 2008) (Sorial and El Sayed, 2017). Morris water maze test has been considered as the gold standard to evaluate spatial memory and learning which, however, relies heavily in a good motor function as the animals need to swim during the experiments. Indeed, many studies also reported preserved locomotor activity in this model indicating no interference of STZ with motor function during memory test (Hoyer et al., 1999) (Bloch et al., 2017) (Saxena et al., 2011).

1.6.2 Glucose hypometabolism

Later, the icv-STZ model became more widely used because glucose hypometabolism is a prominent feature of AD which occurs 2-3 decades before AD symptoms and brain atrophy (see above; Grieb 2016). The presence of glucose hypometabolism was expected in this model (Pathan et al., 2006) (Nitsch et al., 1989). However, recent studies indicate a contradictory result. The hippocampal glucose hypometabolism observed in this model is only small (ca. 10%) in a FDG-PET study (Duelli et al., 1994) (Knezovic et al., 2018).

1.6.3 Mitochondrial dysfunction

An indication of changes in mitochondrial function and biogenesis have been reported. Complex IV seems to be the most sensitive towards icv-STZ toxicity, followed by complex I and II. On the other hand, complexes III and V seem relatively spared (Zafeer et al., 2019). A decrease in citric acid cycle enzyme activities were also reported (Correia et al., 2013). However, the changes of both the protein level of mitochondrial complexes and the enzyme activities of the citric acid cycle were only small.

Some changes in mitochondrial complexes may cause changes in the ATP level. As expected, the changes in the ATP level were much lower than the changes in mitochondrial complexes (Ishrat et al., 2006). The decreased enzyme activities also failed to decrease the level of citric acid cycle intermediates (Nitsch and Hoyer, 1991).

1.6.4 Increased oxidative stress markers

Some changes in mitochondrial complexes may also cause changes in oxidative stress markers. Several such changes have been reported, concerning, for instance, the final products of lipid peroxidation (malondialdehyde), reactive oxygen species, endogenous antioxidant peptide (glutathione), and endogenous antioxidant enzyme (glutathione peroxidase, glutathione reductase, and superoxide dismutase). However, these changes in the hippocampus were only small (maximum +/- 50%) (Ishrat et al., 2006) (Zafeer et al., 2019) (Du et al., 2015). Up to two-fold increase of intracellular ROS measured by DCFDA (2',7'-dichlorofluorescein diacetate) assay was reported (Zafeer et al., 2019), however, this assay has been reported to have some limitations (Halliwell and Whiteman, 2004).

1.6.5 Cholinergic deficits

Indications of cholinergic deficit in this model have also been reported by measuring AChE, ChAT, and ACh (Sorial and El Sayed, 2017, Saxena et al., 2008 and Tota et al., 2011). However, these cholinergic markers poorly reflect dynamic cholinergic transmission, i.e. they do not correlate directly with ACh release. Furthermore, there is an indication of hyperactivity of the remaining cholinergic neurons (Shoham et al., 2007) as has been reported in another toxicity model (Toledano and Álvarez, 2004; see 1.4.2).

Notably, some of these cholinergic parameter changes were ameliorated by sibilin (p.o 100 and 200 mg/kg; dose-dependently; Tota et al., 2011), indometacin (i.p 10 mg/kg; Sorial and El

Sayed, 2017), valproic acid (i.p 100-200 mg/kg; Sorial and El Sayed, 2017), donepezil (p.o 5 mg/kg; Saxena et al., 2008) and tacrine (p.o 5 mg/kg; Saxena et al., 2008), dimethyl fumarate (0.4% w/w dimethyl fumarate in the food pellet; Majkutewicz et al., 2016), and Coenzyme Q10 (10 mg/kg b.wt., i.p. in corn oil; Ishrat et al., 2006). In many instances, the mechanism of action of these drugs is unknown; some drugs may interact with streptozotocin and influence the etiology of the STZ-induced damage.

1.6.6 A β peptide and p-Tau

Regarding two pathological hallmarks of AD namely A β ₁₋₄₂ peptide and p-Tau, apparently, longer studies such as 5 weeks are needed. These toxic substances were more easily observed in hippocampus than cortex (Correia et al., 2013) (Du et al., 2015). A two-fold increased of p-Tau level were observed after 3 months, however, it slowly decreased and was back to normal after 9 months (Osmanovic-Barilar et al., 2015). Regarding A β ₁₋₄₂ peptide, the increase was small (Correia et al., 2013).

1.6.7 Insulin receptor signaling impairment

Even though our study does not address changes in insulin receptor signaling, a brief discussion on insulin receptor signaling impairment in this model is worthwhile.

Indication of insulin signaling impairment have been reported in rats pups 2 weeks after injection. In this study, mRNA expression of insulin and insulin receptor substrate-1 were reduced (ca. -50%) (Lester-Coll et al., 2006). Hippocampal insulin receptor levels were also decreased in another study (-20%) (Osmanovic-Barilar et al., 2015). However, in this study, the insulin-degrading enzyme (IDE) was also decreased (-60%), which may indicate a preservation of insulin level. In another study, phosphorylation of the downstream kinases were also decreased (-30%) (Deng et al., 2009), as well as GLUT1, GLUT3 and protein O-GlcNAcylation level.

The increased insulin resistance markers following icv-STZ is considered as the cause of glucose hypometabolism which leads to AD-like symptoms. Therefore, a new AD hypothesis was suggested: disturbance of the insulin-signaling pathway or type-3 diabetes in the brain (Fig. 1.9) (Salkovic-Petrisic et al., 2013) (de la Monte et al., 2006). Several clinical studies based on this new hypothesis are being conducted. Indeed, a role of insulin in neuroplasticity has been postulated in a recent study (Grillo et al., 2015).

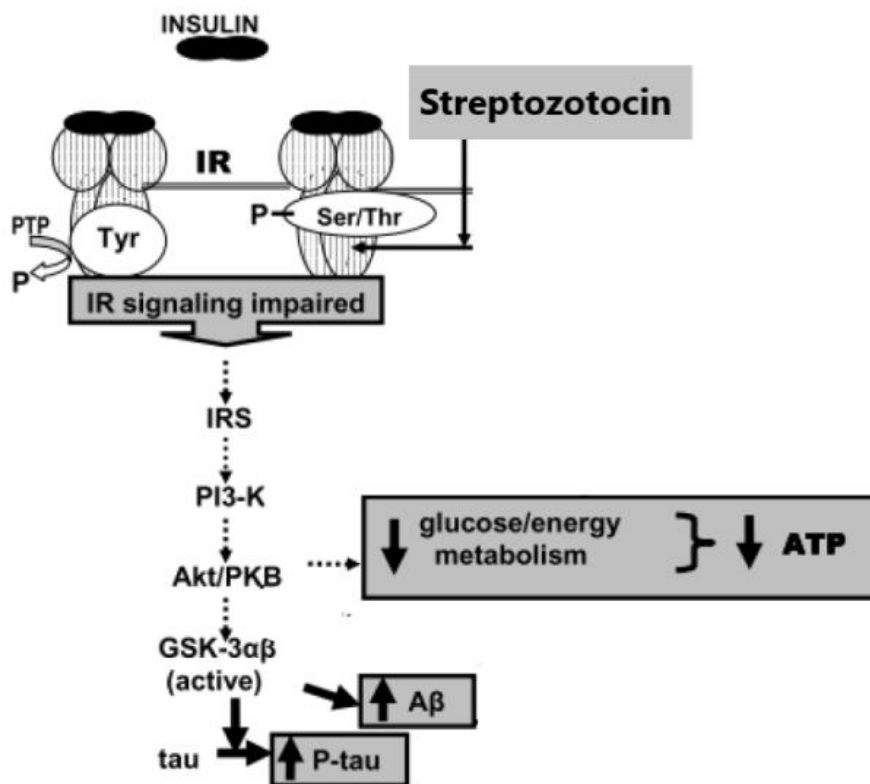


Figure 1. 9. Proposed mechanism of icv-STZ induced brain insulin resistance. Dashed arrow: impairment. (Picture was taken from (Ping-Sun, 2015) with modification.

1.6.8 Comparison of icv-STZ model and 3xTg mice

Chen et al. (2012) and Rai et al. (2014) compared icv-STZ model and 3xTg mouse model that bear mutations on presenilin 1, APP, and tau genes (Oddo et al., 2003). Both models showed impaired memory, neuroinflammation, hyperphosphorylated tau, altered synaptic proteins and insulin signaling in the brain. However, icv-STZ model shows more severe neuroinflammation and more down-regulation of genes related to insulin signaling and glucose metabolism. Notably, glial activation and inflammation preceded memory impairment and neuronal apoptosis.

In his review Grieb (2016) explains that insulin receptors as the first target of icv-STZ are unlikely because (1) insulin receptors undergo rapid intracellular turnover and (2) molecular structure of streptozotocin and insulin are completely different, therefore, interaction is not plausible. Therefore, it seems that neuroinflammation is more plausible to induce AD-like symptoms following icv-STZ than impaired insulin signaling (Fig. 1.10).

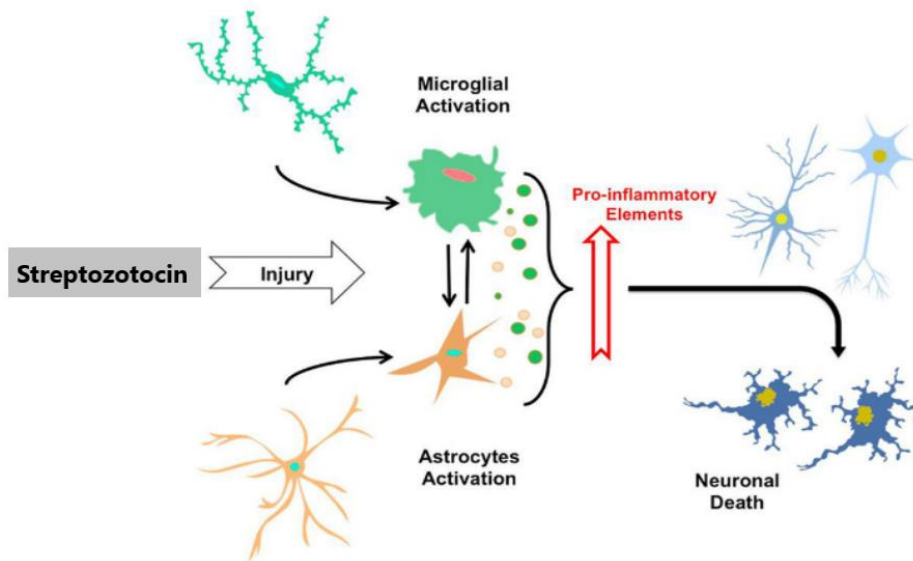


Figure 1. 10. Proposed mechanism of icv-STZ induced brain injury. The picture was taken from (Morales et al., 2014) with modification.

1.7 Objectives of the study

An alternative hypothesis in understanding sporadic Alzheimer’s disease (sAD) is urgently needed because prior models did not yield effective therapies despite decades of research. The alternative hypothesis, however, needs to be investigated thoroughly. Otherwise, it leads to ineffective AD research due to a lack of similarity between the disease model and human AD. As discussed in the previous segment, icv-STZ model seems promising to be used as a toxin-induced, non-transgenic AD model connecting diabetes mellitus (DM) with AD. This model offers an alternative hypothesis for AD: a glucose hypometabolism hypothesis. However, the mechanisms how icv-STZ induced AD-like symptoms are unclear, especially in the aspects of glucose hypometabolism and cholinergic deficit.

To gain a better understanding of icv-STZ pathology and similarities to human AD, we investigated the cholinergic and metabolic effect of STZ-induced hippocampal injury using microdialysis technique in freely moving animals, respirometry, and immunohistochemistry (IHC). First, GFAP staining was used to confirm the injury. Second, Fluoro jade staining was used to evaluate neurodegeneration. Third, the mitochondrial respiratory function was examined to explain the mechanism of injury. Fourth, cholinergic markers (ChAT, AChE, and CHT-1) were measured. Fifth, microdialysis experiments were done to examine whether the injury affects brain metabolism and cholinergic transmission.

Microdialysis is a sophisticated technique in which a probe is implanted in the area of interest (specific brain region) allowing sample collection from the extracellular (interstitial) space. Notably, this technique can be done in awake animals under behavioral or pharmacological stimulation. Metabolites and neurotransmitters in the interstitial space reflect neuronal activity in the surrounding area of the microdialysis probe and allow us to monitor real-time concentration with a customized time interval. Some biomarkers monitored in this study are energy metabolites (glucose, lactate, pyruvate, β -hydroxybutyrate), components of membranes (glycerol and choline), and an oxidative stress marker (isoprostane). β -hydroxybutyrate (BHB) is an alternative energy substrate produced by the liver which can be converted to acetyl-Co A in brain mitochondria to feed the TCA cycle. During glucose hypometabolism, some changes in the BHB level are expected.

The key questions in this study are:

1. Does icv-STZ cause toxicity in the hippocampus? While it has been known that STZ toxicity in the pancreas is mediated by GLUT2, the brain itself lacks GLUT2. To confirm icv-STZ toxicity and to connect this study to the literature, histology studies were performed. GFAP and Fluoro-Jade staining were done because many previous studies reported gliosis and neurodegeneration in this model.
2. Does icv-STZ affect mitochondrial respiratory function in the hippocampus? The mitochondrion is an organelle that plays an important role in normal brain function. Impairment of mitochondrial respiratory function indicates mitochondrial defects which may explain the mechanism of icv-STZ toxicity. Some studies have reported mitochondrial impairment in this model. However, a complete picture of mitochondrial complex activities is lacking.
3. Is the toxic effect of icv-STZ brain region-specific? As AD brains showed brain region-specific impairment, a good AD model should also possess similar brain region-specific changes. Therefore, icv-STZ toxicity on mitochondria was also evaluated in the striatum. The following key questions were also answered by investigating changes in both the hippocampus and striatum.
4. Does icv-STZ toxicity affect cholinergic markers (ChAT, AChE, CHT-1) in the hippocampus and striatum? Extensive literature reported only ChAT, AChE, or VACHT which does not correlate well with ACh level. To answer this question, their activities were measured in homogenates or, in the case of CHT-1, in the P2 fraction containing synaptosomes.

5. Which changes take place in the extracellular space of the hippocampus and striatum during behavioral and pharmacological stimulation? Microdialysate samples were collected during the stimulations and the following substances were measured.
- a. ACh as cholinergic transmission marker was measured by high-performance liquid chromatography/electrochemical detection (HPLC/ECD).
 - b. Glucose and its metabolites, lactate and pyruvate, were measured by a microanalyzer (CMA 600).
 - c. β -hydroxybutyrate (BHB) as an alternative energy metabolite was measured by gas chromatography/mass spectrophotometry (GC/MS).
 - d. Glycerol and choline as markers for membrane damage were measured by a microanalyzer (CMA 600) and HPLC/ECD, respectively.
 - e. Isoprostane as an oxidative stress marker was measured by ELISA.

2 Materials and Methods

2.1 Materials

All organic solvents, chemicals and reagents used in the experiments were of analytical or highest purity grade available. Most were purchased from Sigma-Aldrich Chemical Company (St. Louis Missouri, USA), Merck (Darmstadt, Germany) and other leading suppliers. Lists of instruments, chemicals, supporting materials, drugs and their sources are given in the following tables.

Table 2. 1. List of equipments

| Equipment | Source |
|--|--|
| Analytical balance (AT261 Delta Range) | Mettler, Giessen, Germany |
| Anesthesia adapter (Rat) | Harvard apparatus, USA |
| Anesthetic vaporizer | Kent Scientific, Toorington, CT, USA |
| Autosampler GC-MS (7683 Series Injector) | Agilent, Santa Clara, CA, USA |
| Autosampler HPLC (SIL-20AC) | Shimadzu Europa GmbH, Duisburg, Germany |
| Block Heater BH 602T | Maple Scientific, Staffordshire, UK |
| Camera Microscope Nikon DS-Qi2 | Nikon GmbH, Dusseldorf, Germany |
| Capillary column (VF-5ms EZ-Guars) | Agilent, Santa Clara, CA, USA |
| Centrifuge (Heraeus Fresco 21) | Thermo Scientific, Braunschweig, Germany |
| Centrifuge (Sigma 1-14) | Vertrieb novodirect, Kehl, Germany |
| CMA 120 Plastic Bowl | Harvard Bioscience, USA |
| CMA 600 | CMA Microdialysis AB, Solna, Sweden |
| Cold light lamp PL 2000 | Carl Roth, Karlsruhe, Germany |
| Cryostat CryostarNX50 | Thermo Fisher Scientific, Waltham, USA |
| Diaphragm pump GC-MS | Agilent, Santa Clara, CA, USA |
| Electrochemical detector (platinum electrode WE-PT, reference electrode RE-500) | Eicom, San Diego, CA, USA |
| Evaporator (Sample Concentrator BC 301) | Maple Scientific, Staffordshire, UK |
| GC-MS (HP 6890) | Agilent, Santa Clara, CA, USA |
| Glass cuvette Quartz Suprasil® | Helma, Germany |
| Homeothermic Monitoring System | Harvard Apparatus, Holliston, MA, USA |
| Hot glue Gluematic 3002 | Steinel, Herzbrock-Clarholz, Germany |
| Hot plate magnetic stirrer | IKA Combimag RCT, Staufen, Germany |
| HPLC column (Eicompac AC-Gel) | Eicom, San Diego, CA, USA |
| HPLC enzyme reactor (AC-ENZYM II-3) | Eicom, San Diego, CA, USA |
| HPLC HTEC-500 | Eicom, San Diego, CA, USA |
| HPLC precolumn (PC-03) | Eicom, San Diego, CA, USA |
| Microscope Nikon Eclipse Ni-U (Objective : 4x Plan Fluor and 20x Plan Apo λ) | Nikon GmbH, Dusseldorf, Germany |
| Microscope filter: TRITC, FITC-3540C-000 Brightline Filterset | Semrock, New York, USA |

| Equipment | Source |
|---|---|
| Microscope light Intensilight C-HGFI | Nikon GmbH, Dusseldorf, Germany |
| Millipore water purification system | Millipore, Schwalbach, Germany |
| Motor handpiece (MHX/E) | Xenox, Niersbach, Germany |
| Multipette® M4 | Eppendorf, Wesseling-Berzdorf, Germany |
| Oxygraph-2K (Oroboros®) | Oroboros instruments, Austria |
| pH-Meter | Mettler Toledo, Gießen, Germany |
| Pipette Labmate Pro | HTL, Warschau, Poland |
| Pipette Transferpette® -8/-12 | Brand, Wertheim, Germany |
| Potter S Homogenizer | B. Braun, Melsungen, Germany |
| Quadrupole mass spectrometer (5973 Network mass selective detector) | Agilent, Santa Clara, CA, USA |
| Scintillation counter (Victor Wallac 1420) | Perkin Elmer, Rodgau, Germany |
| Scintillation tube Minis2000 | Zinsser Analytic, Frankfurt, Germany |
| Shakers IKA-Vibrax-VXR electronic | Staufen, Germany |
| Spectrophotometer (Victor X Multilabel Plate Reader) | Perkin Elmer, Rodgau, Germany |
| Spectrophotometer Spectronic® | Spectroline, USA |
| Stereotaxic instruments | Stoelting, Chicago, IL, USA |
| Syringe (Hamilton 1001 RN) | Sigma-Aldrich, Munich, Germany |
| Syringe (Hamilton 1701A SN) | Sigma-Aldrich, Munich, Germany |
| Syringe pump (KDS 200) | KD Scientific, Holliston, MA, USA |
| Syringe 5 µL (Agilent) | Agilent, California, USA |
| Tissue chopper (McIlwain Tissue Chopper) | MickleLab, Guildford, UK |
| Trepan 224 018 HP | Hager und Meisinger, Neuss, Germany |
| Ultrasonic bath (Elmasonic S 30 H) | Elma Schmidtbauer, Singen, Germany |
| Vortex Heidolph Reaxtop | Heidolph Instruments, Schwalbach, Germany |
| Water bath (Julabo EM) | Julabo, Seelbach, Germany |

Table 2. 2. List of chemicals and solvents

| Chemicals/Solvents | Source |
|--------------------------------------|---|
| [³ H]-Acetyl-coenzym A | American Radiolabeled Chemicals, St. Louis, USA |
| [³ H]-Cholin | American Radiolabeled Chemicals, St. Louis, USA |
| 5,5'-Dithiobis-(2-Nitrobenzoic acid) | Sigma-Aldrich, Munich, Germany |
| Acetic acid 100% | Merck, Darmstadt, Germany |
| Aceton | Merck, Darmstadt, Germany |
| Acetonitril | Merck, Darmstadt, Germany |
| Acetyl CoA (acetyl coenzyme A) | Sigma-Aldrich, Germany |
| Acetylcholinesterase | Sigma-Aldrich, Munich, Germany |
| Acetylcholine perchlorate | Sigma-Aldrich, Munich, Germany |
| Acetylthiocholine iodide | Sigma-Aldrich, Munich, Germany |
| Adenosine diphosphate | Sigma-Aldrich, Germany |

| Chemicals/Solvents | Source |
|---|-------------------------------------|
| Albumin (Bovine Serum) | Sigma-Aldrich, Munich, Germany |
| Albumin, IgG-frei | Carl Roth GmbH & Co, Germany |
| Antimycin A | Sigma-Aldrich, Germany |
| Argon gas | Praxair, Düsseldorf, Germany |
| Ascorbate sodium salt | Sigma-Aldrich, Munich, Germany |
| Bovine serum albumin, essentially fatty acid free | Sigma-Aldrich, Germany |
| Butyrylthiocholine | Sigma-Aldrich, Munich, Germany |
| Calcium chloride | Merck, Darmstadt, Germany |
| Carbogen | Praxair, Düsseldorf, Germany |
| Carbonilcyanide <i>p</i> -trifluoromethoxyphenylhydrazone (FCCP) | Sigma-Aldrich, Germany |
| Choline chloride | Sigma-Aldrich, Munich, Germany |
| Citrate synthase from porcine heart | Sigma-Aldrich, Germany |
| CMA 600 Calibrator | CMA Microdialysis AB, Solna, Sweden |
| CMA 600 Reagent | CMA Microdialysis AB, Solna, Sweden |
| Coomassie® Brilliant blue | Biorad, Germany |
| Cryomedium (Tissue-Tek® O.C.T.®) | Sakura Finetek, Germany |
| Cytochrome c from equine heart | Sigma-Aldrich, Germany |
| Dipotassiumhydrogenphosphate | Merck, Darmstadt, Germany |
| Disodiumhydrogenphosphate | Merck, Darmstadt, Germany |
| D-Sucrose | Sigma-Aldrich, Germany |
| DTNB (5,5'-Dithiobis(2-nitrobenzoic acid)) | Sigma-Aldrich, Germany |
| EDTA-2-Sodium | Carl Roth, Karlsruhe, Germany |
| EGTA (ethylene glycol-bis(β-aminoethyl ether)-N,N,N',N'-tetraacetic acid) | Sigma-Aldrich, Germany |
| Epinephrine (Suprarenin®) | Sanofi, France |
| Ethanol 96% | Merck, Darmstadt, Germany |
| Fast-Green FCF | Sigma-Aldrich, Munich, Germany |
| Fluoro-Jade C | Merck, Darmstadt, Germany |
| Fluoromount G | Southern Biotech, UK |
| Glucose | Merck, Darmstadt, Germany |
| Helium gas | Praxair, Düsseldorf, Germany |
| Hemicholinium-3 | Sigma-Aldrich, Munich, Germany |
| HEPES | Sigma-Aldrich, Germany |
| HEPES-Natrium | Alfa Aesar, USA |
| Hydrochloric acid solution 1N | Merck, Darmstadt, Germany |
| Isoflurane® | Abbott, Wiesbaden, Germany |
| Lactobionic acid | Sigma-Aldrich, Germany |
| L-Malic acid | Sigma-Aldrich, Germany |
| Magnesium chloride | Merck, Darmstadt, Germany |
| Magnesium sulfate | Sigma-Aldrich, Munich, Germany |
| Methanol | Carl Roth, Karlsruhe, Germany |
| N,O-Bis(trimethylsilyl)trifluoroacetamide | Sigma-Aldrich, Munich, Germany |
| Neostigmine bromide | Acros Organics, Geel, Belgium |

| Chemicals/Solvents | Source |
|--|----------------------------------|
| Nitrogen gas | Praxair, Düsseldorf, Germany |
| Oligomycin | Sigma-Aldrich, Germany |
| Oxalacetic acid | Sigma-Aldrich, Germany |
| Paraformaldehyde | Merck, Germany |
| Potassium chloride | Merck, Darmstadt, Germany |
| Potassium dihydrogen phosphate | Merck, Darmstadt, Germany |
| Potassium hydrogen carbonate | Merck, Darmstadt, Germany |
| Potassium hydroxide | Sigma-Aldrich, Germany |
| Protease inhibitor cocktail | Roche, Switzerland |
| Pyridine | Sigma-Aldrich, Munich, Germany |
| Pyruvic acid sodium salt | Sigma-Aldrich, Germany |
| Rotenone | Sigma-Aldrich, Germany |
| Roti®-Liquid Barrier Marker | Carl Roth, Karlsruhe, Germany |
| RotisolV® HPLC Gradient Grade Water | Carl Roth, Karlsruhe, Germany |
| Scintillation liquid Irga-Safe | Perkin Elmer, Rodgau, Germany |
| Scopolamine bromide | TCI Europe, Zwijndrecht, Belgium |
| Sodium-1-decansulfonate | Merck, Darmstadt, Germany |
| Sodium 3-hydroxybutyrate | Sigma-Aldrich, Munich, Germany |
| Sodium azide | Sigma-Aldrich, Germany |
| Sodium chloride | Merck, Darmstadt, Germany |
| Sodium dihydrogenphosphate | Merck, Darmstadt, Germany |
| Sodium hydrogencarbonate | Merck, Darmstadt, Germany |
| Sodium hydrogenphosphate | Merck, Darmstadt, Germany |
| Sodium hydroxide 0.1 M | Merck, Darmstadt, Germany |
| Sodium hydroxide pellet | Merck, Darmstadt, Germany |
| Sodium lactate | Sigma-Aldrich, Munich, Germany |
| Sodium phosphate | Merck, Darmstadt, Germany |
| Sodium salicylate | Sigma-Aldrich, Munich, Germany |
| Sodium tetraphenylborate | Sigma-Aldrich, Munich, Germany |
| Sterile saline solution | B. Braun, Melsungen, Germany |
| Succinate disodium salt | Sigma-Aldrich, Germany |
| Sucrose | Merck, Darmstadt, Germany |
| Sudan black B | Sigma-Aldrich, Germany |
| Synthetic air (21% O ₂ , 79% N ₂) | Air Liquide, Düsseldorf, Germany |
| Taurine | Sigma-Aldrich, Germany |
| Tetraisopropylpyrophosphamide (iso-OMPA) | Sigma-Aldrich, Munich, Germany |
| Tetramethyl-p-phenylenediamine dihydrochloride (TMPD) | Sigma-Aldrich, Germany |
| Toluol | Merck, Darmstadt, Germany |
| Triethanolamine | Sigma-Aldrich, Germany |
| Trimethylsilylchloride | Sigma-Aldrich, Munich, Germany |
| Tris(hydroxymethyl) aminomethane | Sigma-Aldrich, Germany |
| Triton X-100 | Sigma-Aldrich, Germany |

| Chemicals/Solvents | Source |
|------------------------------------|--------------------------------------|
| Ultra pure water (Millipore Water) | Merck Millipore, Schwalbach, Germany |
| Water for injection | Fresenius Kabi, Bad Homburg, Germany |

Table 2. 3. List of supporting materials and tools

| Products | Source |
|---|---|
| Adhesive primer (Multilink A/B) | Ivoclar Vivadent, Liechtenstein |
| Alcohol swabs | B. Braun, Melsungen, Germany |
| Bupivacain-Gel | Local pharmacy, Germany |
| Canula Sterican® (25G, 0.9 x 4 mm) | B. Braun, Melsungen, Germany |
| Cryomold Sakura biopsy | Sakura Finetek, Germany |
| Cyanoacrylate super gel glue UHU | UHU, Germany |
| Dental cement PermaCem Smartmix Dual | DMG, Hamburg, Germany |
| Dialysis membrane FXC or Diax 600 (Polysulfone, cut off: 30 kDa) | Fresenius Medical Care, Germany |
| Disposable needle | B. Braun, Melsungen, Germany |
| Disposable syringes | B. Braun, Melsungen, Germany |
| Disposable tips | Greiner Bio One, Germany |
| Disposable weighing bowls | Carl Roth, Karlsruhe, Germany |
| Drill bit (224RF018) | Meisinger, Germany |
| Epoxy glue | Sunchrom, Germany |
| Eppendorf tube | Greiner Bio-One, Frickenhausen, Germany |
| Eppendorf tubes (0.65, 1.5, 2.0 ml) | B. Braun, Melsungen, Germany |
| Eye ointment Bepanthen® | Bayer, Leverkusen, Germany |
| Fused Silica Capillary Tubing (0.074 mm ID) | Polymicro Technologies, USA |
| Guillotine for rats and guinea pigs | Hugo Sachs, Germany |
| Hamilton gastight syringes (1ml) | Hamilton Company, USA |
| Microscope cover slip 24x60mm | Carl Roth, Karlsruhe, Germany |
| Microscope slide 24x60mm (Thermo Scientific™ SuperFrostPlus™ Adhesion slides) | Thermo Fisher Scientific, Waltham, USA |
| Polyethylene tube SX01 (ID: 0.28 mm, AD: 0.61 mm) | A. Hartenstein, Würzburg, Germany |
| Polyethylene tube SX02 (ID: 0.38 mm, AD: 1.29 mm) | A. Hartenstein, Würzburg, Germany |
| Polyethylene tube Tygon ST R3607 (ID: 0.38 mm, AD: 1.29 mm) | Ismatec, Wertheim-Mondfeld, Germany |
| Polyethylene tube Tygon ST R3607 (ID: 0.76 mm, AD: 1.62 mm) | Ismatec, Wertheim-Mondfeld, D |
| Q-tips cotton | DM store, Germany |
| Razor blade | Wilkinson Sword, Solingen, Germany |
| Super plastic glue with activator (Pattex) | Henkel AG, Germany |
| Surgical tools | Fine Science Tools, Heidelberg, Germany |
| Suture clips (Michel) | B. Braun (Aesculap), Melsungen, Germany |

| Products | Source |
|--------------------------|-------------------------------|
| Vials and Inlets (GC-MS) | Agilent, Santa Clara, CA, USA |

Table 2. 4. Kits Used

| Kit | Source |
|--|----------------------|
| 8-Isoprostane express EIA kit [®] | Cayman Chemical, USA |

Table 2. 5. Primary Antibody Used

| Primary Antibody | IHC Dilution | Species | Catalog No., Source |
|-------------------------|---------------------|----------------|----------------------------|
| GFAP | 1:1000 | rabbit | Z0334, Dako, Denmark |

Table 2. 6. Secondary Antibody Used

| Secondary Antibody | IHC Dilution | Species | Catalog No., Source |
|---------------------------|---------------------|----------------|--------------------------------|
| Anti-rabbit AF555 | 1:500 | Goat, IgG | A21429, Life Technologies, USA |

2.2 Buffers and solutions

Acetic acid solution 0.1%

0.1% acetic acid in milliQ water

Acetyl-CoA (12.2 mM)

25 mg acetyl CoA + 2.5 ml milliQ water

aCSF

147 mM NaCl

2.7 mM KCl

1.2 mM MgCl₂

1.2 mM CaCl₂

5,5'-Dithiobis (2-nitrobenzoic acid) (1.01 mM)

pH=8.1

2 mg DTNB + 5 ml of 1 M Tris-HCl-buffer of pH 8.1.

Fluoro-Jade C stock solution 0.01%

0.01% Fluoro-Jade C in milliQ water (protect from light)

Fluoro-Jade C working solution 0.0001%

600 µL Fluoro-Jade C stock solution in 60 mL acetic acid solution

Hepes sucrose buffer

Sucrose 320 mM

Hepes sodium 10 mM

KMnO₄ 0.06 %

0.06 % KMnO₄ in milliQ water

Mitochondrial respiratory medium (MiR05, Oroboros®)

pH= 7.1

0.5 mM EGTA

3 mM MgCl₂

60 mM Lactobionic acid

20 mM Taurine

10 mM KH₂PO₄

20 mM HEPES

110 mM D-Sucrose

1g/l Bovine serum albumin, essentially fatty acid free

Oxalacetate (10 mM)

pH= 8.0

6.6 mg oxalacetate + 5 ml of 0.1 M triethanolamine-HCl-buffer of pH 8.0.

Paraformaldehyde (PFA) solution 4%

pH= 7.4

4% Paraformaldehyde in PBS

PBS-Triton (PBST)

0.1 % Triton X-100 in PBS

Phosphate buffer saline (PBS)

pH= 7.4

137 mM NaCl

2.7 mM KCl

8.1 mM NaH₂PO₄

1.8 mM KH₂PO₄

Triethanolamine-HCl-buffer (0.1 M)

pH= 8.0

1 ml of 0.5 M triethanolamine-HCl-buffer of pH 8.0 + 4 ml milliQ water

Triethanolamine-HCl buffer (0.5 M, pH 8.0) + EDTA (5 mM)

8.06 g triethanolamine/100 ml milliQ water (adjust pH)

186.1 mg EDTA

Tris-HCl buffer (1.0 M,)

pH= 8.1

2.4228 g Tris/20 ml milliQ water

Tris-HCl buffer (0.1 M)

pH=7.0

2 ml 1M Tris-HCl buffer, pH 8.1+ 20 ml milliQ water

Triton X-100 (10% solution)

10 g Triton X-100

add 90 ml milliQ water

2.3 Experimental animals

Icv-STZ induced brain injury was induced in male Wistar rats of 190-220 g body weight (5 weeks of age) (Janvier Labs, Le Geneste St. Isle, France). Animals were housed in a controlled room (22°C, 50%– 65% humidity; day/night cycle of 12/12 h) with free access to water and standard laboratory diet (65% carbohydrates, 24% protein, and 11% fat; Altromin[®], Germany). After 7 days of acclimatization, they were randomly divided into 2 or 3 groups for treatments.

After weighing, they were anesthetized with isoflurane (5% induction and 2% maintenance in synthetic air). Deep anesthesia was confirmed by checking the intradigital reflex. Then, the skull was immobilized by placing an ear bar and Bepanthen[®] was applied on both eyes for lubrication. Next, alcohol swab was used to disinfect the scalp in the area of surgery. After that, sagittal incision was made starting from middle of both eyes to middle of both ears to expose the pericranium. Bupivacain was applied as a long lasting local anesthesia and then the skull was scraped. The bleeding was controlled by applying cotton bud. After the bleeding stopped and the skull was dry, a small hole was made in the skull by a dental drill at lateral ventricle

coordinate (from bregma AP: -0.8; L: ± 1.5 ;DV: -3.6) according to a rat brain atlas (Paxinos and Watson,1998) and confirmed later with fast green injection.

Next, STZ was prepared freshly and protected from light. The treated group received high dose of STZ (1.5 mg/kg in WFI, 5 μ l) or low dose of STZ (0.6 mg/kg in saline solution, 5 μ l) while the control group received saline solution. A 5 μ l Hamilton syringe (Agilent PART #5182-0836) was used to administer the compound with a rate of 1 μ l/ min into the brain lateral ventricle. Three days later, the high dose group received one more icv STZ (1.5 mg/kg in WFI, 5 μ l) while the control group received saline solution. After icv injection, the hole was closed with dental cement and the skin incision was closed with suture clip. Animal health status were recorded and body weights were checked twice a week until the end of the study (day 21 after icv STZ). All the experiments were done in accordance with the guidelines by regional ethical committee (Regierungspräsidium Darmstadt, Germany (FR/1005)).

It should be noted that initial experiments used 0.6 mg/kg and 3 mg/kg STZ as doses for icv injection. Due to mortality associated with 3 mg/kg icv-STZ, the dose was split as described above, and mortality was avoided. The results of the early experiments were not used in the present thesis.

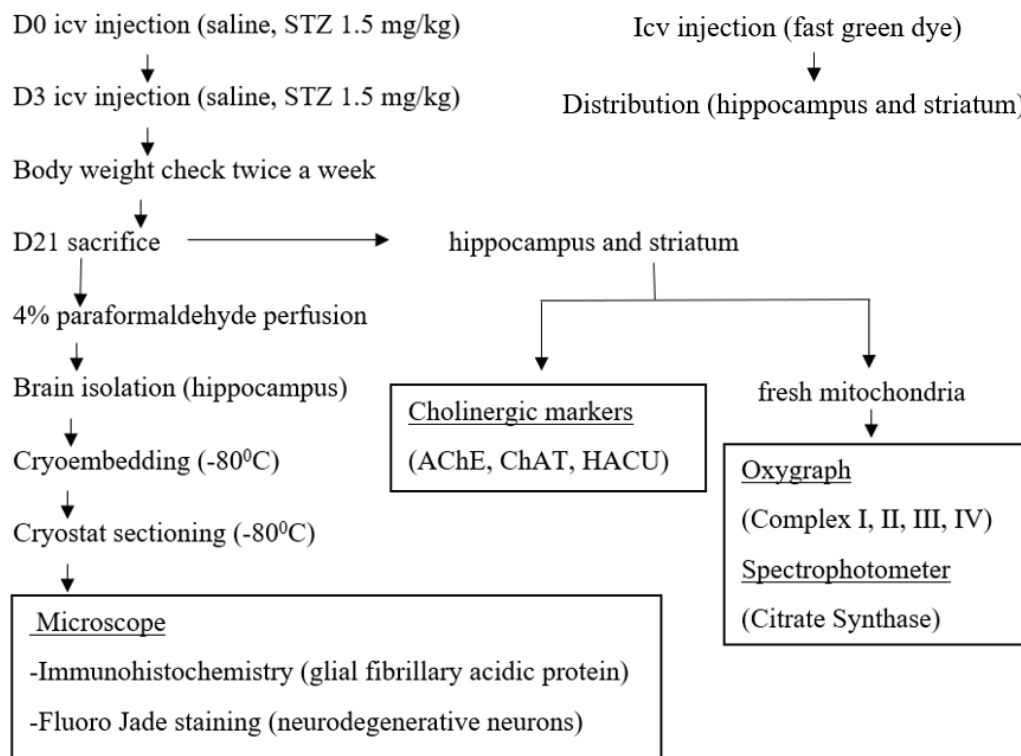


Figure 2. 1. Flow diagram of the histology, mitochondrial respiration and cholinergic marker studies.

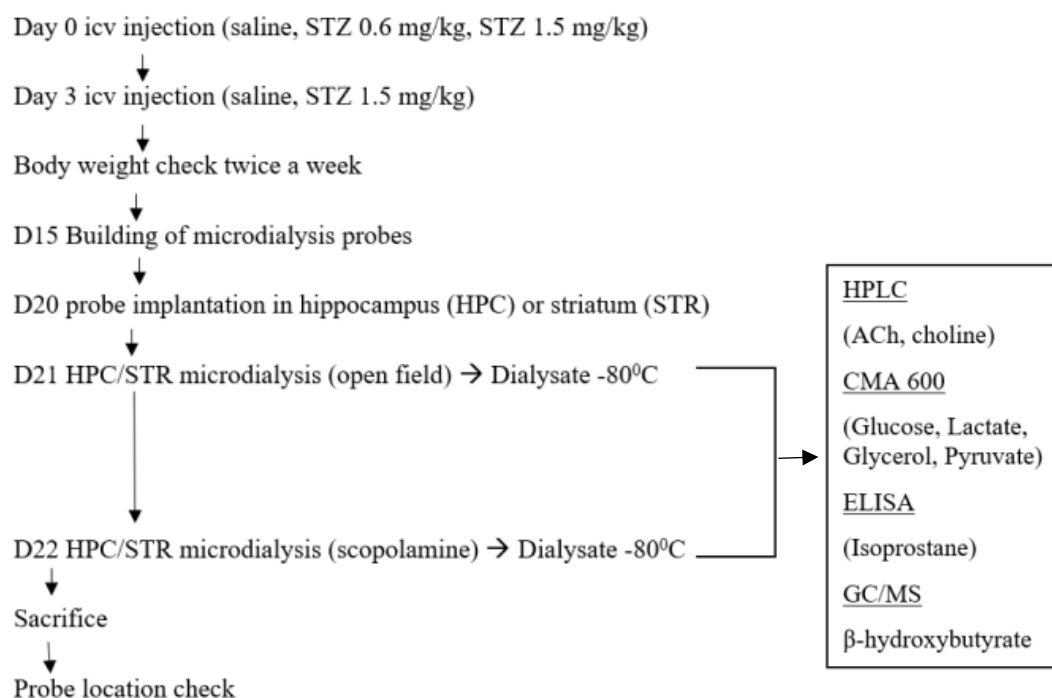


Figure 2. 2. Flow diagram of microdialysis study

2.4 Sample collection

After 21 days, either the rats were sacrificed or microdialysis study was performed to collect samples for cholinergic or metabolic markers from hippocampus and striatum. After microdialysis study was done, the rats were sacrificed followed by probe location confirmation.

For histology study, the rats were sacrificed with i.p. injection of ketamine (2x80 mg/kg) and xylazine (2x10 mg/kg) and transaortically perfused with 500 mL 4°C saline and 400 mL 4% PFA in PBS through the ascending aorta as described by Gerfen (1997). The brain was taken out and a 3 mm coronal section of each hemisphere were made. Next, postfixation was done by immersing the section for 4 hours in 15 mL 4% PFA in PBS at room temperature. Then, sucrose infiltration was done by replacing 4% PFA in PBS with 20% sucrose in PBS (4°C) overnight until the section sunk. The next day, the section was transferred into embedding media (Tissue-Tek OCT® compound) in a cryomold followed by alufoil wrapping and on dry ice freezing. Finally, all the samples were kept at -80°C until cryosectioning. Cryostat sections of 14 µm thickness were made at -20°C followed by 1.5 hours air drying. Then, the air-dried sections were kept at -80°C until staining.

While homogenates for mitochondrial respiratory function determination were prepared freshly, homogenates for cholinergic marker study (AChE, ChAT, and HACU) were kept at -80°C before measurement. Based on König (2019), after sacrifice under isoflurane, isolated hippocampus (HPC) and striatum (STR) were homogenized quickly in HEPES/sucrose buffer (1g/mL) using Potter homogenizer (B. Braun) at 1,000 rpm and 15 strokes. Then, aliquots of 60 μL were kept in -80°C for acetylcholinesterase (AChE) and choline acetyltransferase (ChAT) activity measurement. For high affinity choline uptake (HACU), P2 fraction from 1000 μL homogenate was prepared by multiple step centrifugation as follows:

1. 1,000 x g, 10 min, 4°C \rightarrow collect 700 μL supernatant (discard sediment)
2. 17,000 x g, 10 min, 4°C \rightarrow collect sediment
3. Resuspend pellet with 0.5 ml of HEPES/Sucrose buffer
4. This P2 fraction was kept in -80°C

2.5 Histology study

2.5.1 Fluoro-Jade staining

Fluoro-Jade C staining was performed based on Schmued et al. (2005). After at least 1 night at -80°C , sections containing hippocampus (HPC) were air dried for 30 minutes at room temperature (RT). All reagents were prepared freshly except the stock solution of Fluoro-Jade C and ethanol 70%. Air dried sections were then soaked in 70% ethanol for 3 min followed by washing in milliQ water for 3x1 min. The next steps were performed in the dark. The sections were soaked in 0.06% KMNO_4 for 15 min followed by washing in milliQ water for 3x1 min. After that, the sections were stained with 0.0001% Fluoro-Jade C in 0.1% acetic acid for 15 min followed by washing in milliQ water for 3x1 min. Finally, the sections were allowed to air dry over night at room temperature. The next day, the sections were soaked in xylene for 3 min followed by coverslipping with DPX and then allowed to air dry at RT.

2.5.2 Immunohistochemistry of glial fibrillary acidic protein (GFAP)

Reactive gliosis was investigated using GFAP staining according to Kallenborn-Gerhardt et al. (2014). After at least 1 night in -80°C , sections were allowed to dry at room temperature (RT). Then, grease pencil was used to encircle the section. After the grease was dry, the sections were immersed in PBS in a staining jar for 3x10 min on a shaker for washing. Next, the sections were permeabilized using PBST (0.1% Triton X-100 in PBS) for 5 min and blocked using 10% normal goat serum in 3% BSA in PBS for 60 min at RT. Then, the sections were incubated

with the first primary antibody in 3% BSA in PBS overnight at 4°C. The next day, after washing in PBS for 3x10 min, the sections were incubated with secondary antibody in PBS for 2 hours in the dark. The next steps were also in the dark. After 3x10 min washing with PBS, the sections were quenched with 0.06% Sudan black for 5 min at RT followed by 3x5 min washing with PBS. After coverslipping with Fluoromount G, the sections were kept in 4°C in the dark until dry.

2.5.3 Microscopic evaluation

Fluorescence signal was detected using a FITC (Fluorescein isothiocyanate) filter for Fluoro-Jade C and TRITC (Tetramethylrhodamine isothiocyanate) filter for GFAP. Pictures were processed by Nikon software NIS-Elements and combined by Adobe Photoshop CS.

2.6 Mitochondrial respiration study

2.6.1 Isolation of mitochondria from hippocampus and striatum

Isolation of mitochondria was carried out based on Imran et al. (2015) with modifications. After washing in cold PBS, freshly isolated hippocampi (HPC) and striata (STR) were weighed and quickly transferred into Potter vessel. The vessel previously was filled with 2 mL MiR05 medium containing protease inhibitors (MiR05-PI). Homogenization was done at 1,000 rpm with 15 strokes. Until this step, 4 tubes of homogenate (control and treated rats @ 2 tube for HPC and STR) were collected. The next step is multiple centrifugation for washing and isolating mitochondria.

1. 1,400 x g, 7 min, 4° C → collect supernatant (discard sediment)
2. 1,400 x g, 3 min, 4° C → collect supernatant (discard sediment)
3. 10,000 x g, 5 min, 4° C → collect pellet (discard supernatant)
4. resuspend pellet with 1 ml MiR05
5. 1,400 x g, 3 min, 4° C → collect supernatant (discard sediment)
6. 10,000 x g, 5 min, 4° C → collect pellet (discard supernatant)
7. resuspend mitochondrial pellet with 0.5 ml of MiR05 medium
8. Isolated mitochondria were kept on ice until use

An aliquot of mitochondrial suspension was kept frozen at -80°C for the citrate synthase activity determination. The other materials (substrates, inhibitors and uncoupler) were kept on ice until used.

2.6.2 Mitochondrial respiratory measurement

First, Oroboros Oxygraph[®] (O2K) chambers were filled with 2 ml of MiR05 medium and set at 37°C with 750 rpm stirrer speed. Then, oxygen in the air was allowed to saturate the medium by positioning the O2K stopper loosely. After saturation, the O2K stoppers were positioned tightly and calibration was done. Next, 80 µl of isolated mitochondria was injected directly into the chamber (i.e. chamber A control, chamber B treated). Finally, the activities of each complexes of electron transport chain (ETC) and maximum capacity of ETC were measured by adding specific substrates, inhibitors and uncoupler into the chamber subsequently as follows.

1. Pyruvate (5 mM) and malate (2 mM)

Leak respiration (Leak-I) was detected as a results of proton diffusion accros the membrane.

2. ADP (2 mM)

In the presence of pyruvate (5 mM) and malate (2 mM), complex I respiration was detected and proton gradient was restored as a result of complex V activation.

3. Succinate (10 mM)

Complex I and II respiration or maximum physiological respiration were detected as substrates for all the complexes were present.

4. Cytochrom C (10 µM)

Mitochondrial integrity was detected. If loss of cytochrome C had occurred during mitochondria isolation procedure, cytochrome C addition would restore the integrity of mitochondria.

5. Oligomycin (2 µg/ml)

Leak-II was detected because oligomycin inhibits ATP synthase (complex V) and proton diffusion occured.

6. FCCP (titrated in 0.5 µM aliquots stepwise until maximum respiration)

Maximum uncoupled respiration was detected because of maximum electron transfer through the ETC to complex IV. Addition of FCCP (carbonilcyanide *p*-triflouromethoxyphenylhydrazone), a protonophore, leads to proton diffusion accros the membran. Therefore, high proton gradient is never achieved to slow the electron transfer (Divakaruni et al., 2014).

7. Rotenone (0.5 µM)

Complex II respiration was detected because rotenone inhibits complex I.

8. Antimycin-A

Non-mitochondrial respiration was detected. Antimycin-A inhibits complex III and leads to blockage of mitochondrial respiration.

9. TMPD (0.5 mM) and ascorbic acid (2 mM)

Non-physiological respiration of only complex IV was detected. Reduced state of TMPD (tetramethyl-p-phenylenediamine dihydrochloride) by the help of ascorbic acid supplies electrons to complex IV.

10. Sodium azide (100 mM)

Autooxidation was detected because sodium azide blocks the complex IV.

Because oxygen levels in the chamber decreased during mitochondrial respiration, reoxygenation of the chamber was done by opening the stopper after addition of oligomycin, antimycin A and TMPD/ascorbate.

2.6.3 Citrate synthase activity

Citrate synthase (CS) is the rate-limiting enzyme in the citric acid cycle and is commonly used as a quantitative marker of mitochondria (Larsen et al., 2012; Pohland et al., 2018). In pathological states, increased CS activity per cell sometimes is associated with increased mitochondrial proliferation.(Eigentler et al., 2015). CS activity was determined by colorimetric assay based on 5-thio-2-nitrobenzoic acid (TNB) production as a result of the reaction between the 5',5'-dithiobis 2-nitrobenzoic acid (DTNB) and CoA-SH. The rate of increase of the absorbance is proportional to enzyme activity.

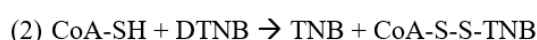
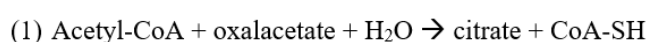


Figure 2. 3. Citrate synthase-catalyzed reaction coupled with DTNB (irreversible reaction).

For CS activity determination, first, mitochondrial samples were thawed on ice while preparing the incubation medium for the reaction. The medium consisted of 795 μL Milli-Q water, 100 μL DTNB, 25 μL Triton X-100 (10%), 50 μL oxalacetate, and 25 μL acetyl-CoA. After the medium was incubated for 5 min in a water bath (30⁰C), 5 μL of mitochondria sample or diluted CS standard was added into the medium and quickly transferred into a quartz cuvette. The rate of increase of the absorbance (the slope) was measured on a spectrophotometer at 412 nm using a kinetic program. The slope had to be linear for 200s. CS standard (Sigma) was used for quality control of the reagent and assay conditions. CS standards were diluted 500 times in 0.1 M Tris-HCl buffer pH 7.0.

2.7 Cholinergic marker study

2.7.1 Protein level determination

All cholinergic markers (AChE, ChAT, and HACU) were normalized to protein level. Bradford method was used for protein level determination based on colorimetry. The Bradford dye, a triphenylmethane dye (Coomassie Brilliant Blue G250, CBBG) is present as a cation and has a red-brown color with a maximum absorption at 470 nm. After binding to arginyl and lysyl side chains of protein in acidic solution, the complex results in a stable, anionic blue color with a maximum absorption at 595 nm (Bradford, 1976). Standard curve was made using albumin (BAS-RIA Grade, Fraction V, minimum 96%, Sigma-Aldrich) diluted with Milli-Q water (Table 7).

Table 2. 7. Albumin concentration for the standard curve

| Albumin concentration | | | | | |
|------------------------------|---------|----------|----------|----------|----------|
| 0.5 µg/mL | 5 µg/mL | 10 µg/mL | 15 µg/mL | 20 µg/mL | 25 µg/mL |

After thawing on ice, the samples were shaken briefly and diluted in Milli-Q water 1:10. Then, 50 µL of each sample were pipetted in triplicate into a 96-well plate and 200 µL of Bradford solution (BioRad Protein Assay; with Milli-Q 1:4) were added. The color measurement was carried out using Wallac 1420 Explorer at 570 nm.

2.7.2 Acetylcholinesterase activity

Acetylcholinesterase activity was measured based on hydrolysis of acetylthiocholine using photometric method (Ellman et al., 1961). Triton X-100 in PBS solution was used to permeabilize the membranes and release AChE. Acetylthiocholine (ATC) was used as the substrate of AChE while butyrylcholinesterase was blocked by iso-OMPA (König et al., 2019). The thiocholine product then reacted with 5,5'-dithiobis-2-nitrobenzoic acid (DTNB) producing a yellow 2-nitro-5-thiobenzoate anion (Figure 3.14) that was then measured at 412 nm by a photometer. As a standard, commercially available AChE (Sigma-Aldrich) ranging from 0-1 U/mL in 0.5% Triton X-100/PBS was used (Table 8).

Table 2. 8. Acetylcholinesterase concentration for standard curve

| Acetylcholinesterase-Concentration | | | | | |
|---|-----------|----------|-----------|----------|--------|
| 1 u/mL | 0.75 u/mL | 0.5 u/mL | 0.25 u/mL | 0.1 u/mL | 0 u/mL |

After thawing on ice and shaken briefly, 45 μL homogenate in HEPES/sucrose buffer was treated with 5 μL of 5% Triton-X followed by 10s vortex and centrifugation at 12,000 g and 4°C for 10 minutes. Then, 10 μL of the supernatant (n=2) was mixed with 40 μL of 0.5% Triton X-100/PBS solution. Meanwhile, a cooled 96-well microplate was filled with @ 65 μL Ellman buffer (0.1 M NaH_2PO_4 , 0.1 M Na_2HPO_4 , pH 8) and 25 μL of 800 μM iso-OMPA solution. Then, 10 μL sample or standard (n=3) was added into each well. The rest of the sample was kept for Bradford protein determination. Next, 1.5 mL of 20 mM ATC solution was mixed with 1.5 mL of 10 mM DTNB solution and 12 mL of Ellman buffer. Finally, 100 μL of the freshly prepared solution was added into each well with multichannel pipette. The reaction kinetic was measured by Wallac 1420 Explorer at 412 nm (20 times for 20 seconds).

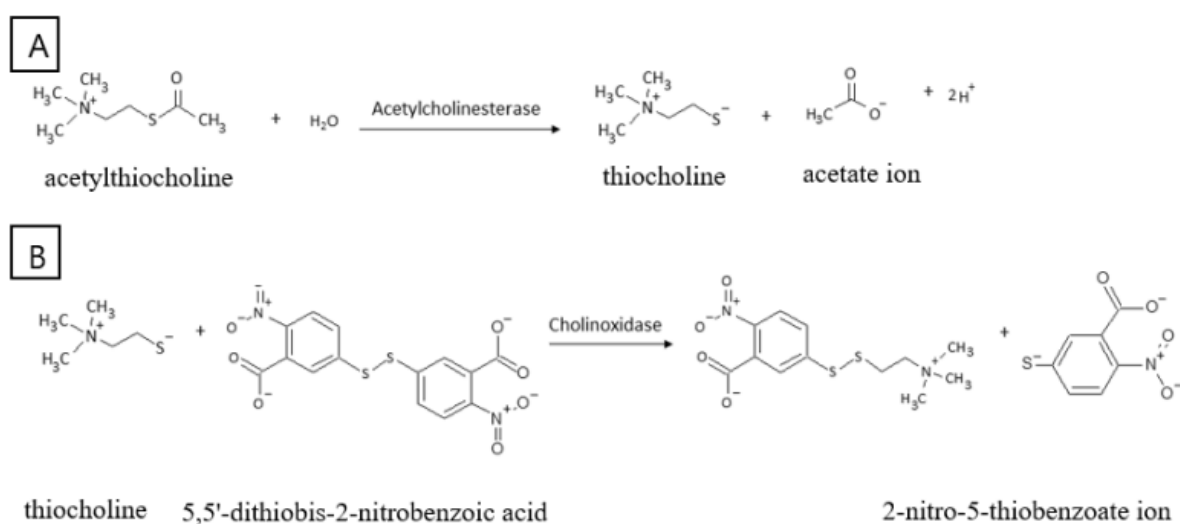


Figure 2. 4. Hydrolysis of the acetylthiocholine catalyzed by AChE

2.7.3 High-affinity choline uptake (HACU)

P2 fraction of homogenate contains synaptosomes with presynaptic terminal characteristics, for example transporter activity. Two choline transporters participate in the synthesis of ACh by providing choline, commonly known as high-affinity choline uptake (HACU) and low affinity choline uptake (LACU). Because HACU is inhibited by hemicholinium-3, its uptake then can be calculated by measuring total uptake and hemicholinium-sensitive uptake of radioactively labeled choline using scintillation instrument (König et al., 2019).

After thawing on ice, the P2 fraction was centrifuged at 16,000 g in 4°C 10 min. The pellet was then resuspended with 500 μL Krebs-Henseleit buffer (KHB buffer) (Table 2.9) and divided into two tubes (A and B @ 250 μL) followed by centrifugation at 16,000 g in 4°C 10 min. The pellet in each tube was then resuspended with either 500 μL KHB or 500 μL KHB

containing 10^{-6} M hemicholinium-3, respectively, for duplicate HACU measurement (@200 μ L) and duplicate protein determination (@50 μ L). After incubation in a water bath at 30°C for 10 minutes, 50 μ l [3 H]-choline (20 μ Ci/ml) (Biotrend, Cologne, Germany) was added into each tube followed by incubation in a water bath for 5 minutes. To stop the reaction, 1 mL of ice-cold KHB was added followed by storing on ice for 2 min. After centrifugation at 16,000 g in 4°C for 10 minutes, the pellets was washed with 500 μ L KHB followed by centrifugation at 16,000 g in 4°C for 10 minutes. Next, the pellet was resuspended in 500 μ L methanol to disintegrate the membranes and release [3 H]-choline. Afterwards, it was transferred into scintillation vials and spiked with scintillation fluid (Irga-Safe, Perkin Elmer). Finally, [3 H]-choline was measured using scintillation counter.

Table 2. 9. Composition of the Krebs-Henseleit buffer

| Substance | NaCl | KCl | CaCl ₂ | MgSO ₄ | NaHCO ₃ | Na ₂ HPO ₄ | Glucose |
|--------------------|------|-----|-------------------|-------------------|--------------------|----------------------------------|---------|
| Concentration (mM) | 115 | 7.1 | 1.2 | 1.2 | 25 | 1.5 | 12.9 |

2.7.4 Choline acetyltransferase activity

Choline acetyltransferase (ChAT) activity was measured based on König et al. (2019). Tritium-labeled acetyl-CoA and choline were used as the substrates of ChAT. After extraction into tetraphenylborate, [3 H]-ACh radioactive radiation was measured with a scintillator.

All steps was done on ice until incubation. After thawing on ice, 60 μ l brain homogenates was centrifuged for 10 minutes at 4°C and 12,000 g. The supernatant was collected and protein determination was done using Bradford method. The concentration of protein in a 250 μ L final medium was 0.25 μ g/ μ L.

Table 2. 10. Composition of ChAT reaction medium

| | |
|--|-------------------------------------|
| Homogenate supernatant x μ L | 62.5 μ g protein |
| Sodium chloride | 0.3 M |
| EDTA sodium | 0.02 M |
| Na ₃ PO ₄ (pH 7.4) | 0.05 M |
| Triton X-100 | 0.5% |
| Neostigmine bromide | 1 mM |
| Choline chloride | 2 mM |
| [3 H]-acetyl coenzyme A | 0.5 μ Ci |
| Milli-Q x μ L | up to a total volume of 210 μ L |

First, the reaction medium was mixed without the supernatant and [³H]-acetyl-CoA. After heating in a water bath (37°C; 5-10 minutes), the supernatant and 0.5 μCi [³H]-acetyl-CoA were added followed by shaking and incubation at 37°C for 10 minutes. Then, 250 μL of ice-cold PBS buffer was added to stop the reaction. Extraction of the resulting [³H]-ACh was done by vortexing with an extraction solution (0.5% Na tetraphenylborate in 85% toluene/15% acetonitrile) followed by centrifugation at 14,000 g for 7 minutes. The supernatant was collected into a scintillation vial and 4 ml of scintillant fluid (Irga-Safe, Perkin Elmer) was added. Finally, the intensity of the radioactive radiation was measured with a scintillation instrument using blank and standard.

2.8 Microdialysis study

Microdialysis study was performed in freely moving animals with self-build microdialysis probe as described by Lietsche et al. (2014). Dialysate was collected from extracellular space of hippocampus and striatum during brain perfusion with aCSF in which hydrophilic compounds go through the semi-permeable membran by means of passive diffusion (Fig. 2.5).

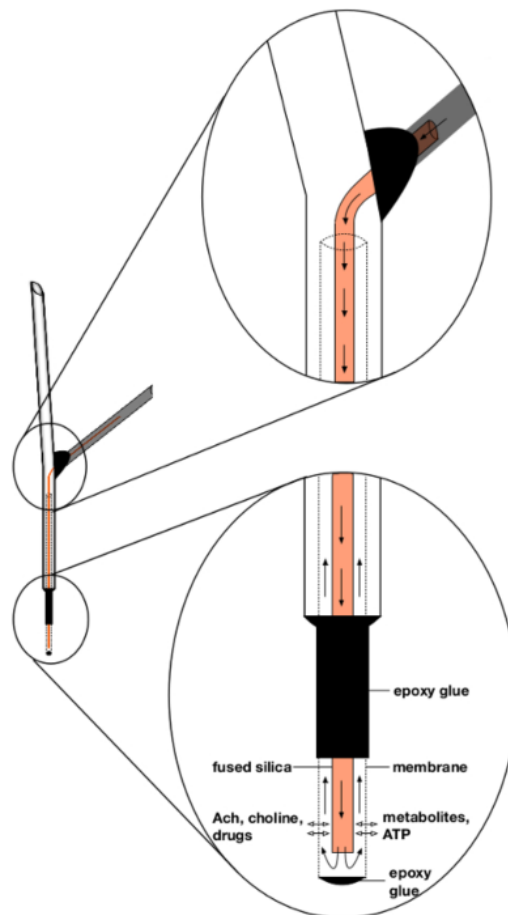


Figure 2. 5. Schematic illustration of a microdialysis probe (Lietsche et al., 2014)

2.8.1 Construction of microdialysis probe

Y-shaped, concentric microdialysis probes with a molecular weight cutoff of 30kDa were made during 2 days according to Lietsche et al. (2014) with slight modification (Figure 2.6). First, a PTFE-tubing was cut into 4 cm length with one end at an angle and then roughened with a sandpaper. Second, a 30 G cannula was inserted into the PTFE-tubing and then pierced at a distance of 1.2 cm from flat end. Third, a 3 cm length fused silica was inserted into the pierced hole and out to the flat end and then secured at a 8 mm projection from the flat end with epoxy glue. The next day, polysulfone membrane was inserted over the 8 mm projection of the fused silica and into the PTFE-tubing and then cut at a 9 mm projection from flat end. Next, the membrane was marked with fine pen to determine the exchange area of 3 mm from the bottom of the membrane. Epoxy glue was mixed according to the manufacturer's instruction and then applied on the bottom of the membrane and the joint between the membrane and the PTFE tubing. For making a metal cannula, a 25 G needle was cut into 8 mm length. The metal cannula was then pulled onto the remaining part of the fused silica and glued with the epoxy glue to secure its position. On the day of microdialysis experiment, hot glue was applied on the joint between metal cannula and PTFE-tubing.

Meanwhile, perfusion tube consists of inlet tube and outlet tip. Inlet tube was used for delivering aCSF for perfusion by connecting the metal cannula of the probe to a 1 mL Hamilton syringe. It was made of a 85 cm length of PE tubing (ID = 0.28 mm) with two pieces of 0.7 cm length Tygon tube (ID = 0.38 mm) at both ends. An activator and cyanoacrylate glue was used to secure the connections. The dialysate was collected from outlet tip (Ultra-tip, Greiner bio-one) connected to the angled cut of PTFE-tube by a 8 mm length adapter tube.

Before using, leaking test was conducted by pumping aCSF at a rate of 2 $\mu\text{L}/\text{min}$ through 1 mL Hamilton syringe connected to inlet tube, microdialysis probe, and outlet tip. Leaked probes were discarded while the functional ones were used for the next experiment.

2.8.2 *In vitro* recovery

In vitro recovery test was done in order to examine the quality and reproducibility of the probe. It was done by dipping the functional probes in a solution containing a known concentration of solute called recovery-mix (Table 11.). Dialysate was collected for 120 minutes (15 minutes/fraction) during perfusion rate of 2 $\mu\text{L}/\text{min}$ and kept at -80°C until the day of analysis.

In vitro recovery was calculated by comparing the concentration of a solute in the dialysate to the recovery mix.

Table 2. 11. Recovery mix

| Solute | Acetylcholine | Choline | Glucose | Lactate |
|------------------------|---------------|---------|---------|---------|
| Concentration in a CSF | 100 nM | 4000 nM | 1 mM | 1 mM |

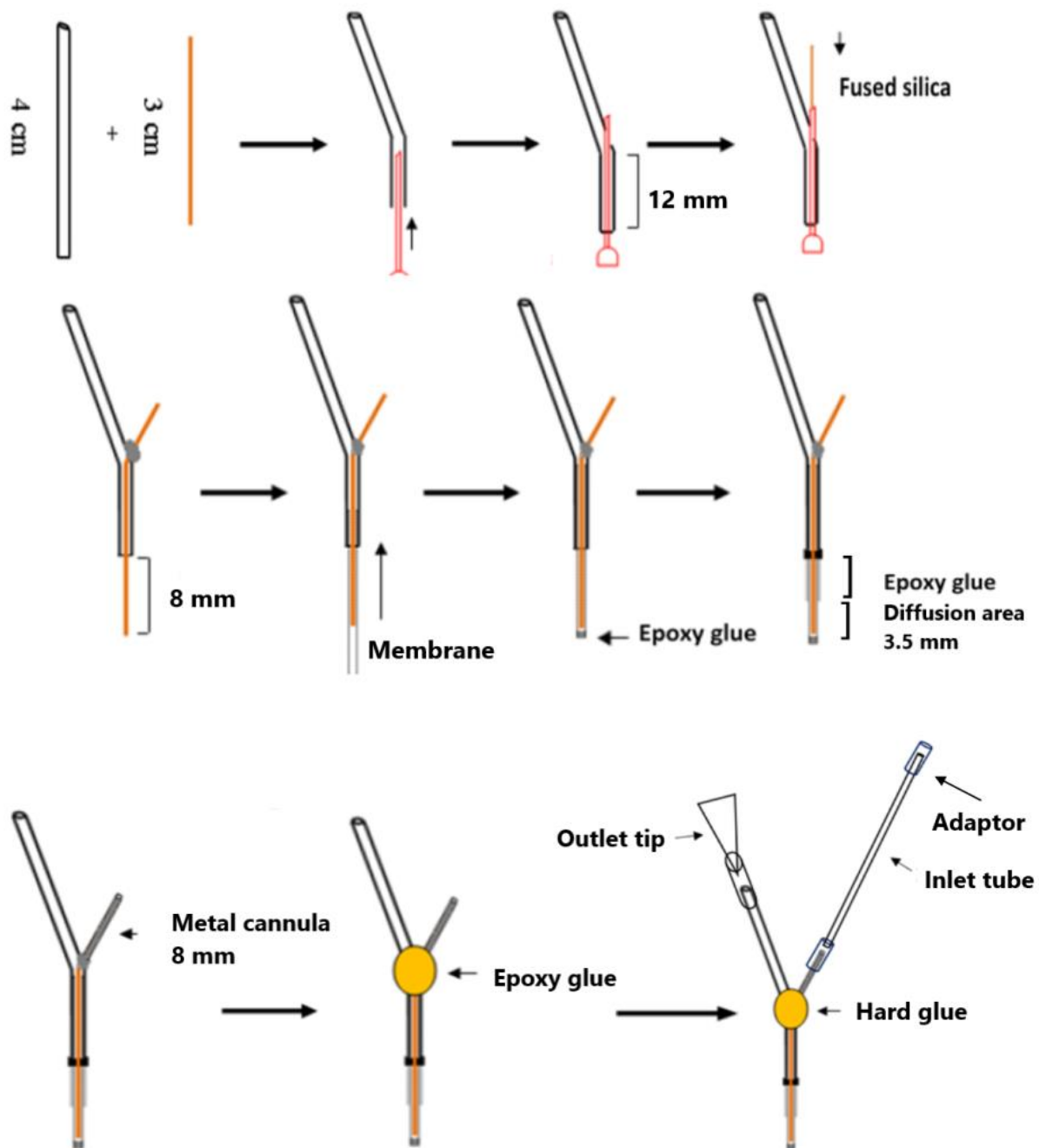


Figure 2. 6. Schematic illustrations of 30 kDa probe assembly. (Courtesy of Imran (2015)).

2.8.3 Microdialysis probe implantation

On day 19, rats were transported to microdialysis cage for implantation the next day. In the morning, leaking test was done and functional probes were collected and dipped in aCSF until used. Then, the rats were weighed and anesthetized with isoflurane (5% induction; 2% maintenance in synthetic air) and placed onto the stereotaxic instrument with their nose inside anesthetic mask (Figure 2.7). Deep anesthesia was confirmed by checking the intradigital reflex. Skull was immobilized by placing two ear bars and Bepanthen® was applied on both eyes for lubrication.



Figure 2. 7. Operation setup for probe implantation. (Courtesy of Imran (2015)).

After disinfection with alcohol swab, the clips on the skull were removed and the wound was opened again to expose the pericranium. Bupivacain was applied as a long-lasting local anesthetic and then the skull was scraped. Bleeding was controlled by applying cotton bud and Suprarenin® on the skull. When the skull was completely dry, a small hole was made in the skull by dental drill at a coordinate from bregma (HPC AP:-5.2; L:-4.8; DV:-7.0; STR AP:+0.2; L:-2.8; DV:-7.5) according to the atlas Paxinos and Watson (1998) and was confirmed after microdialysis experiment.

Next, probe was slowly implanted into hippocampus or striatum. After applying Multi-link primer on the skull for better adhesion, dental cement was applied on the area of primer up to the probe's hot glue region to fix the probe on the skull. After hardening, the skin was clipped to cover the skull and the cement. Finally, the rats were transported back to microdialysis cage for microdialysis experiment the next day. This procedure is illustrated in Figure 2.8 and Figure 2.9.

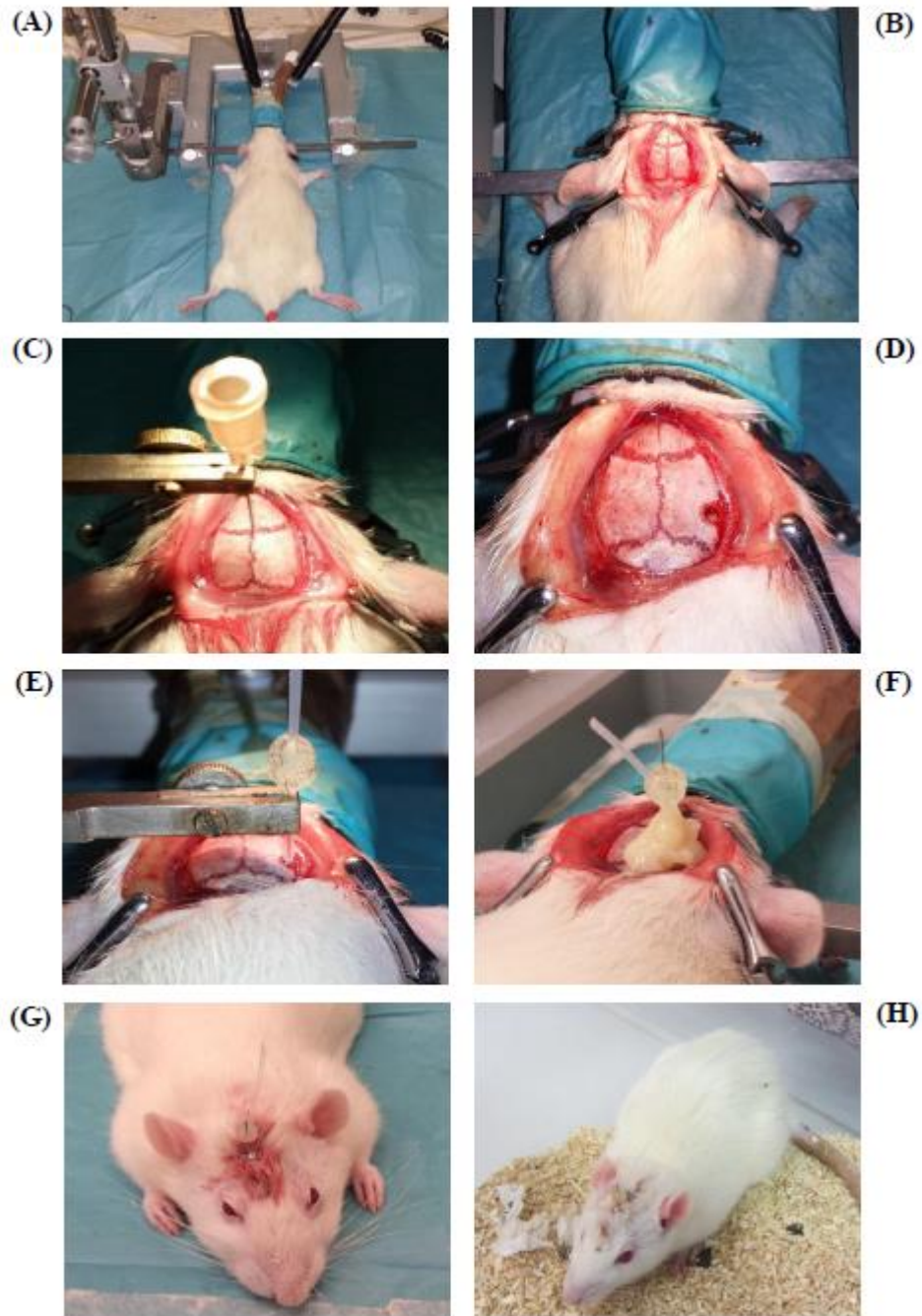


Figure 2. 8. Probe implantation. (A) Rat was placed in stereotaxic apparatus. (B) Midline incision and removal of pericranium. (C) Location of bregma. (D) Hole in skull after adjusting coordinates for right dorsal and ventral hippocampus. (E) Dorsoventral implantation of probe. (F) Fixing with dental cement. (G) Suture clips to close wound. (H) Overnight recovery. (Courtesy of Imran (2015)).

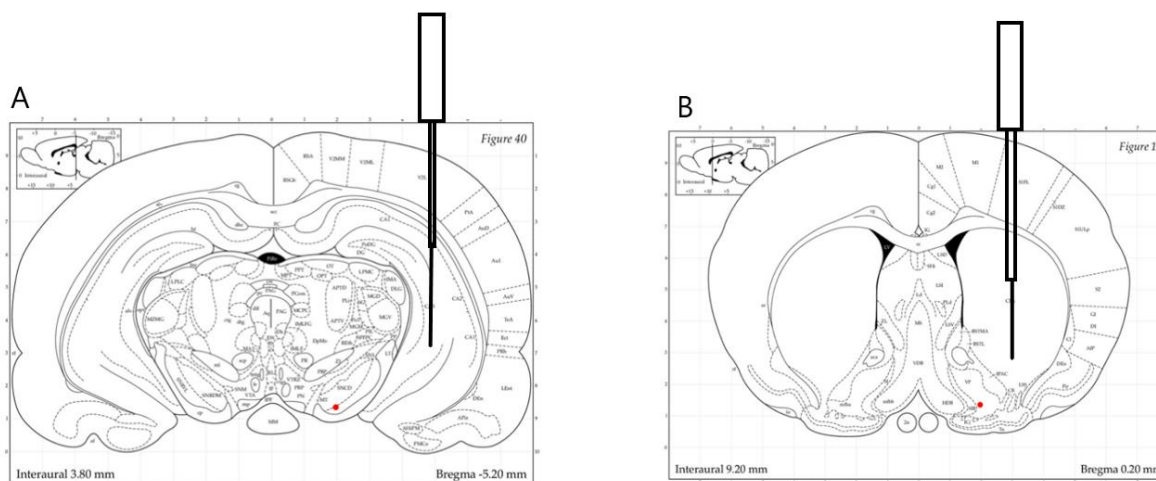


Figure 2. 9. Illustration of probe location. (A) hippocampus and (B) striatum. (<http://labs.gaidi.ca/>).

2.8.4 Microdialysis experiment

Implantation of microdialysis probes induce an alteration of blood-brain barrier permeability, cerebral blood flow, and neurotransmitter release. Therefore, microdialysis experiment was conducted at least 18 hours after probe implantation for their recovery and until maximum 2 days before gliosis occurs around the probes (König et al., 2017).

During microdialysis, the rat was placed in a microdialysis cage with free access to water and food, except during open field test as discussed later. Perfusion solution was prepared by incorporating 0.1 μ M neostigmine in aCSF. Neostigmine is an acetylcholinesterase inhibitor that reduces the degradation of ACh to choline and therefore enables the detection of ACh with HPLC (König, 2019). First, perfusion liquid was filled into a syringe (1 mL gas tight Hamilton syringe in a perfusion pump) and an inlet tube. Then, the inlet tube was connected to the metal sleeve of the probe while the outlet tip was connected to the teflon tube sleeve with the help of an adapter. A constant perfusion rate of 2 μ L/min was used. After 30 minutes of equilibrium between perfusion liquid and tissue, dialysates of 15 minutes intervals were collected for 90 minutes (6x30 μ L). These dialysates were called basal samples.

On day 1 after implantation, open field test was conducted in order to assess new environment stimulation effect (behavioural effect). After basal sample collection, the rat was moved to an open field box. Next, dialysates of 15 minute intervals were collected for 90 minutes (6x30 μ L). These dialysates were called open field samples. Then, the rat was moved back to the microdialysis cage and dialysates of 15 minutes intervals were collected for another 90 minutes (6x30 μ L). These dialysates were called basal samples after open field test.

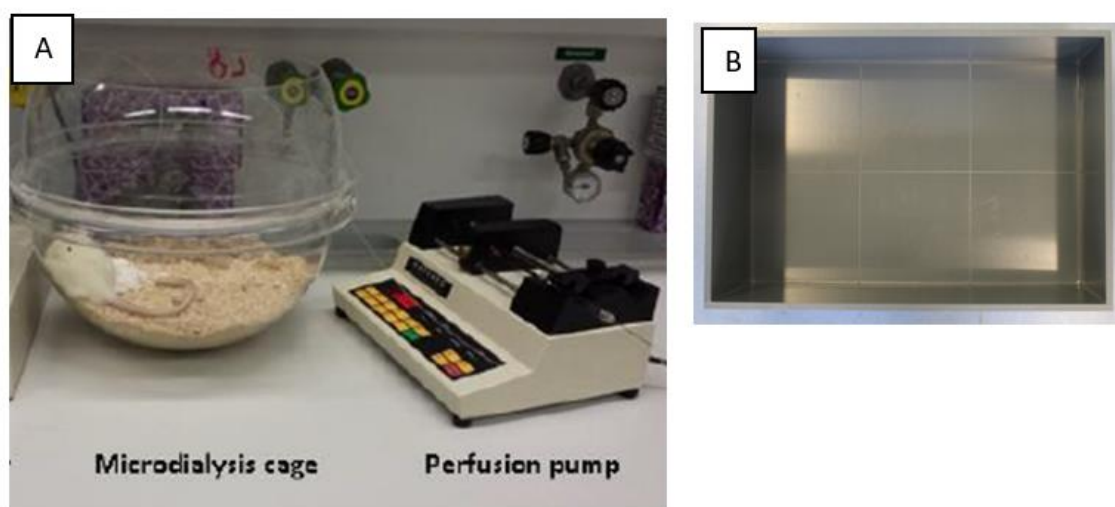


Figure 2. 10. Experimental setup of microdialysis in rats. (A) Microdialysis cage and perfusion pump. (B) Open field box of 35 cm x 32 cm x 20 cm size. (Courtesy of Imran (2015) and König (2019)).

On day 2 after implantation, scopolamine test was conducted in order to assess pharmacological stimulation effect. This was done by incorporating 1 μ M scopolamine in the perfusion solution after day 2 basal sample was collected. Scopolamine is a M2/M4 muscarinic autoreceptor antagonist. The low concentration of scopolamine blocks locally negative feedback mechanism of ACh release resulting in its maximum release from presynaptic neuron. Then, dialysates of 15 minute intervals were collected for 90 minutes (6x30 μ L). These dialysates were called scopolamine samples. Finally, basal samples after scopolamine were collected for 90 minutes (6x30 μ L).

An additional 90 minutes of basal samples (3x60 μ L) were collected for GC measurement (HPC) or ELISA measurement (STR). During microdialysis, the dialysates were collected in a 250 μ L closed tube and kept in closed ice box. At the end of the experiment, they were kept in -80° freezer until day of analysis. After microdialysis experiment, the rats were sacrificed and the brains were taken out for probe location determination.

2.8.5 Analysis of microdialysates

Microdialysates were analyzed with several methods. First, HPLC/ECD method was used to measure ACh and choline levels. Next, colorimetric method was used to measure glucose, lactate, pyruvate, and glycerol by CMA-600 microdialysate analyzer. GC/MS method was used to measure BHB in HPC microdialysates while ELISA method was used to measure isoprostane in STR microdialysates.

2.8.5.1 Choline and acetylcholine

ACh and choline levels were determined by directly injecting 10 μL dialysate into a high performance liquid chromatograph coupled with electrochemical detector system (HPLC/ECD). By different interaction between mobile phase and stationary phase, substances with different polarity are separated and reach the detector at different time points (retention time). Each substance can be detected and quantified by the help of analytical standards.

The HPLC/ECD system consists of an autosampler, mobile phase, a degasser, a pump, a pre-column, a separation column, an enzyme reactor, and an electrochemical detector. The mobile phase consisted of 50 mM KHCO_3 , 134.3 mM EDTA-Na_2 and 1.64 mM sodium decane-1-sulfonate in RotisolV[®] HPLC gradient grade water with a pH of 8.4. The stationary phase is the separation column (Eicompak AC-GEL 2.0 ID x 150mm) with non-polar side chains. The pre-column consisted of the same material as the separating column (but coarser) and traps unwanted compounds from the samples. During operation, the system was maintained at 4-5 MPa and 33⁰C with mobile phase rate at 150 $\mu\text{L}/\text{min}$.



Figure 2. 11. HPLC machine for ACh and Choline determination. (Courtesy of: Imran (2015)).

Because of slightly non-polar properties, ACh has a higher retention time than choline. After separation, both choline and ACh go through enzyme reactor which contains acetylcholinesterase and choline oxidase. As a result, hydrogen peroxide is liberated and reaches platinum electrode on the electrochemical detector. By digital transformation, the released electrons were seen as a chromatogram. Quantification of ACh and choline in the sample was obtained by comparing the area under curve (AUC) of the sample to the AUC of a known concentration of external standard. The limit of detection was 2 fmol/10 μL . The reactions are illustrated in Figure 2.12.

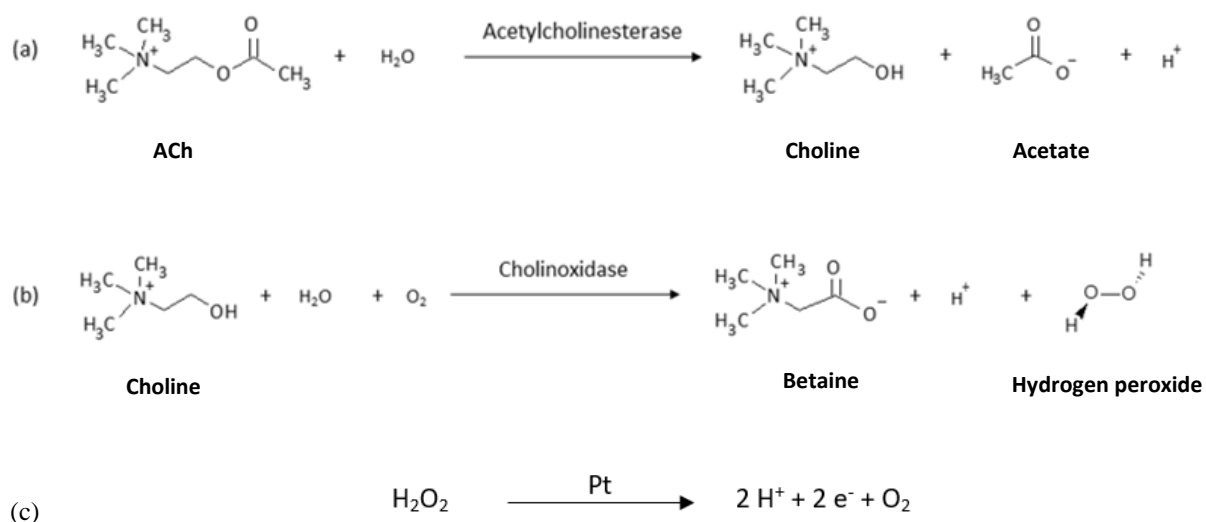


Figure 2. 12. Reaction of analyte in the HPLC/ECD machine. Reaction: (a) and (b) are in the enzyme reactor and (c) is in the electrochemical detector.

2.8.5.2 Glucose, lactate, pyruvate, and glycerol

Glucose, lactate, pyruvate, and glycerol levels in dialysate were measured by colorimetric method using CMA 600 microdialysate analyzer. This device is commonly used in clinical settings to measure tiny volumes of microdialysis samples (1-2 μL) with the help of specific reagents for each analytes. In brief, analytes were enzymatically oxidized by a specific oxidase resulting in H_2O_2 liberation. A second enzyme (peroxidase) catalyze the next reaction resulting in a photoactive red-violet colored compound which is then measured photometrically at 546 nm.

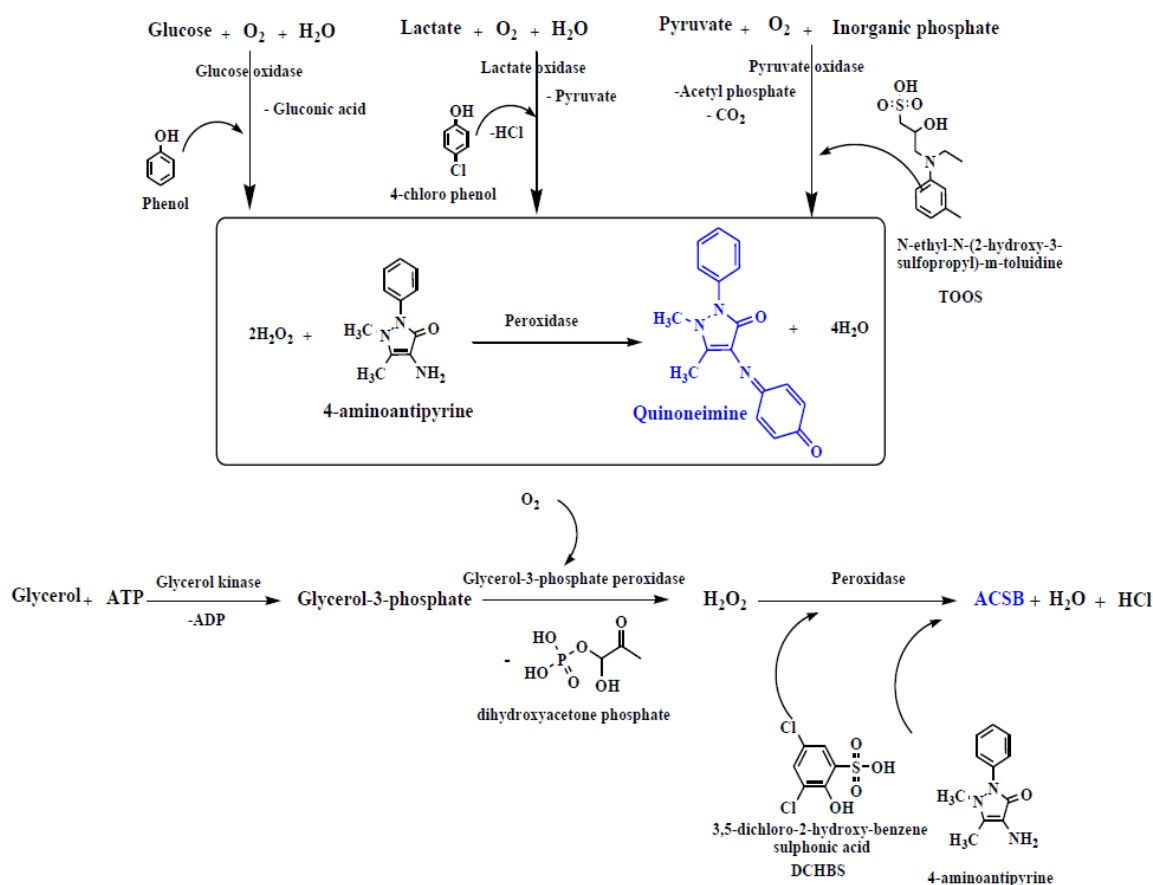


Figure 2. 13. Schematic reaction by CMA 600. Note: Blue is photoactive. (Courtesy of Imran (2015))

2.8.5.3 Beta-hydroxybutyrate (BHB)

Beta-hydroxybutyrate (BHB) level was measured using Gas Chromatography-Mass Spectrophotometry method (Koch et al., 2017). Gas chromatography is a method to separate mixed compounds in which the analytes must be in the gas phase. Carrier gas brings the analytes into a separation column in which each analyte interacts differently with the column resulting in separation and different retention time in the column. Finally, a mass spectrometer detects each analyte and quantitative and qualitative analysis can be done using internal and external standards.

Internal standard is structurally similar compound to the analyte that is added to the samples with a known concentration and undergoes each analytical step together with analyte of interest. Meanwhile, external standard is a similar compound to analyte which is prepared as calibrator and undergoes similar analytical steps but separately from sample. For BHB analysis, sodium salicylate was used as an internal standard and sodium 3-hydroxybutyrate was used as an external standard.

Quantification was done based on peak of specific retention time. First, response factor (Rf) was calculated. Rf is the ratio of internal standard to external standards. Finally, the mass of analyte in the sample was calculated by the ratio of analyte in the sample to internal standard in the sample multiplied by respective Rf, known concentration of internal standard, and total volume.

External standard was prepared by diluting sodium 3-hydroxybutyrate 10 $\mu\text{g}/\mu\text{l}$ in methanol-water (3:2, pH 9.5). After evaporation on a heating block at 60°C under nitrogen, the next step was done under argon (oxygen-free). First, the dry residue was dissolved in pyridine and Hünig base using 40°C ultrasonic bath for 10 minutes. After cooling, derivatization was done using a mixture of BSTFA and TMCS (99:1) and a heating block at 70 °C for 50 minutes. The final concentration of external standard was 50 ng/ μL .

Internal standard was prepared by diluting sodium salicylate 10 $\mu\text{g}/\mu\text{l}$ in methanol-water (3:2, pH 9.5). Then, 15 μL of the internal standard was added to 60 μL microdialysate. Evaporation and the next step are similar to external standard. The final concentration of internal standard in the sample was 50 ng/ μL .

Next, sample was injected to GC-MS (HP 6890, Agilent) machine. After evaporation at 250°C, helium gas carried the sample through a 30 meter long column at a rate of 1 mL/min in an oven. Then, each separated compound entered the mass spectrometer and was ionized and identified for their specific fragmentation patterns. The fragmentation pattern was measured in the SIM mode by comparing with a database (Wiley 275.L).

2.8.5.4 Isoprostane

Isoprostane level in the microdialysates of striatum was measured using a commercially available 8-isoprostane EIA kit coated with mouse anti-rabbit IgG (Cayman Chemicals,USA) with the limit of detection approximately 10 pg/ml. First, 8-isoprostane standard was prepared in a concentration from 1500-2.5 pg/ml. Then, as instructed on the kit, the standard, microdialysate samples, 8-isoprostane tracer and antiserum (50 μl each) were added into the EIA-well plate. Then, the plate was incubated at room temperature on an orbital shaker for 2 hours. After 5x washing with wash buffer, 200 μl of Ellman's reagent (freshly prepared) was added to each well. Next, the second incubation was done in the dark with orbital shaker for 90 minutes. Finally, absorbance was measured at 405 nm using multilable plate reader (Victor™ X3 2030, Perkin Elmer USA). Calculation was done using online support "MyAssays" from

Cayman Chemical website (www.caymanchem.com). The standard curve is shown in Figure 2.14.

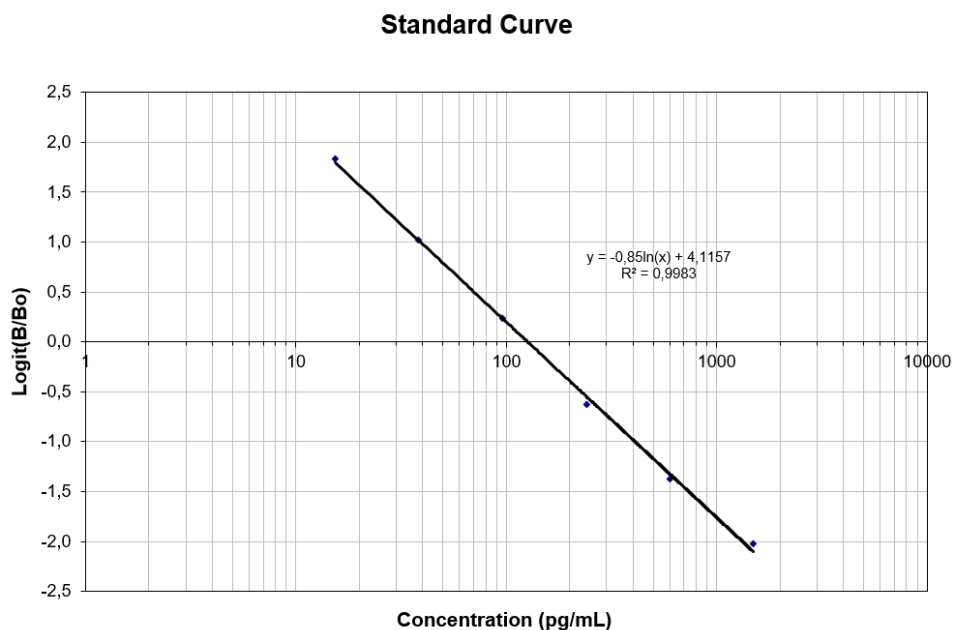


Figure 2. 14. Isoprostane standard curve.

2.9 Statistical analysis

Unless otherwise stated, data are presented as means \pm S.E.M of N experiments. GraphPad Prism[®] Version 5.03 was used for presenting the data and performing statistical analysis. A significance level of 0.05 was chosen for all tests. Unpaired t-test was used for comparing means of two groups while analysis of variance (ANOVA) was used for comparing means of more than two groups followed by Tukey's test. If two factors affect the means and each subject was measured repeatedly, two-way analysis of variance (ANOVA) of repeated measures was used followed by Bonferroni post test.

3 Results

Results are divided into 3 parts. The first part is dedicated to confirm icv-STZ toxicity while the second and third part are divided according to brain region (hippocampus and striatum).

3.1 Confirmatory study for icv-STZ local toxicity

3.1.1 Icv-STZ decreased both body weight and hippocampal weight

Icv-STZ toxicity was obvious 1.5 weeks after high dose administration (2x1.5 mg/kg) as shown by less weight gain compared to other groups (Figure 3.1 A). After 1.5 weeks, the weight gain started to increase more than before. However, at the end of the experiment (on day 21), high dose STZ-treated rats had a 15% less body weight than controls (saline 331±35 g vs high dose 283±24 g, N=17-20; $p<0.01$). Meanwhile, rats which received low dose of icv-STZ (0.6 mg/kg) developed normally during the experiment.

Furthermore, isolated hippocampal weight at the end of the study (21 days after icv-STZ) showed significant reduction by 13% after high dose (170.2±7.2 mg, N=12; 147.9±8.0 mg, N=12; $p<0.05$) (Figure 3.1 B). The hippocampus was then used for determination of mitochondrial respiration (see 3.2.1).

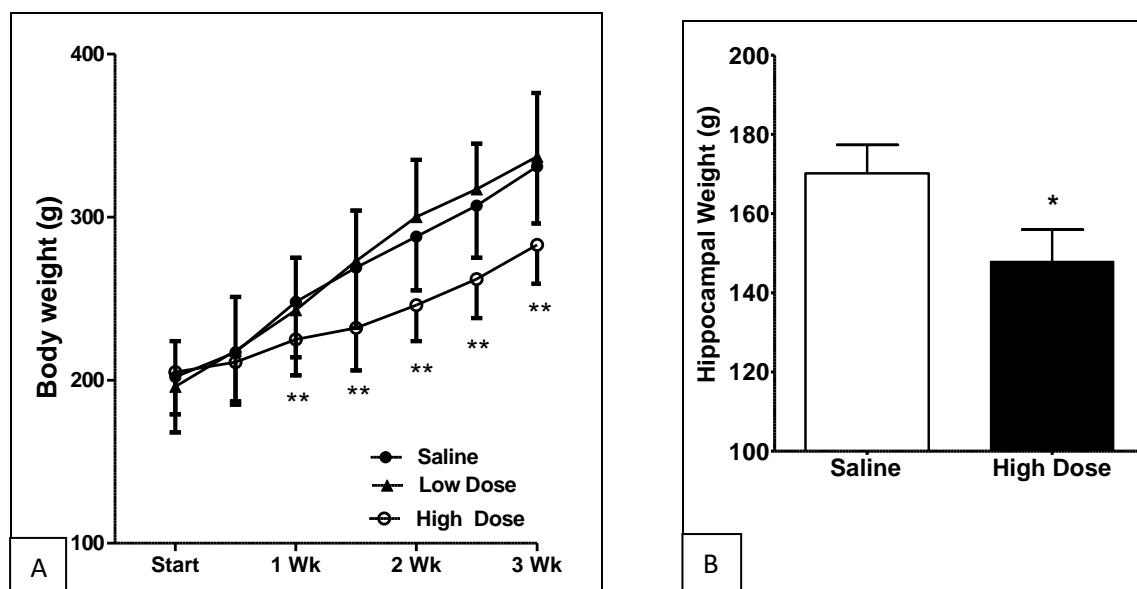


Figure 3. 1. Body weight and hippocampus weight. (A) Body weight of rats treated with saline or streptozotocin (STZ) at low (0.6 mg/kg) or high (twice 1.5 mg/kg) doses. Data are means \pm S.D. of 17-20 experiments. Statistics: two-way ANOVA with Bonferroni post-test: **, $p<0.01$ vs. saline. (B) Hippocampus weight. Data are means \pm S.E.M of 12 experiments. Statistics: one-way ANOVA with Tukey's multiple comparisons test: *, $p<0.05$ vs. saline.

3.1.2 Icv-STZ induced gliosis and neurodegeneration in hippocampus

Cellular toxicity of icv-STZ was investigated through histological observation on dorsal and ventral hippocampus, i.e. a similar location to the implanted probe for microdialysis study (see 3.2.3). Immunohistochemical study using GFAP primary antibody revealed glial activation after high dose of icv-STZ on the whole dorsal and ventral hippocampus, especially at the CA1 region (n=4) (Figure 3.2 B). However, Fluoro-Jade C staining revealed CA1 region neurodegeneration only in 3 out of 9 rats (Figure 3.2 C).

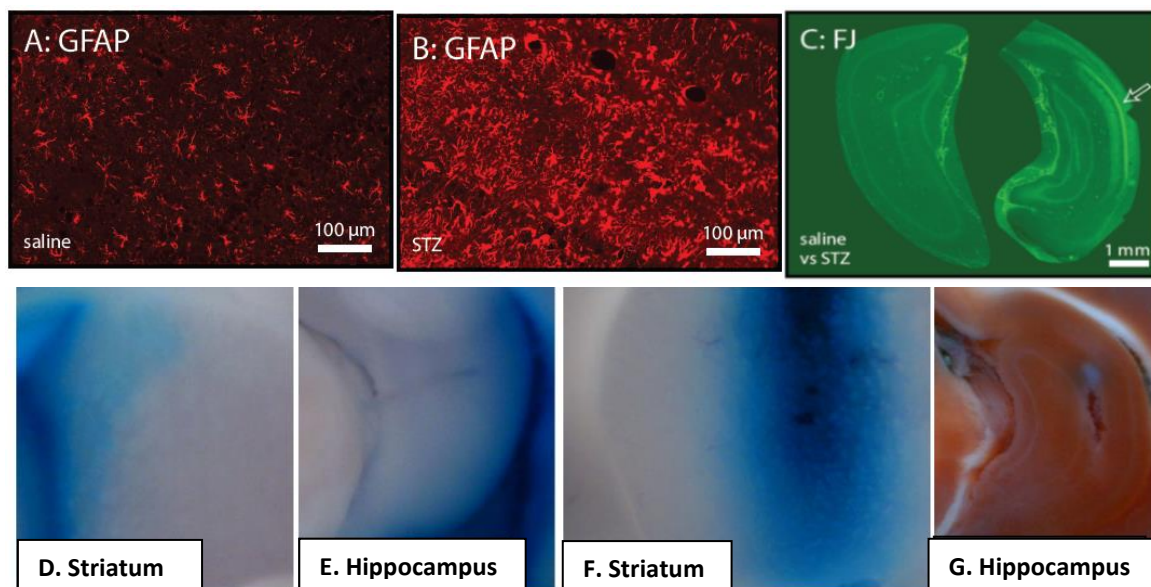


Figure 3. 2. Coronal cryosections of the hippocampus (14 μm) at AP -5.6 mm from bregma. (A) Glial fibrillary acidic protein (GFAP) immunoreactivity in the rat hippocampus 21 days after i.c.v. injection of saline. (B) Strong GFAP immunoreactivity in rat hippocampus 21 days after i.c.v. injection of streptozotocin (STZ). (C) Lower magnification: Fluoro-Jade C staining illustrates extensive STZ-induced degeneration of the CA1 region (arrow). In the saline group, no signal was observed in the CA1 region. (D) Striatal and (E) hippocampal distribution of fast green dye after icv injection. (F) Diffusion of Fast Green dye from implanted probe in striatum (see 3.3.3). (G) Probe location in hippocampus (see 3.2.3).

3.2 Hippocampus

Hippocampus was chosen because it is the most investigated brain region for cognitive function.

3.2.1 High dose of icv-STZ reduced mitochondrial respiration especially on complex II and IV in hippocampus

Figure 3.3 A shows mitochondrial respiration of isolated mitochondria from hippocampi. After normalization with citrate synthase activity, all complexes showed reduction by 9-15% but significant only for complex II (succinate dehydrogenase) and IV (cytochrome c oxidase). High dose of icv-STZ decreased single mitochondrial respiration on complex I (NADH reductase) by 14% (saline 36.4 ± 3.5 ; N=12, high dose 31.4 ± 3.3 ; N=12; $p>0.05$), complex II (succinate dehydrogenase) by 15% (saline 81.1 ± 3.7 ; N=12, high dose 68.9 ± 4.5 N=12; $p<0.05$), complex III (maximum electron transfer system) by 9% (saline 134.1 ± 6.9 ; N=12, high dose 121.7 ± 7.1 ; N=12; $p>0.05$), and complex IV (cytochrome c oxidase) by 14% (saline 326.3 ± 14.6 ; N=12, high dose 280.7 ± 16.7 ; N=12; $p<0.05$).

Citrate synthase activity was used as the quantitative marker for mitochondria content. Citrate synthase activity was measured using Ellman's reagents by colorimetry. The high dose group showed a significant increase of citrate synthase activity by 24% (saline 0.8 ± 0.1 ; N=12 vs high dose 1.0 ± 0.1 ; N=12; $p<0.05$). This indicates that high dose of icv-STZ increased mitochondrial content (Figure 3.3 B).

Quality of mitochondria is also determined by its isolation procedure. During isolation of mitochondria, the membrane may lose its integrity resulting in loss of cytochrome C (Cyt C). In this case, addition of exogenous Cyt C will replace the endogenous Cyt C that leads to increased respiration. Therefore, % increase of respiration after addition of exogenous Cyt C reflects the quality of mitochondria: The more damage to mitochondria, the bigger the percentage. Figure 3.3 C shows that the quality of mitochondria was similar in both groups. Both group lost 14% of cytochrom C during isolation (saline 14.0 ± 1.6 ; N=12 vs high dose 14.6 ± 1.3 ; N=12. Similar quality of mitochondria between saline and high dose showed, at least, that the latter difference of mitochondrial respiratory function was not caused by variations induced by the isolation procedure.

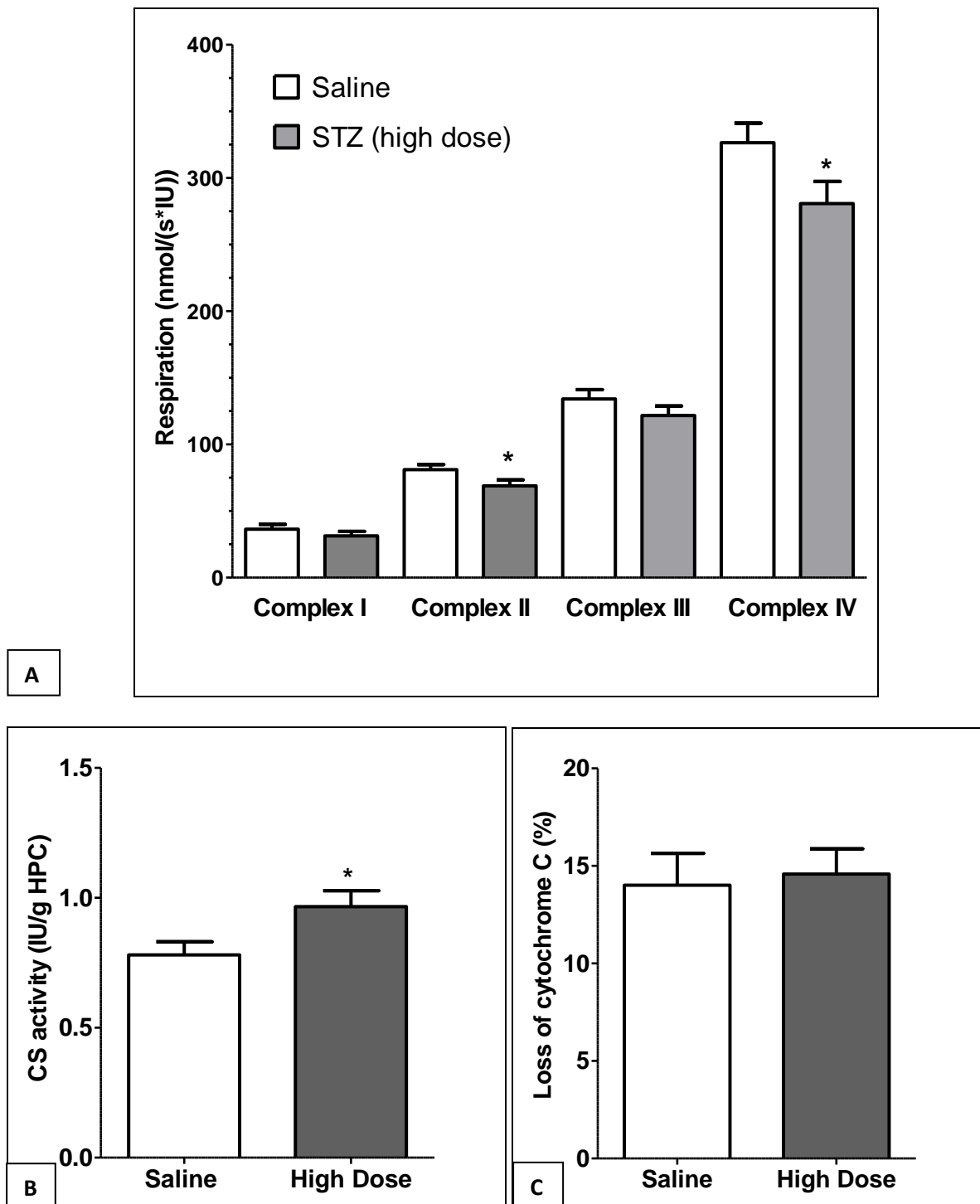


Figure 3.3. Mitochondrial respiration in hippocampus. (A) Changes in oxygen flux in complexes I, II, III and IV of the electron transport chain (ETC). Substrates, uncoupler and inhibitors were used to measure each complex as described in Methods. Raw data as obtained from respirometry were normalized to mitochondrial citrate synthase activity. (B) Citrate synthase activity normalized by hippocampus weight. (C) Loss of cytochrome C during isolation of mitochondria. Statistical analysis: Data are means \pm S.E.M. (N=12) and were analyzed by unpaired t-test. * $p < 0.05$ compared to saline.

3.2.2 Cholinergic marker study in hippocampus

Cholinergic neuronal markers involved in extracellular ACh level were investigated in hippocampal homogenates. HACU (high affinity choline uptake) which plays a significant role on intracellular choline availability for ACh synthesis was investigated by radioactive method. ChAT which catalyzes ACh synthesis was also investigated by radioactive method. Meanwhile, AChE which catalyze ACh degradation was investigated by colorimetry method. After normalization to protein content, the high-dose group revealed a slight decrease in HACU activity by 16% ($p>0.05$). However, significant decreases were observed both in ChAT and AChE activity by 28% ($p<0.01$) and 30% ($p<0.001$), respectively (Table 3.1).

Table 3. 1. Cholinergic parameters as determined in rat hippocampus three weeks after icv-STZ administration. **, $p<0.005$; ***, $p<0.001$ vs. controls. The data was kindly provided by Helene Lau.

| Activity | Controls | High-dose STZ |
|---|-----------------|-----------------------|
| Choline acetyltransferase (ChAT) (ACh nmol/h/mg protein) | 39.7 ± 1.7 | $29.2 \pm 2.5^{**}$ |
| Acetylcholinesterase (AChE) (AChE mU/mg Protein) | 111.2 ± 3.7 | $76.92 \pm 8.0^{***}$ |
| High-affinity choline uptake (HACU) (DPM/ μ g Protein) | 358 ± 42 | 300 ± 30 |
| Low-affinity choline uptake (LACU) (DPM/ μ g Protein) | 138 ± 7 | 139 ± 10 |

3.2.3 Microdialysis study: Effect of icv-STZ on metabolic and cholinergic profile in hippocampus during cholinergic challenge

Extracellular metabolite levels during cholinergic challenges were monitored 21 days after icv-STZ using microdialysis technique in dorsal ventral hippocampus. Open field test was used as physiologic challenge while local scopolamine administration was used as pharmacologic challenge. Before and during each challenge, samples of 6 time points were collected (15 minutes/time points; except for isoflurane: 30 minutes). Basal value samples was collected before the challenge (Table 3.1). For analysis, acetylcholine and choline were determined by

HPLC/ECD, glucose and lactate were determined by colorimetry using CMA600, and β -hydroxybutyrate (BHB) was determined by GC/MS.

Table 3. 2. Extracellular concentrations of hippocampal metabolites as determined by microdialysis under basal conditions (not corrected for recovery). *, $p < 0.05$ vs. controls.

| Metabolite | Controls | Low dose STZ | High dose STZ |
|-------------------------------------|-----------------|-----------------|------------------|
| Acetylcholine (nM) | 8.71 \pm 1.33 | 7.29 \pm 0.84 | 7.48 \pm 1.58 |
| Choline (μ M) | 0.69 \pm 0.06 | 0.82 \pm 0.07 | 0.94 \pm 0.06* |
| Glucose (μ M) | 204 \pm 29 | 202 \pm 13 | 233 \pm 25 |
| Lactate (μ M) | 192 \pm 34 | 135 \pm 20 | 150 \pm 9 |
| β -Hydroxybutyrate (μ M) | 6.12 \pm 1.23 | 6.85 \pm 0.90 | 7.08 \pm 0.84 |

Basal β -hydroxybutyrate did not change significantly after both low and high dose of STZ; only a slight, dose-dependent increase was observed (Table 3.2). On the other hand, basal choline was increased dose-dependently and significantly.

Basal extracellular glucose level also did not change 21 days after either low or high dose of icv-STZ. Only a slight increase of glucose was observed after high-dose STZ (+14%; saline 204 \pm 29 μ M vs high dose 233 \pm 25 μ M, N=6; $p > 0.05$). Physiologic challenge showed a slight increase of glucose level in all groups (saline 252 \pm 37 μ M, low dose 247 \pm 34 μ M, high dose 245 \pm 19 μ M, N=6; $p > 0.05$) (Figure 3.5A).

Meanwhile, extracellular lactate levels were reduced insignificantly after both low and high dose of icv-STZ compared to saline (-24%; basal saline 192 \pm 34 μ M, low dose 135 \pm 20 μ M, high dose 150 \pm 9 μ M, N=6; $p > 0.05$). Physiologic challenge did not cause a major change in lactate levels but only induced a slight increase of lactate levels in all groups (saline 215 \pm 29 μ M, low dose 185 \pm 24 μ M, high dose 171 \pm 20 μ M, N=6; $p > 0.05$) (Figure 3.5 B). When the whole data from basal, open field test, and scopolamine test were analyzed together, both low and high dose of icv-STZ decreased lactate level insignificantly by 23% (saline 206 \pm 7 μ M, low dose 159 \pm 14 μ M, high dose 159 \pm 7 μ M; $p > 0.05$).

Surprisingly, despite decrease in cholinergic enzymes, cholinergic transmission was unchanged after both doses of icv-STZ. Similar basal ACh levels were observed on day-1 (saline 8.7 \pm 1.3 nM, low dose 7.3 \pm 0.8 nM, high dose 7.5 \pm 1.6 nM, N=6; $p > 0.05$). During open field test, similar increases were also observed at minute 30 in all groups (saline 16.8 \pm 3.0 nM, low dose 16.8 \pm 2.5 nM, high dose 21.6 \pm 4.6 nM, N=6; $p > 0.05$) (Figure 3.6 A). On day-2, similar basal ACh levels were also observed (saline 6.4 \pm 0.7 nM, low dose 7.5 \pm 1.3 nM, high dose 10.6 \pm

2.1 nM, N=6; $p>0.05$). During scopolamine test, all groups also showed similar maximum increase at minute 75 (saline 36.1 ± 5.9 nM, low dose 29.2 ± 8.2 nM, high dose 34.2 ± 6.3 nM, N=6; $p>0.05$) (Figure 3.6 B).

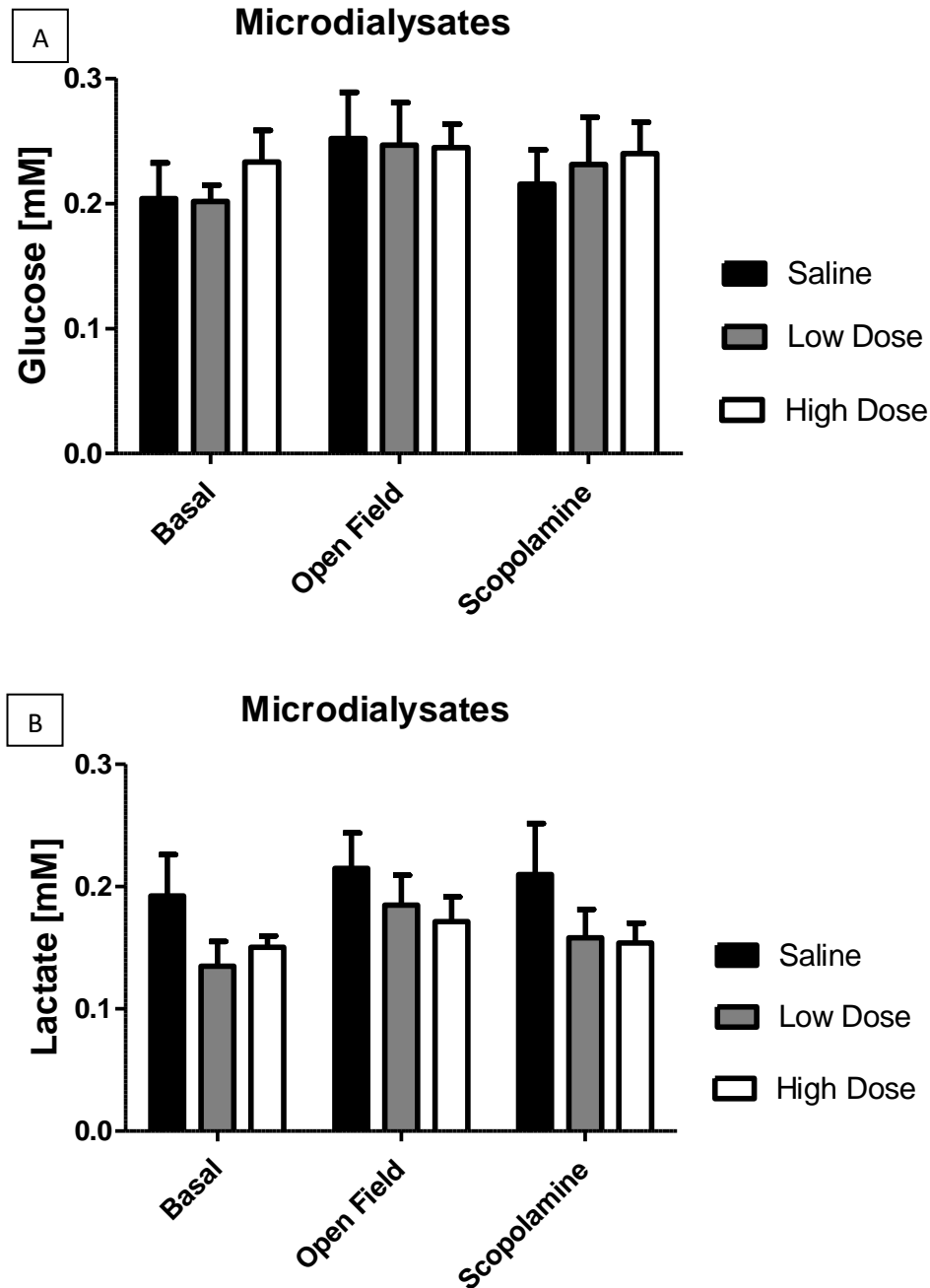


Figure 3. 4. Metabolite levels in hippocampal microdialysates during behavioral and cholinergic challenges. (A) Glucose; (B) Lactate concentrations were measured in microdialysates under basal conditions, during open field exploration, and during infusion of scopolamine. Data are averages of six samples (90 minutes) and are means \pm S.E.M. (N=6). Statistics: one-way ANOVA followed by Tukey's multiple comparison test. $p > 0.05$ compared to saline.

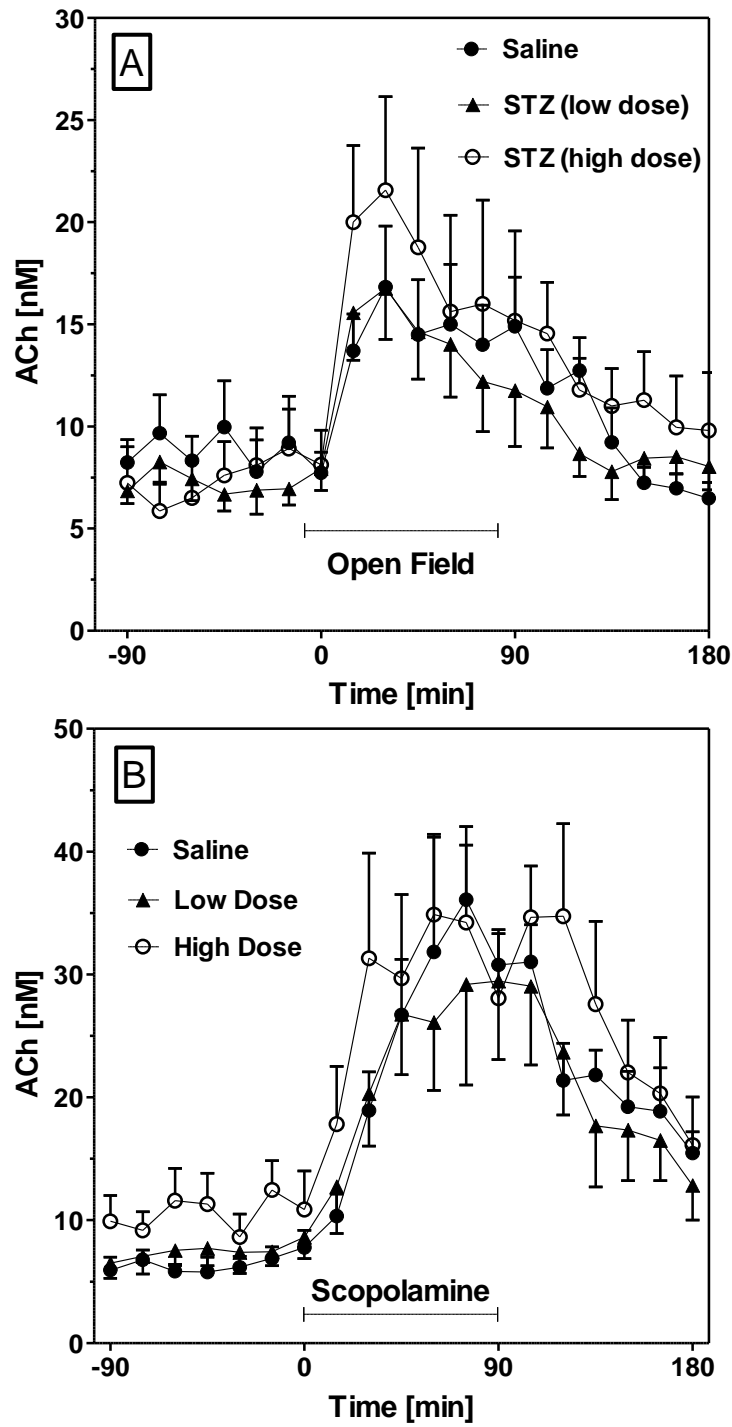


Figure 3. 5. Acetylcholine (ACh) levels in rat hippocampal microdialysates during behavioral and cholinergic challenges. (A) Open field test (from time 0 until 90 min). (B) Infusion of scopolamine (0.1 μ M) (from time 0 until 90 min). Data are means \pm S.E.M. (N=6-7) and were analyzed by one-way ANOVA followed by Tukey's multiple comparison test.

3.3 Striatum

Striatum was investigated because it contains short projecting cholinergic interneurons and is involved in movement.

3.3.1 Preserved mitochondrial respiratory function after high dose of icv-STZ in striatum

Mitochondrial study of isolated mitochondria from striatum showed no change on both mitochondrial respiration and mitochondrial content. Effect of mitochondrial isolation procedure are similar in both saline and STZ group, leading to 15% loss of cytochrom C.

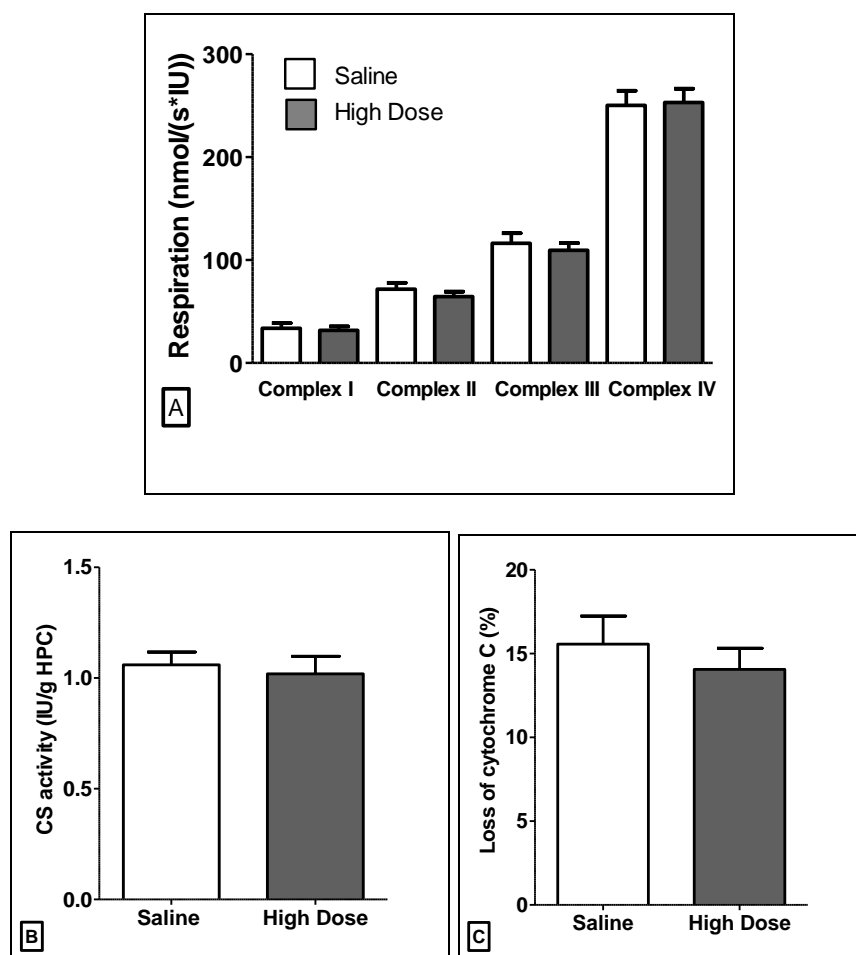


Figure 3. 6. Mitochondrial respiration in striatum. (A) Changes in oxygen flux in complexes I, II, III and IV of the electron transport chain (ETC). Substrates, uncoupler and inhibitors were used to measure each complex as described in Methods. Raw data as obtained from respirometry were normalized to mitochondrial citrate synthase activity. (B) Citrate synthase activity normalized by striatal weight. (C) Loss of cytochrom C during isolation of mitochondria. Statistical analysis: Data are means \pm S.E.M. (N=9) and were analyzed by unpaired t-test. * $p < 0.05$ compared to saline.

3.3.2 Cholinergic marker study in striatum

Similar to the experiment in hippocampus, three cholinergic neuronal markers involved in extracellular ACh release were also investigated in striatum. After normalization to protein content, the high-dose group revealed significant increases in both HACU activity and AChE activity by 31% and 7%, respectively (* $p < 0.05$). However, preserved ChAT activity was observed (Table 3.3).

Table 3. 3. Cholinergic parameters as determined in rat striatum three weeks after icv-STZ administration. *, $p < 0.05$ vs. controls. The data was kindly provided by Helene Lau.

| Activity | Controls | High-dose STZ |
|---|-------------------|--------------------|
| Choline acetyltransferase (ChAT) (ACh nmol/h/mg protein) | 97.83 \pm 2.38 | 99.67 \pm 3.244 |
| Acetylcholinesterase (AChE) (AChE mU/mg Protein) | 411.1 \pm 10.20 | 441.5 \pm 10.35* |
| High-affinity choline uptake (HACU) (DPM/ μ g Protein) | 393 \pm 13 | 514 \pm 40* |
| Low-affinity choline uptake (LACU) (DPM/ μ g Protein) | 157 \pm 7 | 153 \pm 6 |

3.3.3 Microdialysis study: Effect of icv-STZ on metabolic and cholinergic profile in striatum during cholinergic challenge

Similar to the experiment in hippocampus, extracellular metabolite levels during cholinergic challenges were monitored 21 days after icv-STZ using microdialysis technique in striatum. The differences with hippocampus are as follows. First, pyruvate and glycerol was also measured by colorimetry using CMA 600. Second, isoprostanone was measured instead of β -hydroxybutyrate.

Table 3. 4. Extracellular concentrations of striatal metabolites as determined by microdialysis under basal conditions (not corrected for recovery). *, $p < 0.05$ vs. controls.

| Metabolite | Controls | Low dose STZ | High dose STZ |
|----------------------|---------------|---------------|---------------|
| Acetylcholine (nM) | 30.86 ± 4.57 | 24.86 ± 3.90 | 42.16 ± 5.22 |
| Choline (µM) | 924.5 ± 47.76 | 865.6 ± 39.15 | 972.6 ± 104.3 |
| Glucose (µM) | 233.3 ± 15.4 | 203.8 ± 12.1 | 294.4 ± 22.1* |
| Lactate (µM) | 97.0 ± 11.0 | 104 ± 8.3 | 130.1 ± 13.1 |
| Pyruvate (µM) | 6.9 ± 0.91 | 11.6 ± 1.5 | 13.5 ± 2.5 |
| Glycerol (µM) | 2.69 ± 0.38 | 3.77 ± 0.64 | 4.76 ± 1.07 |
| Isoprostanes (pg/ml) | 26.4 ± 1.5 | 23.2 ± 2.2 | 31.4 ± 2.9 |

Basically, nothing changed in striatal basal value of ACh, choline, lactate, pyruvate, glycerol, and isoprostane after both low and high dose. Meanwhile, slight increases in a dose-dependent manner were observed on glycerol and pyruvate (Table 4).

Significant increase by 26 % on basal glucose levels were observed but only after high STZ dose (saline 233.3 ± 15.4 µM vs high dose 294.4 ± 22.1 µM, * $p < 0.05$). Significant increases of lactate levels were also observed after low and high dose but only during scopolamine test by 59 % and 107 %, respectively (saline 87.1 ± 3.0 µM; low dose 137.6 ± 18.7 µM; high dose 180.0 ± 12.1 µM, * $p < 0.05$). In this case, after cholinergic challenge the high dose group kept releasing lactate (Fig. 3.7 B).

In line with the cholinergic markers which showed increased HACU and AChE in striatum, extracellular ACh also increased slightly after high-dose STZ by 37 % (saline 30.86 ± 4.57 nM, high dose 42.16 ± 5.22 nM, N=6; $p > 0.05$). The physiologic challenge during open field test induced a 33% increase of ACh release in saline group but a 50% increase in both STZ groups (Figure 3.8 A). On day-2, the basal ACh levels were similar to day-1 (saline 33.74 ± 5.41 nM vs high dose 37.48 ± 7.26 nM, N=6; $p > 0.05$). During scopolamine test, all groups showed a similar maximum increase of ACh (saline 107.20 ± 15.59 nM, low dose 94.87 ± 19.20 nM, high dose 100.3 ± 21.67 nM, N=6; $p > 0.05$) (Figure 3.6 B).

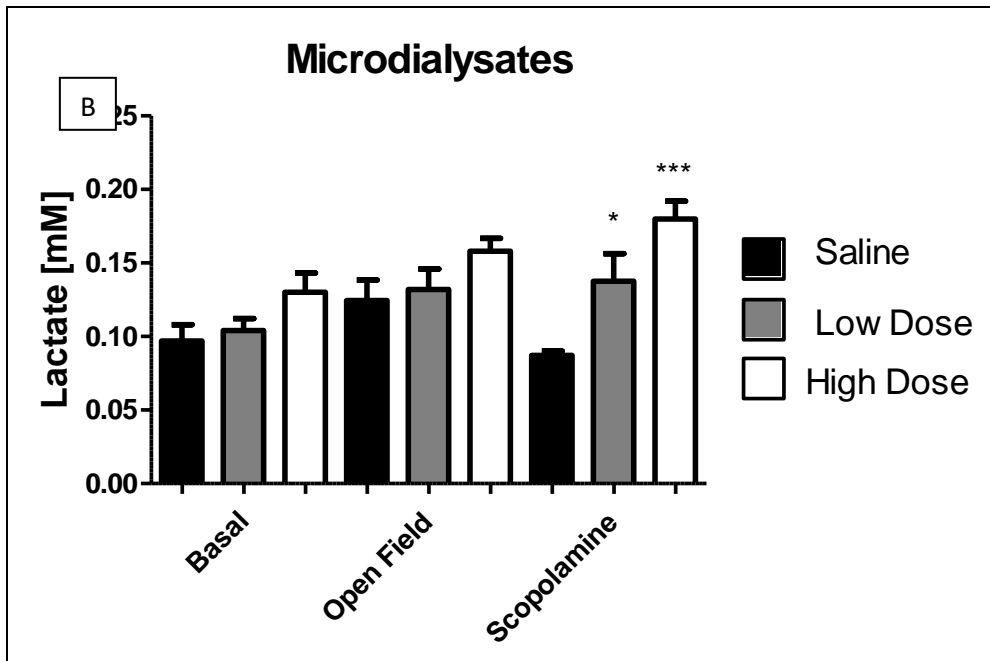
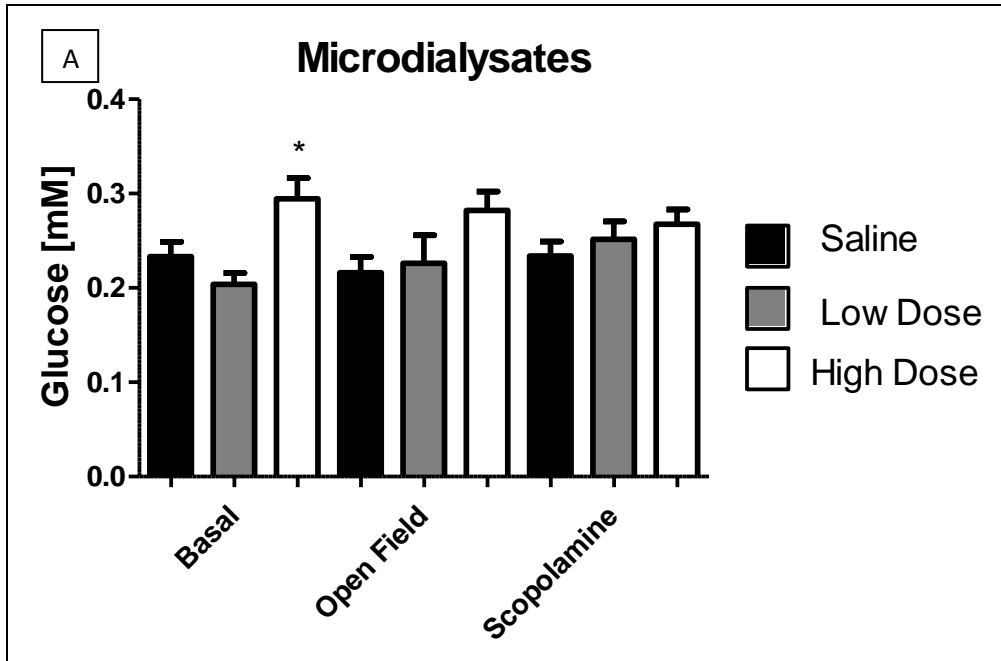


Figure 3. 7. Metabolite levels in striatal microdialysates during behavioral and cholinergic challenges. (A) Glucose; (B) Lactate concentrations were measured in microdialysates under basal conditions, during open field exploration and during infusion of scopolamine.

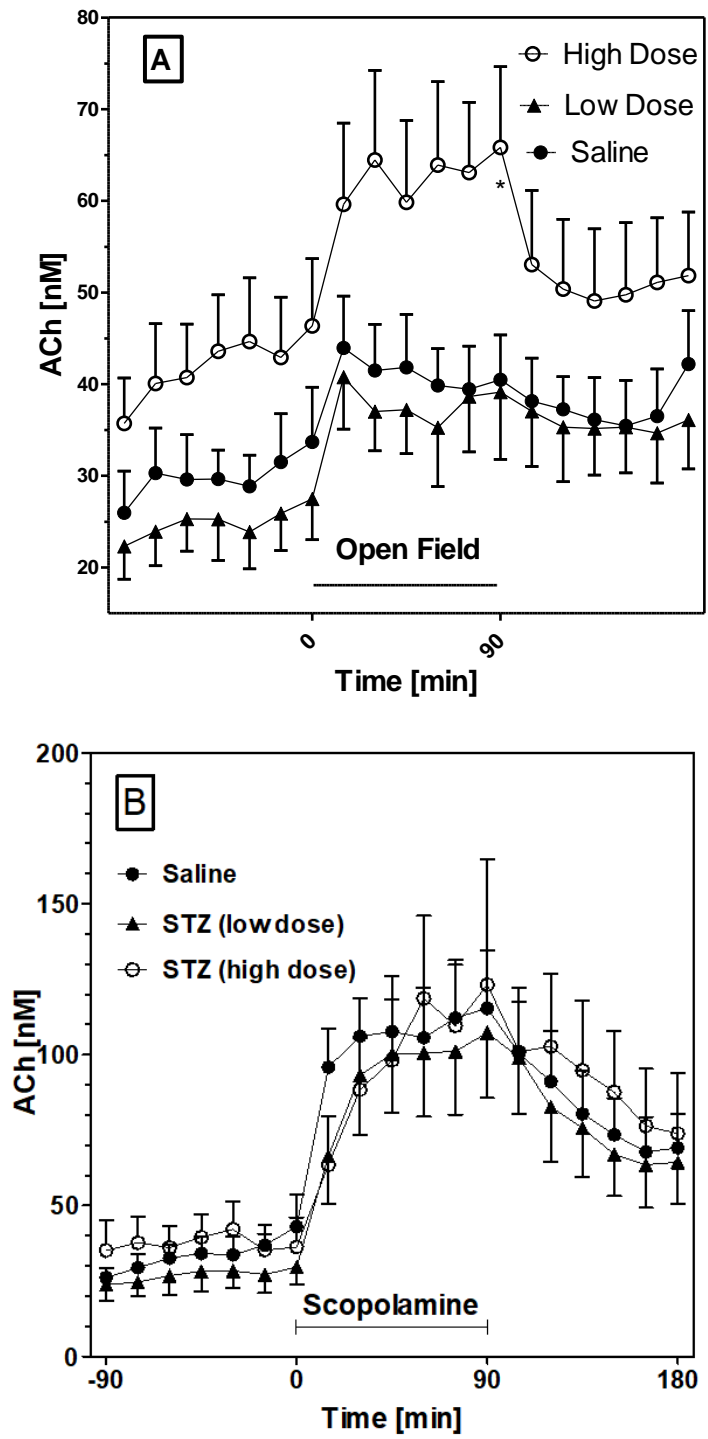


Figure 3. 8. Acetylcholine (ACh) levels in rat striatal microdialysates during behavioral and cholinergic challenges. (A) Open field test (from time 0 until 90 min). (B) Infusion of scopolamine (0.1 μ M) (from time 0 until 90 min). Data are means \pm S.E.M. (N=6-7) and were analyzed by one-way ANOVA followed by Tukey's multiple comparison test.

3.4 In vitro recovery

In vitro-recovery test was performed before microdialysis study in order to ascertain similar quality of the self-built probes. Similar flow rate as used in *in vivo*-experiment (2 μ L/min) and a mixed solution of main analytes of interest (ACh, choline, glucose and lactate) were used. The mixed solution contained ACh 100 nM, Choline 4 μ M, Glucose 1 mM, and Lactate 1 mM which is similar to brain extracellular fluid. Meanwhile, the one-fourth concentration contained ACh 25 nM, Choline 1000 nM, Glucose 0.25 mM, and Lactate 0.25 mM. As seen in Figure 3.4, higher concentration of analytes tended to produce lower *in vitro*-recoveries but the differences were not significant (High vs Low; ACh 9.5 \pm 2.1% vs 10.0 \pm 3.7%; Choline 11.4 \pm 2.1% vs 13.4 \pm 4.6%; Glucose 10.4 \pm 2.4% vs 14.7 \pm 5.4%; Lactate 9.9 \pm 2.5% vs 14.1 \pm 4.3%). Overall, values of 10%-15% were obtained for recoveries.

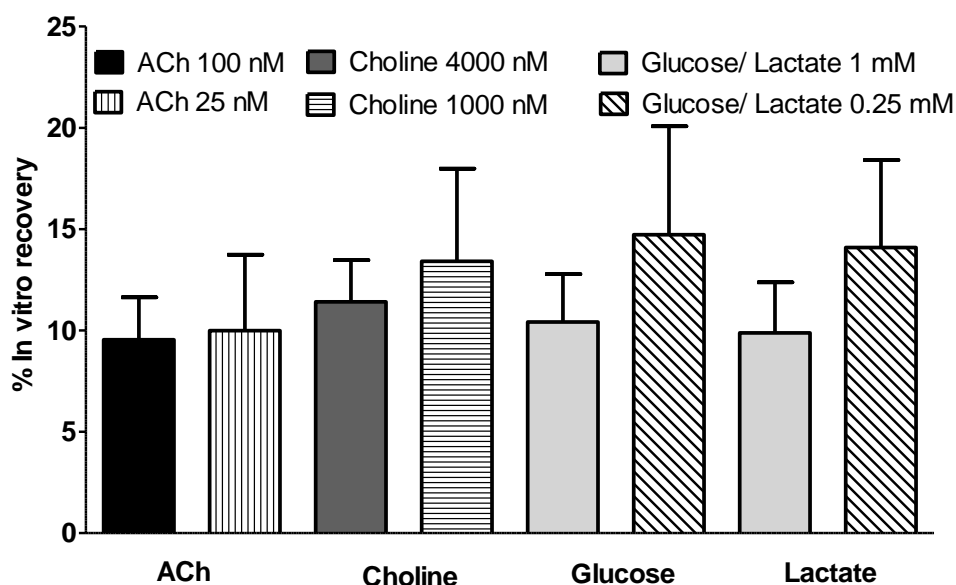


Figure 3. 9. In vitro recovery of acetylcholine, choline, glucose, and lactate. Data are means \pm S.D. (N=5) and were analyzed by unpaired t-test. $p>0.05$.

4 Discussion

4.1 Introduction: Alzheimer's disease and diabetes in the brain

The fact that brain glucose hypometabolism precedes AD clinical symptom (see 1.3.2) and diabetes increases the risk of AD led to an alternative AD hypothesis: AD may resemble diabetes in the brain or “diabetes type 3”. This hypothesis suggests that insulin receptor signaling impairment in the brain results in glucose hypometabolism leading to clinical AD symptoms (de la Monte, 2014). To test this hypothesis, numerous studies used wild type rats receiving an intracerebroventricular administration of streptozotocin (icv-STZ). Streptozotocin (STZ) is a glucosamine-nitrosourea compound commonly used to induce experimental diabetes. After systemic administration, its specific uptake by GLUT-2 glucose transporter induces pancreatic β -cell death through DNA alkylation leading to hyperglycemia and glucose hypometabolism due to impairment of insulin receptor signaling (Grieb, 2016). A similar pathological mechanism was proposed to explain icv-STZ toxicity. It has been suggested that cognitive deficits occur as a result of glucose hypometabolism due to insulin receptor signaling impairment (Osmanovic-Barilar et al., 2015). More than 50 studies (Salkovic-Petrisic et al., 2013) have been published based on this hypothesis, and the authors linked this hypothesis to other AD hypotheses such as $A\beta$ and p-Tau, mitochondrial deficits, and cholinergic deficits.

However, there are some indications of a different pathological mechanism of icv-STZ to peripheral STZ. (1) Insulin in the brain is from periphery because only one group reported insulin gene expression in the brain (Devaskar et al., 1993) (Devaskar et al., 1993). (2) Brain hypometabolism is not easily induced by STZ because brain glucose metabolism is largely insulin-independent and ketone bodies, such as BHB, may serve as an alternative energy substrate in the absence of glucose (3) AD like-pathologies observed in the icv-STZ animal model may not be related to human AD but may reflect pure toxicity. Shoham et al. (2003) suggested that the memory impairment in this model may also be caused by axon and myelin damage of the fornix, anterior hippocampus, and periventricular structure which play an important role in learning and spatial memory (4) Two glucose analogues, 5-thio-D-glucose and 3-O-methyl glucose, which prevent the development of hyperglycemia after peripheral STZ administration, fail to prevent icv-STZ induced memory impairment (Grünblatt et al., 2007) (6) intracerebral administration of a non-polar nitrosamine compound (N-

nitrosodiethylamine), which does not require the GLUT-2 transporter, elicits similar effects as STZ such as impaired spatial learning and increases of lipid peroxidation, cell loss, pro-inflammatory cytokines, and insulin resistance markers (Tong et al., 2009). It follows that this response is not dependent on GLUT-2 but rather reflects the toxicity of the alkylating compound.

Our study aims to investigate to what extent this model mimics human AD, particularly the cholinergic dysfunction which correlates well with clinical symptoms of AD and is the target of current drug therapy (Hampel et al., 2018). Furthermore, glucose metabolism was also investigated to test the glucose hypometabolism hypothesis of this model.

4.2 Methodical considerations: the microdialysis technique

Investigation of the cholinergic function using the microdialysis technique in freely-moving animals is the main focus of this study. Using this technique, the cholinergic transmission can be investigated under cholinergic challenge and without influence from anesthesia. Furthermore, the changes in metabolism during these challenges can also be observed in real time.

For this purpose, a self-built probe with a semi-permeable membrane (pore size of 30 kDa) was used (Lietsche et al., 2014). Besides being inexpensive, a self-built probe enables us to adjust probe size and the dialysis area to a specific brain region of interest. The pore size allows small hydrophilic compounds from brain extracellular space to diffuse passively into the perfusate. Therefore, extracellular ACh level and glucose metabolites (glucose, lactate, pyruvate) can be measured directly without purification. Furthermore, an alternative energy metabolite (beta-hydroxybutyrate/BHB), membrane breakdown markers (extracellular choline and glycerol), and markers of oxidative stress (isoprostanes) can also be measured from microdialysates samples. The uniform quality of the probes was assessed by an *in-vitro* recovery test before the study. Approximately 10% of *in vitro*- recoveries were obtained for ACh, choline, glucose, and lactate (see 3.4).

Microdialysis experiments were conducted 18 hours after probe implantation to restore implantation-induced brain damage, such as impairments of blood-brain barrier permeability and cerebral blood flow, as well as abnormal neurotransmitter release. To minimize gliosis surrounding the probe, which reduces ACh recovery, the experiments were limited up to 2 days after the implantation (König et al., 2017).

However, the microdialysis technique has some limitations. (1) Neuroinflammation markers such as cytokines are too big for our dialysate membrane. (2) A sophisticated analytical method is required for the low limit of detection of analytes, especially for ACh. (3) The method has a poor time resolution of several minutes.

4.3 Methodical considerations: experimental set-up

In the present study, Wistar rats were used because they are less easily stressed and easier to handle than mice (Ellenbroek and Youn, 2016). Most importantly, their brain size is larger than mouse which means that it is easier to target a specific brain region for precise icv injection and microdialysis probe implantation. Furthermore, a bigger brain size means that it is easier to collect a sufficient amount of samples from specific brain regions.

In the present study, we investigated hippocampus and striatum. The hippocampus is innervated by long projecting cholinergic neurons from septum and is severely affected in AD patients. In comparison, striatum contains cholinergic interneurons but is less affected in AD patients. It must be kept in mind that striatal damage may be falsely interpreted as memory impairment during behavioral study because of its function on motor control (see 1.3.1).

We used 5 weeks old rats because 30 days after birth, GLUT-1 and GLUT-3 transporters reach adult level and 90% of adult levels, respectively (Duelli and Wolfgang, 2001). These transporters may mediate STZ cell uptake because of (1) a similar structure of STZ vs. glucose and (2) a low expression of brain GLUT-2 that transport STZ into pancreatic β -cells (Duelli and Wolfgang, 2001).

We used exclusively male rats in this study because they are more sensitive towards icv-STZ (Biasibetti et al., 2017) (Bao et al., 2017). In their studies memory impairment was observed at all-time points (after 2, 4, 5, and 8 weeks) in males but not in females. ChAT level was decreased at all time points (-25%; after 2, 4, and 8 weeks) in males but not in females (only after 8 weeks). By contrast, a similar increase of GFAP level was observed in both males and females, with the highest time point after 2 weeks (+100%) followed by a gradual decline after 4 and 8 weeks (+50%) (Biasibetti et al., 2017). Microscopic structure showed a reduction of dendrite number and dendritic spines (-30%; -50%), as well as synaptic markers, in males but not in females. Furthermore, both A β and p-Tau related markers were also increased in male. These changes were associated with low estradiol levels in both serum and hippocampus of male rats (Bao et al., 2017).

4.4 Icv-STZ distribution and cellular damage

A brief review of damage in the hypothalamus compared to the hippocampus after icv-STZ is described in this section. The hypothalamus is susceptible to STZ damage because it is not only exposed to the ventricular system (third ventricle) but also contains GLUT-2.

Following icv-STZ, the bulk flow of CSF rapidly clears STZ from the injection site resulting in a limited distribution of STZ in ventricle-near parenchyma (see 1.4.2). Tanycytes, i.e. glucose-sensing cells bearing GLUT-2 in the hypothalamus, are exposed to STZ (Grieb, 2016). However, damage to tanycytes as the only factor responsible for AD-like symptoms is unlikely. Hippocampal damage, at least, also plays a role because one hour following icv-STZ, widespread gliosis was observed in the hippocampus. By contrast, intense gliosis was observed only in the third ventricle wall of the hypothalamus (Knezovic et al., 2017). In another study, neurodegeneration has also been detected after 1 day in the near ventricle area of the hypothalamus, septum, and hippocampus (pyramidal neurons of CA1 region) (Santos et al., 2012). Oxidative stress and inflammatory markers were also increased in mouse hippocampus despite preserved histological structure (hematoxylin eosin-staining) (Amiri et al., 2016). Hypothalamus function on feeding regulation was also preserved despite memory impairment. By contrast, icv-alloxan, another GLUT-2 mediated diabetogenic substance, impaired feeding response but failed to impair memory (Ritter et al., 1982) (Sapcanin et al., 2008).

We performed an icv-fast green experiment to obtain pictures of hippocampal and striatal distribution following icv injection. The pictures show the distribution of the dye to the hippocampus and striatum through the nearby ventricle (Fig.3.2). The CA1, CA2, and CA3 regions of hippocampus were stained. By contrast, caudate and putamen of the striatum were minimally stained. Of note, the septal area, the origin of septohippocampal fibers, was not stained. However, fast green dye has a larger molecular weight than STZ (800 Da vs 265 Da) and may diffuse more slowly.

4.5 Early icv-STZ toxicity

In our study, we noted toxicity during the first ten day by measuring weight loss, but all other measurements were done at 3 weeks after icv-STZ. Therefore, in this section, a brief review of early toxicities (<3 weeks) are presented. Of note, these toxicities are related to our markers of interest.

Between seven and ten days following icv-STZ, both cholinergic neurons (ChAT label) in the basal forebrain and cholinergic terminals (VAChT label) in the hippocampus were unchanged (Shoham et al., 2007) despite weight loss (Pathan et al., 2006). Intact memory was also observed despite microglia activation, gliosis, increased markers of ROS, and inflammation in the hippocampus (Shoham et al., 2007) (Rai et al., 2014). By contrast, in another study, memory impairment was reported (Costa et al., 2016). In this study, both hippocampal acetylcholinesterase (AChE) and butyrylcholinesterase (BuChE) activities were increased (+60%) whereas striatal AChE and BuChE activities were unchanged. Indications of hypometabolism were also observed in hippocampus but not in striatum, namely decreased glucose uptake (-30%) and decreased brain ATP level (-50%) (Costa et al., 2016).

After 2 weeks, ChAT activity and ChAT gene expression were also decreased and AChE gene expression was increased. ChAT activities were reduced in the hippocampus and striatum (-20%) (Paidí et al., 2015). Indication of impaired insulin signaling was also observed, namely decreased p-GSK level (-40%) (Osmanovic-Barilar et al., 2015). At this time point, neuronal counts in CA1 and CA3 regions were decreased (-30%) and memory was impaired (Solmaz et al., 2015). TNF- α level was also increased (up to 5x) and was ameliorated by exenatide, a GLP-1 analog (i.p.; 20 μ g/ kg/day) (Solmaz et al., 2015).

This summary demonstrates inconsistent memory impairment and variable cholinergic changes in the first 3 weeks following icv-STZ. Of note, the reported cholinergic markers were incomplete because of no data on extracellular ACh level. There is also an indication of recovered cholinergic neurons. Interestingly, striatum seems to be less affected by icv-STZ toxicity. Moreover, inflammation seems to mediate icv-STZ toxicity because it was detected earlier than insulin signaling impairment.

4.6 Icv-STZ toxicity after 3 weeks

In our hands, icv-STZ toxicity was clearly detectable at day 7-10 after high dose-STZ based on a significant decrease of body weight which is in line with other studies (Paidí et al., 2015) (Pathan et al., 2006). The body weights were still less than control at the end of the experiment (21 days; -17%). Of note, a high dose of STZ (twice 1.5 mg/kg) was needed to induce weight loss.

Our data also show a reduction of hippocampal weight following high dose-STZ. By contrast, Terwel et al. (1995) reported unchanged hippocampal weight despite a decrease in septal

weight (-35%). Another study also reported unchanged hippocampal weight after 5 weeks of a lower dose, but in the presence of unchanged septal weight (STZ 1.5 mg/kg; Prickaerts et al., 1999). In comparison, another study reported a significant brain weight loss (-17%) (Correia et al., 2013). Summarizing, studies vary but most studies found some sort of degeneration in the brain.

4.6.1 Inflammation and neuronal degeneration after icv-STZ

Our study indicates that inflammation and apoptosis occur in the hippocampus. Of note, the CA1 region is the most affected. Compared to other hippocampus regions, damage to the CA1 region gives a better correlation for AD and memory impairment (Adamowicz et al., 2017) (Adler et al., 2018). After 3 weeks, increases of gliosis, DNA fragmentation (up to 3x-7x), and caspase-3 activity (up to 2x) were observed in rat hippocampus, as well as the occurrence of Bax in hippocampal mitochondria (2.5x; Zafeer et al., 2019). In another study, increases of neurodegeneration (+25% until +50%) and IL-10 labeled cells (+30% up to 2x) were observed in all hippocampus regions (CA1, CA2, CA3, DG). By contrast, IL-6 labeled cells were increased in the CA1 and CA2 regions only (up to 2x) (Majkutewicz et al., 2016). Furthermore, gliosis have been reported in several studies (Santos et al., 2012) (Majkutewicz et al., 2016) (Knezovic et al., 2017).

In our hands, following high dose icv-STZ, reactive astrocytes were detected in the dorsal and ventral hippocampus on day 21. Glial fibrillar acidic protein (GFAP) was used as astrocyte marker because of its better correlation with AD progression than other astrocyte markers such as S100 β (Perez-Nievas and Serrano-Pozo 2018). Increased GFAP indicates reactive astrocytes which were found in our high dose rats, especially in the CA1 region. Of note, our data was not able to distinguish between increased GFAP expression and increased astrocyte proliferation. Indeed, in a post mortem study, reactive astrocytes were not associated with their proliferation (Perez-Nievas and Serrano-Pozo 2018).

We also observed another sign of toxicity by Fluoro-Jade C (FJ) staining in the CA1 region of the hippocampus. FJ is an acidic dye postulated to label basic molecules of degenerating neurons (Schmued et al., 2015). Besides a delayed neurodegeneration, the lack of staining in some of the icv-STZ treated rats might be caused by loss of FJ reactive compound. Unfortunately, the molecular target of FJ is unknown (Santos et al., 2012). In another study, an

apoptosis marker (p53 positive cells), which was previously detected on day 7 after icv-STZ, was diminished after 2 weeks (Lester-Coll et al., 2006).

Although the changes were not statistically significant, some *in vivo*-signs of toxicities were also revealed in our microdialysis study. Icv-STZ dose-dependently increased extracellular choline levels in the hippocampus and extracellular glycerol levels in the striatum. In the striatum, only the high dose of STZ increased extracellular choline. Both extracellular choline and glycerol levels are well-known markers of membrane damage produced by degradation of phospholipids, respectively (De Lima Oliveira et al., 2014) (Klein, 2000).

Taken together, our findings demonstrate that the usual dose of icv-STZ induces severe toxicity starting from day 1 until day 10 after icv-STZ followed by a recovery period. However, the signs of neurodegeneration and gliosis were clearly visible even after three weeks. After icv-STZ toxicity was confirmed as structural changes, we investigated whether these changes were followed by changes in energy metabolism and cholinergic neurotransmission.

4.6.2 Mitochondrial dysfunction

In cholinergic neurons, mitochondria play a pivotal role not only for ATP production but also for generation of acetyl-CoA, a precursor for acetylcholine (Ortiz and Swerdlow, 2018). Following cell uptake, glucose as the preferred energy substrate in the brain undergoes glycolysis in the cytosol and produces pyruvate. Pyruvate is then transported into mitochondria and converted to acetyl-CoA by pyruvate dehydrogenase. Acetyl-CoA then feeds the citric acid cycle. FADH₂ and NADH produced during glycolysis and citric acid cycle undergo oxidation in mitochondrial complexes resulting in the development of a proton gradient across the mitochondrial intermembrane space. The proton gradient serves as the driving force for ATP production. Of note, cytosolic acetyl-CoA is generated from mitochondrial citrate produced during the citric acid cycle.

In the present study, we measured respiratory function of each mitochondrial complex in both striatum and hippocampus of the same rats. For this purpose, we used high-resolution respirometry combined with a substrates-uncoupler-inhibitors titration (SUIT) protocol that enabled us to measure each electron transport chain (ETC) complex activity simultaneously (Hagl et al., 2013). Furthermore, we also measured the quality of the mitochondria by the addition of exogenous cytochrome C (Cyt C). Increased respiration following the addition of exogenous Cyt C indicates mitochondrial membrane damage which may occur during

mitochondria isolation steps. Our data show similar membrane damage in both groups indicating a similar quality of mitochondria between saline and icv-STZ.

To normalize ETC activities, we used citrate synthase (CS) activity. Even though CS activity is less correlated with mitochondrial content than cardiolipin, it is widely used and represents intact mitochondria, therefore, single mitochondrial respiration can be calculated (Larsen et al., 2012) (Eigentler et al., 2015) (Pohland et al., 2018). After normalization to hippocampal weight, we found an increase of CS activity which may indicate increased mitochondrial content. The fact that protein level per mg hippocampus did not increase or even decreased indicates that reduced hippocampal weight was not simply caused by loss of extracellular volume (data not shown). By contrast, protein level in the mitochondrial sample was increased following high-dose icv-STZ (data not shown).

Our hippocampal mitochondrial fraction revealed a decrease of respiration in all complex activities (ca. 14%; normalized by CS activity) that was significant only on complexes II and IV. Similarly, several studies have reported signs of mitochondrial impairment after 3 weeks. Mitochondrial complex I, II, and IV protein levels were decreased in the hippocampus (-30%, -30%, -75% respectively; normalized to protein) whereas complex III and V protein levels were unchanged (Zafeer et al., 2019). Another study also showed a decreased complex I respiration (normalized by protein level) in hippocampal mitochondria (ca. -55%; Paidi et al., 2015). These changes have also been reported after 5 weeks as shown by reduced mitochondrial respiratory function (complex I and II) in both cortical and hippocampal mitochondria (ca. -30%; normalized by tissue weight; Correia et al., 2013).

The increased CS activities in our hippocampal data may indicate changes in mitochondrial biogenesis following mitochondrial damage. This is in line with another study that reported increased mitochondrial fission as shown by decreased Mfn2 (-40%; Zafeer et al., 2019) and increased Drp1 protein levels (up to 2x by Paidi et al., 2015; up to 7x by Zafeer et al., 2019). PGC1 α level was also decreased in the hippocampal nuclear fraction (-30%; Zafeer et al., 2019). PGC1 α is a master regulator of mitochondrial biogenesis which can shift the balance of Drp and Mfn expression in favor of mitochondrial fusion. Of note, an increased number of swollen mitochondria after Ca-challenge following icv-STZ have been reported (up to 2x; Correia et al., 2013).

Decreased complex IV activity in the presence of increased citrate synthase activity was also reported in 8 month old APP/PS2 AD mice (Rhein et al., 2009). In their study, the decrease of

complex IV activity was associated with A β pathology. Furthermore, they also reported a decrease in complex I activity which was associated with tau pathology.

Interestingly, our striatal data show preserved mitochondrial respiration and biogenesis as shown by preserved complexes and CS activity. This is in line with another study that reported region-specific mitochondrial changes in transgenic AD mice (Rhein et al., 2009). However, our study was not able to distinguish which cell type was measured.

In comparison, postmortem AD showed specific changes both on the brain region and complexes. A 50% decrease in complex IV activity was observed in the hippocampus and temporal cortex but not in the frontal cortex and cerebellum. By contrast, complex I, II, and citrate synthase activity were unchanged (Maurer, et al., 2000).

4.6.3 Oxidative stress following icv-STZ

Using an ELISA method, we measured a marker of lipid peroxidation: F2-isoprostanes, specific end products of the peroxidation of arachidonic acid (Halliwell and Whiteman 2004). F2-isoprostanes are quite specific oxidative stress markers for AD as it was not increased in Parkinson's disease and schizophrenia (Pratico et al., 1998). In their study, 8,12-iso-iPF 2α -VI (an isoprostane compound) level in CSF of normal brain is ca.10 pg/mL detected by GC/MS. Despite different analytical method, a similar level of was obtained in CSF of normal patient analyzed by EIA method which detects more than 1 compound (Mir et al., 2014).

ELISA detection of F2-isoprostanes in microdialysates has several advantages despite being similar minor end products of peroxidation. (1) ELISA detection of F2-isoprostanes is more sensitive than ELISA detection of malondialdehyde (MDA) (pg/mL vs ng/mL). (2) It is more representative to *in vivo*-oxidation because it measures other arachidonic acid -catalyzed products rather than a single compound by GC/MS (Ito et al., 2019). (3) There are no influences from lipid content in the diet. (6) F2-isoprostanes in microdialysates cannot be produced by *ex vivo* auto-oxidation (Montuschi et al., 2004).

The isoprostane level in our striatal microdialysates was unchanged. This may be caused by preserved mitochondrial function in the striatum as described before (4.3.2). A slight reduction in the low dose group seems to be in the normal range because isoprostane levels in the hippocampal microdialysates were between 14-84 pg/mL one day after lithium administration in rats (Imran, 2015). This comparison may not be entirely correct but extracellular isoprostane level in the brain of normal rats has never been reported. Another factor that may mask the

increase of isoprostane level is a higher metabolism (Halliwell and Whiteman 2004). We conclude from these data that icv-STZ induces only moderate oxidative stress.

By contrast, in another study using thiobarbituric acid (TBA) assays, lipid peroxidation was increased in rat hippocampus (+50%; Ishrat et al., 2006). However, the validity of the TBA assays has been questioned because many TBA reactive materials are not related to lipid peroxidation *in vivo* (Halliwell and Whiteman 2004).

4.6.4 ATP level and mitochondrial membrane potential

As discussed before, this model shows decreased mitochondrial respiration. A decrease of mitochondrial respiration may result in a decreased proton gradient between the intermembrane space and the mitochondrial matrix leading to a decreased driving force of complex V to generate ATP. Even though we did not measure ATP level, indications of decreased ATP levels have been reported. After 3 weeks, ATP levels were slightly decreased in the cortex (-15% by Lannert and Hoyer 1998; -25% by Ishrat et al., 2006) and hippocampus (-25%; Ishrat et al., 2006). After 6 weeks, the reduction was more pronounced in the hippocampal mitochondrial fraction (-50%; Du et al., 2015). After 9 weeks, the ATP level was still decreased in both cortex and hippocampus (-15%; Hoyer and Lannert 2007). Furthermore, hippocampal mitochondrial membrane potential was also decreased (-25%; Zafeer et al., 2019) that was persisted even after 6 weeks (-50% each; Du et al., 2015). From these data, it may be expected that energy metabolism in the brain is severely impaired. By measuring individual energy metabolites, we hoped to delineate whether STZ has a specific effect e.g. on glycolysis, or whether it has unspecific (toxic) effects.

4.6.5 Energy metabolites

In the following section, we will discuss the results of the energy metabolites level in our microdialysate sample from freely moving animal which consists of glucose, lactate, and β -hydroxybutyrate (BHB). Extracellular glucose and lactate were measured from both hippocampus and striatum. On the other hand, extracellular pyruvate and BHB were measured in either only striatum or hippocampus.

4.6.5.1 Glucose

As discussed in 4.6.2, glucose metabolism is important, especially for cholinergic neurons. We measured extracellular glucose level that reflects the balance between blood supply and brain cell uptake (De Lima Oliveira et al., 2014). Glucose uptake from blood depends on blood glucose level and cerebral blood flow (CBF). In the icv-STZ model, normal blood glucose levels have been reported in many studies (e.g. Santos et al., 2012).

Our data show that extracellular glucose levels remained relatively unchanged 21 days after icv-STZ both in the hippocampus and striatum. Small increases of extracellular glucose in both hippocampus and striatum might be caused by cell death because neurodegeneration was observed in the CA1 region. Clearly, icv-STZ causes no major change in glucose availability in the brain.

In our study, the behavioral and pharmacological stimulation also did not change extracellular glucose levels significantly which is in line with another study in a different AD model (Hartmann et al., 2010). It is worth noting that the hippocampus responded more than striatum to behavioral stimulation, possibly through increasing blood supply during the exploration of the new environment. This indicates that icv-STZ did not alter the ability of the brain to respond to cholinergic stimulus. Taken together, our findings do not support the “diabetes in the brain” hypothesis because a significant increase in extracellular glucose level was not observed.

Our finding corroborates other studies. 3 weeks after icv-STZ, the extracellular glucose level in cerebrospinal fluid (CSF) was slightly decreased (-10%; Knezovic et al., 2018). In a longer period, after 42 days and 3 months, glucose uptake was also slightly decreased in the hippocampus as measured by (14C)-2-deoxyglucose uptake method (-10%; Duelli et al., 1994) and FDG-PET study (-7%; Knezovic et al., 2018). Of note, the above-mentioned studies were done under anesthesia which may mask the real condition.

4.6.5.2 Lactate

Lactate in the brain is mainly produced by astrocytes and transported to extracellular space through MCT1 and MCT4 (monocarboxylate-transporters) from which it is then taken up by neuronal MCT2 as an alternative energy substrate during neuronal activation (Dienel, 2012).

We found a slight decrease in the extracellular lactate level after both doses of icv-STZ in the hippocampus which was slightly increased during exploration in the open field in all groups. This slight increase might be caused by higher neuronal activity and is accompanied by

increased ACh release. Accordingly, another AD model (APPSWE/PS1dE9 mice) also showed decreased basal extracellular lactate level which were increased during higher neuronal activity in hippocampus (Hartmann et al., 2010).

The slight reduction of extracellular lactate after icv-STZ might be caused by a dysfunction of lactate release by astrocytes due to their transformation to reactive astrocytes. In APP/PS1 transgenic mouse model of AD with hippocampal gliosis, reduction of hippocampal lactate levels were associated with reductions of lactate transporter expressions (MCT1, MCT2, MCT 4) (Zhang et al., 2018). Furthermore, decreased intracellular lactate levels were also observed in a non-transgenic AD model after intrahippocampal injection of Aβ peptide in the presence of decreased MCT2 expression (Lu et al., 2015).

By contrast, our striatal data show that both extracellular lactate and pyruvate levels were increased dose-dependently after icv-STZ. The data did not, however, reach statistical significance.

4.6.5.3 β-hydroxybutyrate (BHB)

BHB is an alternative energy substrate for the brain. It is a ketone body produced in liver mitochondria during brain glucose deprivation, such as fasting (Cahill, 2006). Fasting increases fatty acid oxidation in the liver followed by increased acetyl-CoA production, leading to increased systemic BHB level. BHB is then transported into the brain by MCT1 resulting in an increased BHB level in brain extracellular fluid. In brain mitochondria, BHB is then converted to acetyl-CoA which feeds the citric acid cycle (White and Venkatesh, 2010). Similar to lactate, BHB may also be a preferred energy substrate to glucose but only when the level is very high (Dienel, 2012).

We measured the BHB level because indications of glucose hypometabolism have been reported in the hippocampus. However, our data show preserved extracellular BHB level which indicates preserved plasma BHB level.

4.6.6 STZ mechanism of toxicity

Since the mechanism of STZ transport into brain cells is unknown (Grieb, 2016), we used bioinformatics data (Fig. 4.1. and 4.2) to investigate the possibilities (Yuliani et al., 2020). Fig. 4.1 shows that both GLUT-2 and GLUT-4 transporters are expressed in a very low amount in the brain. By contrast, both GLUT-1 and GLUT-3 transporters which have been known to mediate glucose transport in astrocytes and neurons, respectively, are highly expressed in the brain, with GLUT-3 as the highest. Therefore, it is more likely that cellular uptake of STZ in the brain is mediated by GLUT-1 and GLUT-3 as has been suggested by Deng et al. (2009). In their study, both GLUT-1 and GLUT-3 protein levels were decreased in the cerebrum (-50% and -30%, respectively Deng et al., 2009) after 3 weeks of exposure to STZ. However, in another study, both GLUT-1 and GLUT-3 expressions were unchanged after 6 weeks, which was, however, investigated in female mice that is less sensitive to icv-STZ (Chen et al., 2012). Therefore, the non-specific cell death such as in the CA-1 region of the hippocampus and astrocyte activation may explain the decrease of mitochondrial respiratory function and consequently, in glucose uptake in the hippocampus.

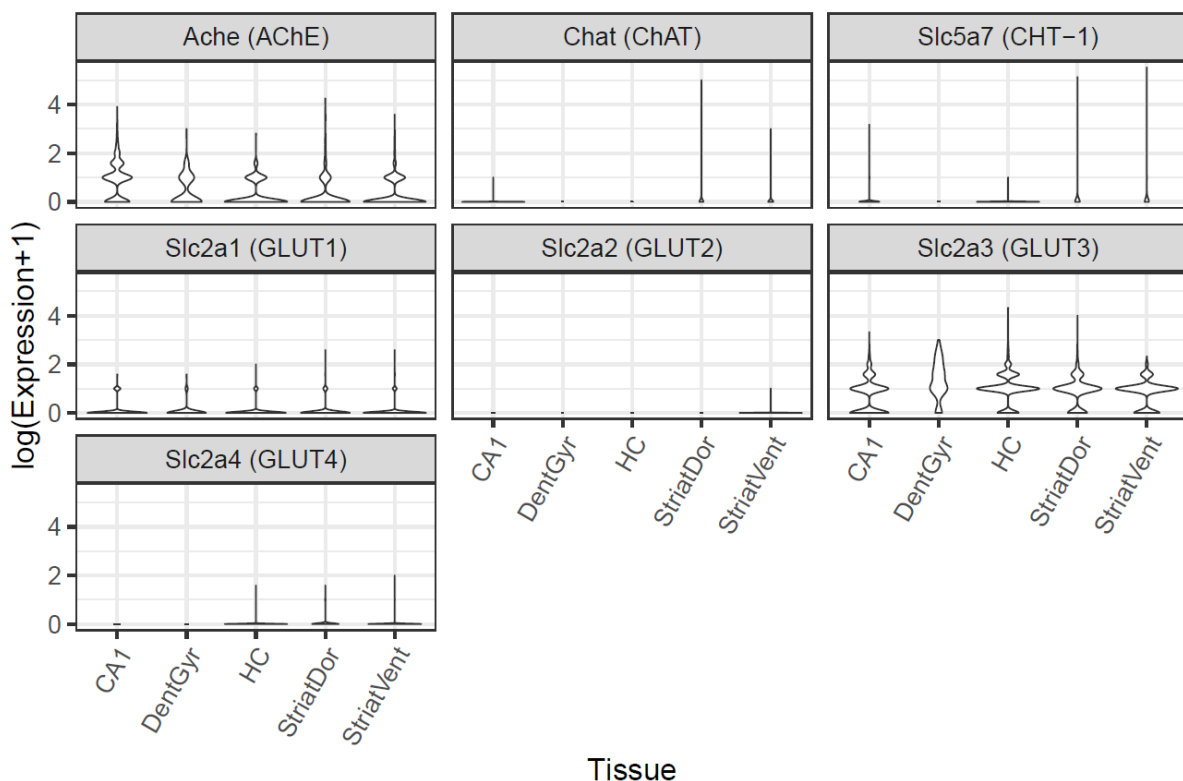


Figure 4. 1. Single-cell expression of cholinergic-associated transcripts and glucose transporters in neurons of hippocampus and striatum of the adult mouse. Hippocampal regions: CA1, dentate gyrus (DentGyr), complete hippocampus (HC); striatal regions: dorsal striatum (StriatDor), ventral striatum (StriatVent) (Yuliani et al., 2020). The figure is kindly provided by Sebastian Lobentanzer.

4.6.7 Cholinergic parameters

In this section, several cholinergic markers (ChAT, AChE, and HACU) will be discussed first followed by a discussion of extracellular ACh levels. Data of the cholinergic markers are needed to understand the meaning of extracellular ACh levels.

4.6.7.1 ChAT activity

ChAT catalyzes the synthesis of ACh from choline and acetyl-CoA in the cholinergic neuron (see 1.3.1). Therefore, it represents cholinergic neurons, and decreased ChAT may lead to decreased ACh synthesis. However, ChAT is not rate-limiting for ACh synthesis, and studies showed preserved ACh synthesis in mice that had half the normal amount of ChAT (Brandon et al., 2004).

In our hands, ChAT activity was decreased significantly (-30%) in the hippocampus after icv-STZ but was unchanged in striatum corroborating other studies. In rat striatum, ChAT activity was unchanged despite increased gliosis marker (Prickaerts et al., 1999). On the other hand, ChAT activity was decreased in the hippocampus (between -50% and -23%) (Ishrat et al., 2006) (Terwel et al., 1995) (Prickaerts et al., 1999).

In the rat medial septum where hippocampal cholinergic neurons originate, ChAT activity was preserved after STZ (Terwel et al., 1995) (Prickaerts et al., 1999), as well as in cholinergic neurons (ChAT label) (Shoham et al., 2007). Apparently, the septum was less affected than the hippocampus which is in contrast to human AD.

However, the ChAT profile was similar between icv-STZ and AD patients in brain regions which were sensitive to AD. Similar to our study, a 30% decrease of ChAT activity was reported 4 hours post mortem in the cortex, a brain region innervated with long projecting cholinergic neurons. Similar to our striatal data, ChAT activity was also unchanged in the putamen of AD patients (Slotkin et al., 1994).

4.6.7.2 AChE activity

The degradation of ACh is catalyzed by acetylcholinesterase (AChE) and non-neuronal (less-specific) butyrylcholinesterase (BuChE). Increased AChE activity may lead to decreased extracellular ACh levels, and decreased AChE activity may lead to increased extracellular ACh levels. Therefore, information on AChE activity is needed to avoid misinterpretation

because increased ACh levels may be caused by either increased cholinergic neuronal firing or simply inhibition of AChE activity.

In our study, we measured the specific AChE activity by inhibiting BuChE activity with iso-OMPA. In our hands, AChE activity was decreased significantly in the hippocampus (-30%) but was increased in the striatum (+7%). By contrast, in other studies, hippocampal AChE activity was increased (+60% by Ishrat et al., 2006 and +40% by Santos et al., 2015) and persisted even after 7 weeks (+40%; Biasibetti et al., 2013). However, the studies did not inhibit BuChE activity. Indeed, in another study, hippocampal AChE expression was decreased (-25%) but BuChE expression was increased (+25%) in the hippocampus 6 weeks following icv-STZ. These findings were obtained from female mice which have been reported to be less sensitive towards icv-STZ toxicity (see 4.3.4.) (Chen et al., 2012). Furthermore, increased hippocampal BuChE activity was also reported in early toxicity studies (Costa et al., 2016) (see 4.5). In this study, however, the hippocampal AChE activity was also increased despite preserved striatal AChE activity.

In comparison to human AD, icv-STZ is different because hippocampal AChE was greatly reduced in AD patient postmortem and a small reduction in AChE activity was reported in the caudate, part of the striatum (Davies 1979).

4.6.7.3 HACU (high affinity of choline uptake)

High-affinity choline transporter (CHT-1) activity or high-affinity of choline uptake (HACU) is one of the rate-limiting steps of ACh synthesis (will be discussed later in 4.6.8). CHT-1 belongs to the Na⁺-dependent glucose transporter family, encoded by the SLC5A7 gene, and is responsible for choline uptake in cholinergic nerve endings (Ribeiro et al., 2016). During neuronal firing, CHT-1 translocates to the synaptic membrane. Therefore, in this study, we used synaptosomal HACU to represent neuronal firing. In our hands, HACU was unchanged in the hippocampus but was increased in the striatum after high dose icv-STZ (+30%).

In comparison to human AD, a completely different HACU profile was observed between icv-STZ and human AD. HACU was increased in the cortex but was unchanged in the striatum of AD patients (Slotkin et al., 1994).

4.6.7.4 Acetylcholine

Extracellular acetylcholine represents cholinergic transmission. Therefore, ACh data completes the cholinergic markers data. In our hand, basal values of extracellular ACh level in the hippocampal microdialysates were unchanged, even slightly increased in the striatum. During the open field test, the exploration of a new environment activates cholinergic transmission as shown by increased ACh levels in the microdialysate samples. This activation is associated with spatial orientation in the hippocampus and increased motor activity in the striatum (König et al., 2017). In our hands, different brain regions show slightly different pictures. Hippocampus responded more to new environment stimulation than striatum. However, the responses were similar in all groups indicating preserved cholinergic transmission after icv-STZ.

On day 2, we investigated the maximum release of ACh in both groups using scopolamine, a muscarinic blocker of M2/M4 autoreceptors. Because M2/M4 receptor activation limits ACh release, scopolamine infusion disinhibits ACh release leading to a maximum release of ACh (Mohr et al., 2013). Both brain regions show a similar several-fold increase of ACh levels during the scopolamine test. Again, the response of the cholinergic transmission was similar in all groups. Of note, our basal extracellular ACh level was lower in the hippocampus than striatum (4x) corroborating another study (Day et al., 1991) (see 1.3.1).

4.6.8 Summary of cholinergic changes and its relation to bioinformatics data

In our hands, extracellular ACh levels correlate well with HACU. In the hippocampus, both ACh and HACU were unchanged. On the other hand, HACU was increased in the striatum that indicated cholinergic neuronal firing leading to a slight increase of ACh level in the striatal microdialysates sample.

A better correlation between ACh and HACU than other cholinergic markers was also found in other studies. (1) ChAT. Even though the decrease of ChAT has been associated with decreased ACh level, a recent study revealed that ChAT is present in kinetic excess because a 50% reduction of ChAT activity in ChAT haploinsufficiency resulted in preserved ACh content (Brandon et al., 2004). (2) AChE. AChE heterozygous mice with a 40-50% decrease of AChE activity showed a 100% increase of ACh release in the presence of a 50% increase of HACU activity (Mohr et al., 2013). (3) ACh. Increased striatal ACh release in the presence of increased HACU has been reported in transgenic mice expressing human α -synuclein (König et al.,

2018). Of note, in another AD model, both Hippocampal HACU and ACh release were preserved in APPSWE/PS1dE9 mice (Hartmann et al., 2010).

The correlation between cholinergic markers as well as glucose transporters are shown in Fig. 4.2 (Yuliani et al., 2020). The correlation was obtained from bioinformatics data and the results are shown as a value between -1 and 1. The higher the correlation, the more closer the numbers to 1. It shows that ChAT and CHT-1 (SLC5A7) are highly co-expressed in all tissues, all neurons, and cholinergic neurons (defined by VACHT expression) whereas AChE is not exclusively cholinergic. Furthermore, GLUT3 has a significant correlation with cholinergic genes while GLUT2 and 4 do not.

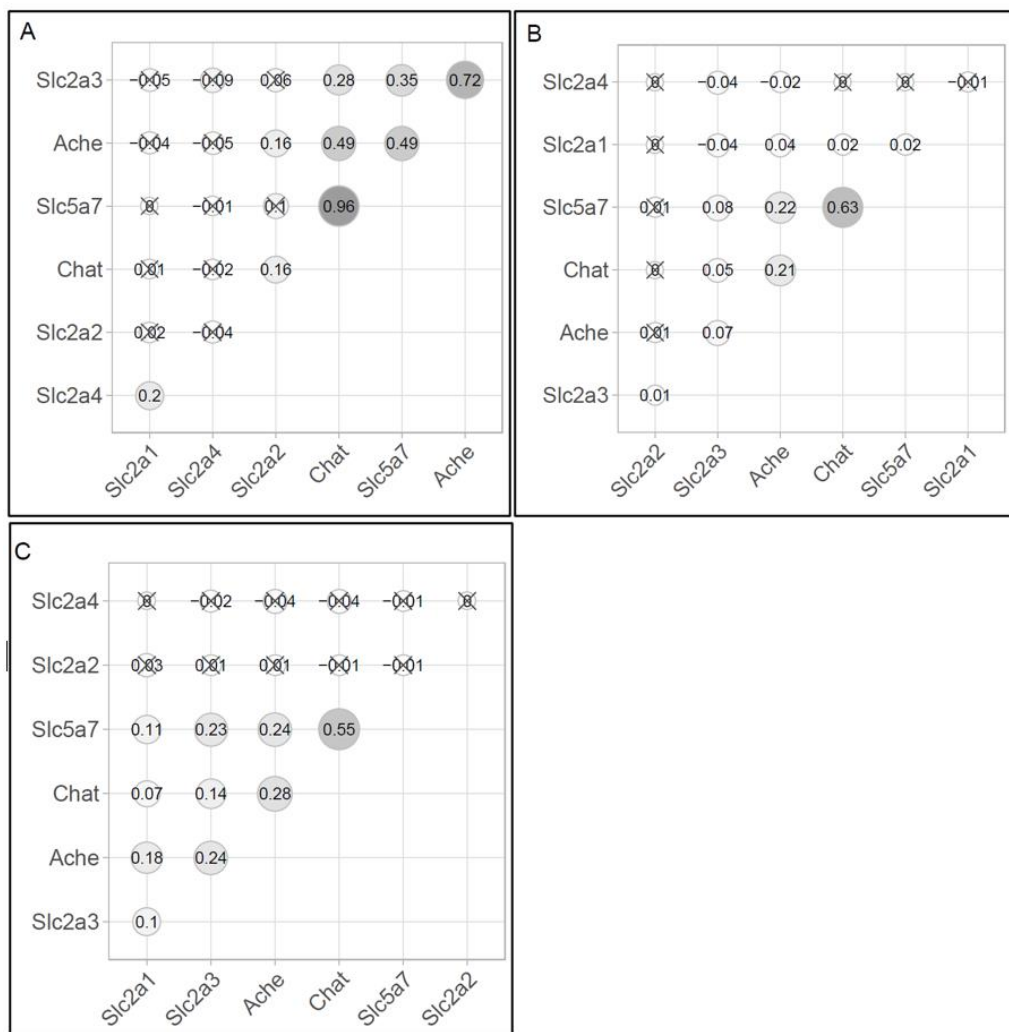


Figure 4. 2. Correlation of expression of cholinergic-associated transcripts and glucose transporters in single cells of the murine nervous system. Size and depth of color of circles denote strength of correlation (range: -1 to 1). Non-significant correlation coefficients ($p > 0.05$) are crossed out. (A) Correlation of transcripts in all tissues (cell-type-level). (B) Correlation in all neurons (single-cell-level). (C) Correlation in cholinergic neurons (single-cell-level) as determined by expression of the vesicular ACh-transporter (VACHT/SLC18A3) (Yuliani et al., 2020). The figure is kindly provided by Sebastian Lobentanzer.

4.6.9 Brain region specificity

A different mechanism of icv-STZ toxicity seemed to occur in different brain regions. Compared to the striatum, the hippocampus seems more prone to icv-STZ toxicity as shown by decreased cholinergic markers (ChAT and AChE) and decreased mitochondrial respiration despite normal availability of extracellular glucose and 3-hydroxybutyrate. However, this condition did not change acetylcholine release as the remaining cholinergic nerve endings were able to fire normally as shown by intact HACU after icv-STZ. In their study, Terwel et al. (1995) suggest that STZ diffused poorly to cholinergic neurons in the septum; this resulted in preserved septal ChAT activity despite decreased hippocampal ChAT activity. Since the hippocampus receives cholinergic innervation from the septum, decreased hippocampal ChAT activity might be caused by axonal and nerve terminal damage. We suggest that the damage was mediated by GLUT-3 because of its higher correlation to a cholinergic neuron than other GLUTs (Fig. 4.2). On the other hand, short projecting cholinergic interneurons in the striatum are relatively spared from STZ toxicity. In our striatal study, icv-STZ only leads to increased cholinergic neuronal firing while lactate release and mitochondrial respiration were preserved. This condition might be caused by either limited diffusion of STZ to cholinergic neurons in the striatum or less sensitivity of the neurons towards STZ. Another study also reported that striatum was relatively spared from icv-STZ toxicity as shown by preserved striatal volume and neuronal density (Kraska et al., 2012).

Taken together, our data indicate that the cholinergic deficit reported in this AD model is either not present (striatum) or at least incomplete (hippocampus). Furthermore, microscopic observation on the hippocampal cholinergic marker (VAcHT label) was unchanged after 8 weeks (Shoham et al., 2007). However, compared to human AD, icv-STZ shows similar brain region specificity with respect to these two brain regions.

4.6.10 Role of other neurotransmitters

While the reasons for the slight increase of ACh after a high dose of icv-STZ in the striatum are not known, we speculate that they may be caused by an increased extracellular glutamate level and a decreased extracellular GABA level. This idea is supported by another study that reported an increased glutamate level and a decreased GABA level in hippocampal homogenate 22 days after icv-STZ (Arora and Deshmukh 2017). Besides, increased glutamate and decreased GABA levels were accompanied by increased glutamatergic neuronal count and decreased GABAergic neuronal count 14 days after icv-STZ in ventrolateral preoptic area

(VLPO) and parabrachial nucleus (PBN) (Cui et al., 2018). In comparison, another AD model induced by acute icv A β toxin showed an increase of extracellular glutamate but an unchanged GABA level (O'Shea et al. 2008). Since GABAergic interneurons and GABAergic terminals predominate in the CA1 of the hippocampus and striatum, respectively (Müller and Remy 2018) (Gonzales and Smith, 2015) (see 1.3.1), we speculate that GABAergic neuronal damage followed by a reduction of inhibitory neurotransmission may indirectly influence cholinergic transmission.

4.7 Conclusion

Centrally administered STZ does not cause diabetes in the brain, but mainly causes unspecific toxicity. STZ toxicity was clearly seen in the reduction of body weight gain, histopathological changes in hippocampus such as astrogliosis and neurodegeneration, and some impairment of energy metabolism three weeks after icv-STZ administration. In contrast, the cholinergic transmission seemed to be well preserved in both hippocampus and striatum but with a different profile in some biomarkers. Cholinergic neurons in the striatum seemed to be well preserved from STZ toxicity whereas minor damage to the hippocampal cholinergic terminals occurs. Overall, the icv-STZ model fails to mimic cholinergic dysfunction, an important part of AD pathology. This model is more suitable for an animal model of hippocampal gliosis with CA1 region injury.

5 References

- Adamowicz DH, Roy S, Salmon DP, Galasko DR, Hansen LA, Masliah E, and Gage FH (2017) Hippocampal β -Synuclein in Dementia with Lewy Bodies Contributes to Memory Impairment and Is Consistent with Spread of Pathology. *J Neurosci* 37(7):1675–84.
- Adler DH, Wisse LEM, Ittyerah R, Pluta JB, Ding SL, Xie L, Wang J, Kadivar S, Robinson JL, Schuck T, Trojanowski JQ, Grossman M, Detre JA, Elliott MA, Toledo JB, Liu W, Pickup S, Miller MI, Das SR, Wolk DA, and Yushkevich PA (2018) Characterizing the Human Hippocampus in Aging and Alzheimer’s Disease Using a Computational Atlas Derived from Ex Vivo MRI and Histology. *Proc Natl Ac Sci USA* 115(16):4252–57.
- Amiri S, Haj-Mirzaian A, Momeny M, Amini-Khoei H, Rahimi-Balaei M, Poursaman S, Rastegar M, Nikoui V, Mokhtari T, Ghazi-Khansari M, Hosseini MJ (2017) Streptozotocin Induced Oxidative Stress, Innate Immune System Responses and Behavioral Abnormalities in Male Mice. *Neuroscience* 340:373-383.
- Arnold SE, Arvanitakis Z, Macauley-Rambach SL, Koenig AM, Wang HY, Ahima RS, Craft S, Gandy S, Buettner C, Stoeckel LE, Holtzman DM, and Nathan DM (2018) Brain Insulin Resistance in Type 2 Diabetes and Alzheimer Disease: Concepts and Conundrums. *Nat Rev Neurol* 14(3):168–81.
- Arora R and Deshmukh R (2017) Embelin Attenuates Intracerebroventricular Streptozotocin-Induced Behavioral, Biochemical, and Neurochemical Abnormalities in Rats. *Mol Neurobiol* 54(9):6670–80.
- Baek SH, Park SJ, Jeong JI, Kim SH, Han J, Kyung JW, Baik SH, Choi Y, Choi BY, Park JS, Bahn G, Shin JH, Jo DS, Lee JY, Jang CG, Arumugam TV, Kim J, Han JW, Koh JY, Cho DH, and Jo DG (2017) Inhibition of Drp1 Ameliorates Synaptic Depression, A β Deposition, and Cognitive Impairment in an Alzheimer’s Disease Model. *J Neurosci* 37(20):5099–5110.
- Ballinger EC, Ananth M, Talmage DA, and Role LW (2016) Basal Forebrain Cholinergic Circuits and Signaling in Cognition and Cognitive Decline. *Neuron* 91(6):1199–1218.
- Balsinha C, Gonçalves-Pereira M, Iliffe S, Freitas JA, Grave J (2019) Health-Care Delivery for Older People with Dementia in Primary Care. In: de Mendonça Lima C, Ivbijaro G (eds) *Primary Care Mental Health in Older People*. Springer, Cham.
- Banks (2014). *Insulin in the Brain : There and Back Again*. *Pharmacol Ther* 136(1):82–93.
- Bao J, Mahaman YAR, Liu R, Wang JZ, Zhang Z, Zhang B, and Wang X (2017) Sex Differences in the Cognitive and Hippocampal Effects of Streptozotocin in an Animal Model of Sporadic AD. *Front Aging Neurosci* 9: 347.
- Bennett RA and Pegg AE (1981) Alkylation of DMA in Rat Tissues Following Administration of Streptozotocin. *Cancer Res* 41. 2786-2790.
- Biasibetti R, Almeida JP, Santos D, Rodrigues L, Wartchow KM, Suardi LZ, Nardin P, Selistre NG, Vázquez D, and Gonç CA (2017) Hippocampal Changes in STZ-Model of Alzheimer’s Disease Are Dependent on Sex. *Behav Brain Res* 316:205–14.

Biasibetti R, Tramontina AC, Costa AP, Dutra MF, Quincozes-Santos A, Nardin P, Bernardi CL, Wartchow KM, Lunardi PS, and Alves CAG (2013) Green Tea (-)Epigallocatechin-3-Gallate Reverses Oxidative Stress and Reduces Acetylcholinesterase Activity in a Streptozotocin-Induced Model of Dementia. *Behav Brain Res* 236:186–93.

Bloch K, Gil-Ad I, Vanichkin A, Hornfeld SH, Koroukhov N, Taler M, Vardi P, and Weizman A (2017) Intracerebroventricular Streptozotocin Induces Obesity and Dementia in Lewis Rats. *J Alzheimer Dis* 60 (1):121–36.

Bradford MM (1976) A rapid and sensitive method for the quantitation of microgram quantities of protein utilizing the principle of protein-dye binding. *Anal Biochem*, 72(1–2): 248–254.

Brandon EP, Mellott T, Pizzo DP, Coufal N, D'Amour KA, Gobeske K, Lortie M, López-Coviella I, Berse B, Thal LJ, Gage FH and Blusztajn JK (2004) Choline transporter 1 maintains cholinergic function in choline acetyltransferase haploinsufficiency. *J Neurosci* 24, 5459–66.

Bubber P, Haroutunian V, Fisch G, Blass JP, Gibson GE (2005) Mitochondrial abnormalities in Alzheimer brain: mechanistic implications. *Ann Neurol* 57(5):695-703.

Cahill GF (2006) Fuel Metabolism in Starvation. *Annu Rev Nutr* 26 (1), 1–22.

Cavanaugh SE, Pippin JJ, and Barnard ND (2014) Animal Models of Alzheimer Disease: Historical Pitfalls and a Path Forward. *Alz Dis* 31(3/4):279–302.

Chen Y, Liang Z, Blanchard J, Dai CL, Sun S, Lee MH, Grundke-Iqbal I, Iqbal K, Liu F, and Gong CX (2013) A Non-Transgenic Mouse Model (Icv-STZ Mouse) of Alzheimer's Disease: Similarities to and Differences from the Transgenic Model (3xTg-AD Mouse). *Mol Neurobiol*. 47(2):711–25.

Chen Y, Tian Z, Liang Z, Sun S, Dai CL, Lee MH, LaFerla FM, Grundke-Iqbal I, Iqbal K, Liu F, and Gong CX (2012) Brain Gene Expression of a Sporadic (Icv-STZ Mouse) and a Familial Mouse Model (3xTg-AD Mouse) of Alzheimer's Disease. *PLoS ONE* 7(12).

Cohen RM, Rezai-Zadeh K, Weitz TM, Rentsendorj A, Gate D, Spivak I, Bholat Y, Vasilevko V, Glabe CG, Breunig JJ, Rakic P, Davtyan H, Agadjanyan MG, Kepe V, Barrio JR, Bannykh S, Szekely CA, Pechnick RN, and Town T (2013) A Transgenic Alzheimer Rat with Plaques, Tau Pathology, Behavioral Impairment, Oligomeric A β , and Frank Neuronal Loss. *J Neurosci* 33(15):6245–56.

Correia SC, Santos RX, Santos MS, Casadesus G, Lamanna JC, Perry G, Smith MA, and Moreira PI (2013) Mitochondrial Abnormalities in a Streptozotocin-Induced Rat Model of Sporadic Alzheimer's Disease. *Curr Alzheimer Res* 10:406–19.

Costa M, Bernardi J, Fiuza T, Costa L, Brand R, and Pereira ME (2016) N-Acetylcysteine Protects Memory Decline Induced by Streptozotocin in Mice. *Chem Biol Interact* 253:10–17.

Cui SY, Song JZ, Cui XY, Hu X, Ma YN, Shi YT, Luo Y, Ge YR, Ding H, Ye H, and Zhang YH (2018) Intracerebroventricular Streptozotocin-Induced Alzheimer's Disease-like Sleep Disorders in Rats: Role of the GABAergic System in the Parabrachial Complex. *CNS Neurosci Ther* 24(12):1241-1252

- Cummings J, Lee G, Ritter A, Sabbagh M, and Zhong K (2019) Alzheimer's Disease Drug Development Pipeline: 2019. *Alzheimers Dement (NY)* 5:272–93.
- Davies P(1979) Neurotransmitter-related enzymes in senile dementia of the Alzheimer type. *Brain Res* 171(2):319-27.
- Day J, Damsma G, Fibiger HC (1991) Cholinergic Activity in the Rat Hippocampus, Cortex and Striatum Correlates With Locomotor Activity: An In Vivo Microdialysis Study. *Pharmacol Biochem Behav* 38:723-729.
- Devaskar SU, Singh BS, Carnaghi LR, Rajakumar PA, Giddings SJ (1993) Insulin II gene expression in rat central nervous system. *Regul Pept* 48(1– 2):55–63.
- Devaskar SU, Giddings SJ, Rajakumar PA, Carnaghi LR, Menon RK, Zahm DS (1994) Insulin gene expression and insulin synthesis in mammalian neuronal cells. *J Biol Chem* 269(11):8445–54.
- De La Monte SM and Tong M (2014) Brain metabolic dysfunction at the core Alzheimer's disease. *Biochem Pharmacol* 88, 548–59.
- De la Monte SM, Tong M, Lester-Coll N, Plater M, and Wands JR (2006) Therapeutic Rescue of Neurodegeneration in Experimental Type 3 Diabetes: Relevance to Alzheimer's Disease. *J Alzheimers Dis* 10:89–109.
- De Lima Oliveira M, Kairalla AC, Fonoff ET, Martinez RCR, Teixeira MJ, and Bor-Seng-Shu E (2014) Cerebral Microdialysis in Traumatic Brain Injury and Subarachnoid Hemorrhage: State of the Art. *Neurocrit Care* 21(1):152–62.
- Deng Y, Li B, Liu Y, Iqbal K, Grundke-Iqbal I, and Gong CX (2009) Dysregulation of Insulin Signaling, Glucose Transporters, O-GlcNAcylation, and Phosphorylation of Tau and Neurofilaments in the Brain: Implication for Alzheimer's Disease. *Am J Pathol* 175(5):2089–98.
- Dienel GA (2012) Brain lactate metabolism: the discoveries and the controversies. *J Cereb Blood Flow Metab* 32,1107-38.
- Drummond E and Wisniewski T (2017) Alzheimer's Disease: Experimental Models and Reality. *Acta Neuropathol* 133(2):155-175.
- Du LL, Chai DM, Zhao LN, Li XH, Zhang FC, Zhang HB, Liu LB, Wu K, Liu R, Wang JZ, and Zhou XW (2015) AMPK Activation Ameliorates Alzheimer's Disease-like Pathology and Spatial Memory Impairment in a Streptozotocin-Induced Alzheimer's Disease Model in Rats. *J Alzheimers Dis* 43(3):775–84.
- Duelli R, Schrock H, Kuschinsky W, and Hoyer S (1994) Intracerebroventricular Injection of Streptozotocin Induces Discrete Local Changes in Cerebral Glucose Utilization in Rats. *Int J Dev Neurosci* 12(8):737–43.
- Duelli R and Wolfgang K (2001) Brain Glucose Transporters: Relationship to Local Energy Demand. *News Physiol Sci* 16.
- Eigentler A, Draxl A, and Wiethüchter A (2015) Laboratory Protocol: Citrate Synthase a Mitochondrial Marker Enzyme. Oroboros Instruments Corp, Innsbruck.

Ellenbroek B and Youn J (2016) Rodent Models in Neuroscience Research: Is It a Rat Race? *Dis Model Mech* 9(10):1079–87.

Ellman GL, Courtney KD, Andres V and Featherstone RM (1961) A new and rapid colorimetric determination of acetylcholinesterase activity. *Biochemical Pharmacology*, 7(2), pp. 88–95.

Ferreira ST, Clarke JR, Bomfim TR, and De Felice FG (2014) Inflammation, Defective Insulin Signaling, and Neuronal Dysfunction in Alzheimer's Disease. *Alzheimers Dement* 10(1 Suppl):S76-83.

Francis PT, Palmer AM, Snape M, and Wilcock GK (1999) The Cholinergic Hypothesis of Alzheimer's Disease: A Review of Progress. *J Neurol Neurosurg Psychiatry* 66(2):137–47.

Frölich L, Müller WE, and Riederer P (2015) Editorial: Siegfried Hoyer's Concept of Alzheimer Pathophysiology. *J Neural Trans* 122(4):495–97.

Furman BL (2015) Streptozotocin-Induced Diabetic Models in Mice and Rats. *Curr Protoc Pharmacol* 70(1):5.47.1-5.47.20.

Gage FH, Kelly PAT, Bjijrklund A, Diemer N (1984) Regional changes in brain glucose metabolism reflect cognitive impairments in aged rats. *J Neurosci* 4(11):2856-2865.

Garcia-Alloza M, Zaldua N, Diez-Ariza M, Marcos B, Lasheras B, Gil-Bea FJ, and Ramirez MJ (2006) Effect of Selective Cholinergic Denervation on the Serotonergic System: Implications for Learning and Memory. *J Neuropathol Exp Neurol* 65(11):1074–81.

Gerfen CR (1997) Basic Neuroanatomical Methods. *Curr Protoc Neurosci*:1.1.1-1.1.11

Gluscock JJ, Osman EY, Coady TH, Rose F, Shababi M, and Lorson CL (2011) Delivery of Therapeutic Agents Through Intracerebroventricular (ICV) and Intravenous (IV) Injection in Mice. *J Vis Exp* (56).

Gonzales KK and Smith Y (2015) Cholinergic Interneurons in the Dorsal and Ventral Striatum: Anatomical and Functional Considerations in Normal and Diseased Conditions. *Ann NY Acad Sci*. 1349(1):1–45.

Grieb P (2016) Intracerebroventricular Streptozotocin Injections as a Model of Alzheimer's Disease: In Search of a Relevant Mechanism. *Mol Neurobiol*. 53(3):1741–52.

Grillo CA., Piroli GG, Lawrence RC, Wrihten SA, Green AJ, Wilson SP, Sakai RR, Kelly SJ, Wilson MA, Mott DD, and Reagan LP (2015) Hippocampal insulin resistance impairs spatial learning and synaptic plasticity. *Diabetes* 64, 3927–36.

Grünblatt E, Salkovic-Petrisic M, Osmanovic J, Riederer P, and Hoyer S (2007) Brain Insulin System Dysfunction in Streptozotocin Intracerebroventricularly Treated Rats Generates Hyperphosphorylated Tau Protein. *J Neurochem* 101(3):757-70.

Hagl S, Kocher A, Schiborr C, Eckert SH, Ciobanu I, Birringer M, El-Askary H, Helal A, Khayyal MT, Frank J, Muller WE, and Eckert GP (2013) Rice Bran Extract Protects from Mitochondrial Dysfunction in Guinea Pig Brains. *Pharmacol Res* 76:17–27.

Halliwel B and Whiteman M (2004) Measuring Oxidative Stress in Vivo and How to Do It. *British J Pharmacol* 142, 231–255.

Hampel H, Mesulam MM, Cuello AC, Farlow MR, Giacobini E, Grossberg GT, Khachaturian AS, Vergallo A, Cavado E, Snyder PJ, and Khachaturian ZS (2018) The Cholinergic System in the Pathophysiology and Treatment of Alzheimer's Disease. *Brain* 141(7):1917–33.

Hartmann J, Kiewert C, and Klein J (2010) Neurotransmitters and energy metabolites in amyloid-bearing APP SWExPSEN1dE9 mouse brain. *J Pharmacol Exp Ther* 332, 364–70.

Hoyer S (1991) Abnormalities of Glucose Metabolism in Alzheimer's Disease. *Ann NY Acad Sci* 640:53–58.

Hoyer S (1996) Oxidative Metabolism Deficiencies in Brains of Patients with Alzheimer's Disease. *Acta Neurol Scand* (26):18–24.

Hoyer S (2004) Glucose Metabolism and Insulin Receptor Signal Transduction in Alzheimer Disease. *Eur J Pharmacol* 490(1–3):115–25.

Hoyer S, Lannert H, Nöldner M, and Chatterjee SS (1999) Damaged Neuronal Energy Metabolism and Behavior Are Improved by Ginkgo Biloba Extract (EGb 761). *J Neural Trans* 106(11–12):1171–88.

Hoyer S and Lannert H (2007) Long-Term Abnormalities in Brain Glucose/Energy Metabolism after Inhibition of the Neuronal Insulin Receptor: Implication of Tau-Protein. *J Neural Trans* (72):195–202.

Hoyer S, Nitsch R, and Oesterreich K (1991) Predominant Abnormality in Cerebral Glucose Utilization in Late-Onset Dementia of the Alzheimer Type: A Cross-Sectional Comparison against Advanced Late-Onset and Incipient Early-Onset Cases. *J Neural Transm Park Dis Dement Sect* 3(1):1-14

Hoyer S, Prem L, Sorbi S, and Amaducci L (1993) Stimulation of Glycolytic Key Enzymes in Cerebral Cortex by Insulin. *NeuroReport* 4(7):991–93.

Hroudová J, Singh N, and Fišar Z (2014) Mitochondrial Dysfunctions in Neurodegenerative Diseases: Relevance to Alzheimer's Disease. *Biomed Res Int* 175062

https://www.genome.jp/kegg-bin/show_pathway?oaa04725 access 26.08.20

<http://labs.gaidi.ca/>

Iiff JJ, Wang M, Liao Y, Plogg BA, Peng W, Gundersen GA, Benveniste H, Vates GE, Deane R, Goldman SA, Nagelhus EA, and Nedergaard M (2012) A Paravascular Pathway Facilitates CSF Flow Through the Brain Parenchyma and the Clearance of Interstitial Solutes, Including Amyloid B. *Sci Transl Med* 4:147.

Imran I, Hillert MH, Klein J (2015) Early metabolic responses to lithium/pilocarpine-induced status epilepticus in rat brain. *J Neurochem* 135, 1007–18.

Imran I (2015) Neurochemical and Metabolic Consequences of Lithium-Pilocarpine-Induced Acute Status Epilepticus. Dissertation. Faculty of Biochemistry, Chemistry and Pharmacy (FB14). Goethe University:Frankfurt am Main.

- Ishrat T, Khan MB, Hoda MN, Yousuf S, Ahmad M, Ansari MA, Ahmad AS, and Islam F (2006) Coenzyme Q10 Modulates Cognitive Impairment against Intracerebroventricular Injection of Streptozotocin in Rats. *Behav Brain Res* 171(1):9–16.
- Ito F, Sono Y, Ito T (2019) Measurement and Clinical Significance of Lipid Peroxidation as a Biomarker of Oxidative Stress: Oxidative Stress in Diabetes, Atherosclerosis, and Chronic Inflammation. *Antioxidants (Basel)* 8(3):72.
- Itoh A, Nitta A, Nadai M, Nishimura K, Hirose M, Hasegawa T, and Nabeshima T (1996) Dysfunction of Cholinergic and Dopaminergic Neuronal Systems in β -Amyloid Protein-Infused Rats. *J Neurochem* 66:1113–17.
- Kallenborn-Gerhardt W, Lu R, Bothe A, Thomas D, Schlaudraff J, Lorenz JE, Lippold N, Real CI, Ferreirós N, Geisslinger G, Del Turco D, and Schmidtko A (2014) Phosphodiesterase 2A localized in the spinal cord contributes to inflammatory pain processing. *Anesthesiology*. 21, 372–82.
- Klein J (2000) Membrane Breakdown in Acute and Chronic Neurodegeneration: Focus on Choline-Containing Phospholipids. *J Neural Transm (Vienna)*. 107(8-9):1027-63.
- Knezovic A, Loncar A, Homolak J, Smailovic U, Osmanovic-Barilar J, Ganoci L, Bozina N, Riederer P, and Salkovic-Petrisic M (2017) Rat Brain Glucose Transporter-2, Insulin Receptor and Glial Expression Are Acute Targets of Intracerebroventricular Streptozotocin: Risk Factors for Sporadic Alzheimer's Disease? *J Neural Transm (Vienna)* 124(6):695-708.
- Knezovic A, Osmanovic-Barilar J, Curlin M, Hof PR, Simic G, Riederer P, Salkovic-Petrisic M (2015) Staging of cognitive deficits and neuropathological and ultrastructural changes in streptozotocin-induced rat model of Alzheimer's disease. *J Neural Transm* 122, 577–92.
- Knezovic A, Osmanovic-Barilar J, Babic A, Bagaric R, Farkas V, Riederer P, and Salkovic-Petrisic M (2018) Glucagon-like Peptide-1 Mediates Effects of Oral Galactose in Streptozotocin-Induced Rat Model of Sporadic Alzheimer's Disease. *Neuropharmacol* 135:48–62.
- Koch K, Berressem D, Konietzka J, Thinnes A, Eckert G, Klein J (2017) Hepatic ketogenesis induced by middle cerebral artery occlusion in mice. *J Am Heart Assoc*: 7, 1–10.
- König M, Berlin B, Schwab K, Frahm S, Theuring F, Wischik CM, Harrington CR, Riedel G, and Klein J (2019) Increased Cholinergic Response in α -Synuclein Transgenic Mice (h- α -SynL62). *ACS Chem Neurosci* 10(4):1915-1922.
- König M, Thinnes A, and Klein J (2017) Microdialysis and Its Use in Behavioural Studies: Focus on Acetylcholine. *J Neurosci Methods* 15;300:206-215.
- König M (2019) Charakterisierung des zentralen cholinergen Systems in α -Synuclein- und Tau-transgenen Mausmodellen. Dissertation Fachbereich 14 Biochemie, Chemie und Pharmazie. Goethe-Universität: Frankfurt am Main.
- Kraska A, Santin MD, Dorieux O, Joseph-Mathurin N, Bourrin E, Petit F, Jan C, Chaigneau M, Hantraye P, Lestage P, and Dhenain M (2012) In Vivo Cross-Sectional Characterization of Cerebral Alterations Induced by Intracerebroventricular Administration of Streptozotocin. *PLoS ONE* 7(9):e46196.

- Lannert H and Hoyer S (1998) Intracerebroventricular Administration of Streptozotocin Causes Long-Term Diminutions in Learning and Memory Abilities and in Cerebral Energy Metabolism in Adult Rats. *Behav Neurosci* 112(5):1199–1208.
- Lenzen S (2008) The Mechanisms of Alloxan- and Streptozotocin-Induced Diabetes. *Diabetologia* 51(2):216–26.
- Larsen S, Nielsen J, Hansen CN, Nielsen LB, Wibrand F, Stride N, Schroder HD, Boushel R, Helge JF, Dela F, and Hey-Mogensen M (2012) Biomarkers of Mitochondrial Content in Skeletal Muscle of Healthy Young Human Subjects. *J Physiol* 590(14):3349–60.
- Lester-Coll N, Rivera EJ, Soscia SJ, Doiron K, Wands JR, and de la Monte SM (2006) Intracerebral Streptozotocin Model of Type 3 Diabetes: Relevance to Sporadic Alzheimer's Disease. *J Alzheimers Dis* 9:13–33.
- Lietsche J, Gorka J, Hardt S, Karas M and Klein J (2014) Self-built microdialysis probes with improved recoveries of ATP and neuropeptides. *J Neurosci Methods* 237, 1–8.
- Lu W, Huang J, Sun S, Huang S, Gan S, Xu J, Yang M, Xu S and Jiang X (2015) Changes in Lactate Content and Monocarboxylate Transporter 2 Expression in A β 25-35-Treated Rat Model of Alzheimer's Disease. *Neurol Sci* 36(6):871–76.
- Majkutewicz I, Kurowska E, Podlacha M, Myślińska D, Grembecka B, Ruciński J, Plucińska K, Jerzemowska G, Wrona D (2016) Dimethyl Fumarate Attenuates Intracerebroventricular Streptozotocin-Induced Spatial Memory Impairment and Hippocampal Neurodegeneration in Rats. *Behav Brain Res* 308:24–37.
- Masters CL, Bateman R, Blennow K, Rowe CC, Sperling RA, and Cummings JL (2015) Alzheimer's Disease. *Nat Rev Dis Primers* 1, 15056 .
- Maurer I, Zierz S, and Möller HJ (2000) A Selective Defect of Cytochrome c Oxidase Is Present in Brain of Alzheimer Disease Patients. *Neurobiol Aging* 21(3):455-62
- Mayer G, Nitsch R, and Hoyer S (1989) Impairments in Passive Avoidance Learning after Cerebral Inhibition of Cerebral Glucose Metabolism. *J Neural Trans Gen Sect* 1(1–2):103–4.
- Mesulam M (2004) The Cholinergic Lesion of Alzheimer's Disease: Pivotal Factor or Side Show? *Learn Mem* 11(1):43–49.
- Mir F, Lee D, Ray H, and Sadiq SA (2014) CSF Isoprostane Levels Are a Biomarker of Oxidative Stress in Multiple Sclerosis. *Neurol Neuroimmunol Neuroinflamm* 1(2):e21.
- Mohr F, Zimmermann M, and Klein J (2013) Mice Heterozygous for AChE Are More Sensitive to AChE Inhibitors but Do Not Respond to BuChE Inhibition. *Neuropharmacol* 67:37–45.
- Montuschi P, Barnes PJ, Roberts LJ (2004) Isoprostanes: Markers and Mediators of Oxidative Stress. *FASEB J* 18(15):1791-800.
- Morales I, Guzmán-Martínez L, Cerda-Troncoso C, Farías GA, and Maccioni RB (2014) Neuroinflammation in the Pathogenesis of Alzheimer's Disease. A Rational Framework for the Search of Novel Therapeutic Approaches. *Front Cell Neurosci* 22;8:112.

- Müller C and Remy S (2018) Septo–Hippocampal Interaction. *Cell Tissue Res* 373(3):565–75.
- Nestler EJ, Hyman SE, Malenka R C (2015). *Molecular neuropharmacology: A foundation for clinical neuroscience*. 3rd Ed. New York: McGraw-Hill, Medical Pub. Div.
- Nitsch R and Hoyer S (1991) Local Action of the Diabetogenic Drug, Streptozotocin, on Glucose and Energy Metabolism in Rat Brain Cortex. *Neurosci Lett* 128:199–202.
- Nitsch R, Mayer G, and Hoyer S (1989) The Intracerebroventricular Streptozotocin-Treated Rat : Impairment of Cerebral Glucose Metabolism Resembles the Alterations of Carbohydrate Metabolism of the Brain in Alzheimer’s Disease. *J Neural Transm* 109–10.
- Nitta A, Itoh A, Hasegawa T, and Nabeshima T (1994) Beta-Amyloid Protein-Induced Alzheimer’s Disease Animal Model. *Neurosci Lett* 170(1):63–6
- O’Shea SD, Smith IM, McCabe OM, Cronin MM, Walsh DM, and O’Connor WT (2008) Intracerebroventricular Administration of Amyloid β -Protein Oligomers Selectively Increases Dorsal Hippocampal Dialysate Glutamate Levels in the Awake Rat. *Sensors* 8(11):7428–37.
- Oddo S, Caccamo A, Shepherd JD, Murphy MP, Golde TE, Kaye R, Metherate R, Mattson MP, Akbari Y, and Laferla FM (2003) Triple-Transgenic Model of Alzheimer’s Disease with Plaques and Tangles: Intracellular A and Synaptic Dysfunction. *Neuron* 39: 409–421
- Oliver DMA and Reddy PH (2019) Molecular Basis of Alzheimer’s Disease: Focus on Mitochondria. *J Alzheimers Dis* 72(s1):S95–116.
- Ortiz PJM and Swerdlow RH (2018) Mitochondrial Dysfunction in Alzheimer’s Disease: Role in Pathogenesis and Novel Therapeutic Opportunities. *Br J Pharmacol* 176(18):3489–3507.
- Osmanovic-Barilar J, Knezovic A, Grünblatt E, Riederer P, and Salkovic-Petrisic M (2015) Nine-Month Follow-up of the Insulin Receptor Signalling Cascade in the Brain of Streptozotocin Rat Model of Sporadic Alzheimer’s Disease. *J Neural Trans* 122(4):565–76.
- Paidi R, Nthenge-Ngumbau D, Singh R, Kankanala T, Mehta H, and Mohanakumar K (2015) Mitochondrial Deficits Accompany Cognitive Decline Following Single Bilateral Intracerebroventricular Streptozotocin. *Curr Alzheimer Res* 12(8):785–95.
- Pathan AR, Viswanad B, Sonkusare SK, and Ramarao P (2006) Chronic Administration of Pioglitazone Attenuates Intracerebroventricular Streptozotocin Induced-Memory Impairment in Rats. *Life Sci* 79(23):2209–16.
- Pavía J, Alberch J, Álvarez I, Toledano A, de Ceballos ML (2000) Repeated intracerebroventricular administration of beta-amyloid(25–35) to rats decreases muscarinic receptors in cerebral cortex. *Neurosci Lett* 278(1–2):69–72.
- Paxinos G, Watson C. *The rat brain in stereotaxic coordinates* .4th edition. 1998; Academic Press, San Diego.
- Pepeu G and Giovannini MG (2017) The Fate of the Brain Cholinergic Neurons in Neurodegenerative Diseases. *Brain Res* 1670:173–84.

- Perez-Nievas BG and Serrano-Pozo A (2018) Deciphering the Astrocyte Reaction in Alzheimer's Disease. *Front Aging Neurosci* 10:114.
- Perez O, Judit M, Swerdlow RH (2018) Mitochondrial Dysfunction in Alzheimer's Disease: Role in Pathogenesis and Novel Therapeutic Opportunities. *Br J Pharmacol* 176(18):3489-3507.
- Pieper AA, Brat DJ, Krug DK, Watkins CC, Gupta A, Blackshaw S, Verma A, Wang ZQ, and Snyder SH (1999) Poly(ADP-Ribose) Polymerase-Deficient Mice Are Protected from Streptozotocin-Induced Diabetes. *Proc Natl Acad Sci USA* 96(6):3059-64.
- Pohland M., Pellowska M, Asseburg H, Hagl S, Reutzel M, Joppe A, Berressem D, Eckert SH, Wurglics M, Schubert-Zsilavec M, and Eckert GP (2018) MH84 Improves Mitochondrial Dysfunction in a Mouse Model of Early Alzheimer's Disease. *Alzheimers Res Ther* 10(1):18.
- Pratico D, Lee MYV, Trojanowski JQ, Rokach J, and Fitzgerald GA (1998) Increased F2-Isoprostanes in Alzheimer's Disease: Evidence for Enhanced Lipid Peroxidation in Vivo. *FASEB J* 12(15):1777-83.
- Prickaerts J, Fahrig T, and Blokland A (1999) Cognitive Performance and Biochemical Markers in Septum, Hippocampus and Striatum of Rats after an i.c.v. Injection of Streptozotocin: A Correlation Analysis. *Behav Brain Res* 102(1-2):73-88.
- Prince M and Jackson J (2009) World Alzheimer Report 2009. *Alzheimer's Disease International* 1-96.
- Racchi M, Mazzucchelli M, Porrello E, Lanni C, and Govoni S (2004) Acetylcholinesterase Inhibitors: Novel Activities of Old Molecules. *Pharmacol Res* 50(4):441-51.
- Rai S, Kamat PK, Nath C, and Shukla R (2014) Glial Activation and Post-Synaptic Neurotoxicity: The Key Events in Streptozotocin (ICV) Induced Memory Impairment in Rats. *Pharmacol Biochem Behav* 117:104-17.
- Rees T, Hammond PI, Soreq H, Younkin S, and Brimijoin S (2003) Acetylcholinesterase Promotes Beta-Amyloid Plaques in Cerebral Cortex. *Neurobiol Aging* 24(6):777-87.
- Rhein V, Song X, Wiesner A, Ittner LM (2009) Amyloid-and Tau Synergistically Impair the Oxidative Phosphorylation System in Triple Transgenic Alzheimer's Disease Mice. *Proc Natl Acad Sci USA*. 106(47):20057-20062.
- Ribeiro FM, Black SAG, Prado VF, Rylett RJ, Ferguson SSG, Prado MAM (2006) The "ins" and "outs" of the high-affinity choline transporter CHT1. *J Neurochem* 97(1):1-12.
- Rice AC, Ladd AC, and Bennett JP (2015) Postmortem Alzheimer's Disease Hippocampi Show Oxidative Phosphorylation Gene Expression Opposite That of Isolated Pyramidal Neurons. *J Alzheimers Dis* 45(4):1051-59.
- Ritter S, Murnane JM, Ladenheim EE (1982) Glucoprivic Feeding Is Impaired by Lateral or Fourth Ventricular Alloxan Injection. *Am J Physiol* 243:R312.
- Salas IH and De Strooper B (2019) Diabetes and Alzheimer's Disease: A Link Not as Simple as It Seems. *Neurochem Res* 44(6):1271-78.

- Salkovic-Petrisic M, Knezovic A, Hoyer S, and Riederer P (2013) What Have We Learned from the Streptozotocin-Induced Animal Model of Sporadic Alzheimer's Disease, about the Therapeutic Strategies in Alzheimer's Research. *J Neural Trans* 120(1):233–52.
- Sang S, Pan X, Chen Z, Zeng F, Pan S, Liu H, Jin L, Fei G, Wang C, Ren S, Jiao F, Bao W, Zhou W, Guan Y, Zhang Y, Shi H, Wang Y, Yu X, Wang Y, Zhong C (2018) Thiamine diphosphate reduction strongly correlates with brain glucose hypometabolism in Alzheimer's disease, whereas amyloid deposition does not. *Alzheimers Res Ther* 10(1):26.
- Santos TO, Mazucanti CHY, Xavier GF, and Torráo AS (2012) Early and Late Neurodegeneration and Memory Disruption after Intracerebroventricular Streptozotocin. *Physiol Behav* 107(3):401-13.
- Santos DB, Colle D, Moreira ELG, Peres KC, Ribeiro RP, Dos Santos AA, De Oliveira J, Hort MA, De Bem AF, and Farina M (2015) Probucol mitigates streptozotocin-induced cognitive and biochemical changes in mice. *Neurosci* 284:590–600.
- Sapcanin A, Sofic E, Tahirovic I, Salkovic-Petrisic M, Hoyer S, Riederer P (2008) Antioxidant Capacity in Rat Brain After Intracerebroventricular Treatment With Streptozotocin and Alloxan. *Neurotox Res* 13(13):97–104.
- Saxena G, Singh SP, Agrawal R, and Nath C (2008) Effect of Donepezil and Tacrine on Oxidative Stress in Intracerebral Streptozotocin-Induced Model of Dementia in Mice. *E J Pharmacol* 581(3):283–89.
- Saxena, Gunjan, Ishan K. Patro, and Chandishwar Nath (2011) ICV STZ Induced Impairment in Memory and Neuronal Mitochondrial Function: A Protective Role of Nicotinic Receptor. *Behavi Brain Res* 224(1):50–57.
- Schmued LC, Stowers CC, Scallet AC and Xu L (2005) Fluoro-Jade C results in ultra high resolution and contrast label- ing of degenerating neurons. *Brain Res.* 1035: 24–31.
- Shoham S, Bejar C, Kovalev E, and Weinstock M (2003) Intracerebroventricular Injection of Streptozotocin Causes Neurotoxicity to Myelin That Contributes to Spatial Memory Deficits in Rats. *Exp Neurol* 184(2):1043–52.
- Shoham S, Bejar C, Kovalev E, Schorer-Apelbaum D, and Weinstock M (2007) Ladostigil Prevents Gliosis, Oxidative-Nitrative Stress and Memory Deficits Induced by Intracerebroventricular Injection of Streptozotocin in Rats. *Neuropharmacol* 52(3):836–43.
- Slotkin TA, Nemeroff CB, Bissette G, and Seidler FJ (1994) Overexpression of the High Affinity Choline Transporter in Cortical Regions Affected by Alzheimer's Disease Evidence from Rapid Autopsy Studies. *J Clin Invest* 94(2): 696–702.
- Solmaz V, Çınar BP, Yiğittürk G, Çavuşoğlu T, Taşkıran D, and Erbaş O (2015) Exenatide Reduces TNF- α Expression and Improves Hippocampal Neuron Numbers and Memory in Streptozotocin Treated Rats. *Eur J Pharmacol* 765:482–87.
- Sorial ME and El Sayed NSED (2017) Protective Effect of Valproic Acid in Streptozotocin-Induced Sporadic Alzheimer's Disease Mouse Model: Possible Involvement of the Cholinergic System. *Naunyn-Schmiedebergs Arch Pharmacol* 390(6):581–93.

Terwel D, Prickaerts J, Meng F, and Jolles J (1995) Brain Enzyme Activities after Intracerebroventricular Injection of Streptozotocin in Rats Receiving Acetyl-L-Carnitine. *Eur J Pharmacol* 287(1):65-71.

Toledano A and Álvarez MI (2004) Lesions and Dysfunctions of the Nucleus Basalis as Alzheimer's Disease Models: General and Critical Overview and Analysis of the Long-Term Changes in Several Excitotoxic Models. *Curr Alzheimer Res* 1:189–214.

Tong M, Neusner A, Longato L, Lawton M, Wands JR, and De La Monte SM (2009) Nitrosamine Exposure Causes Insulin Resistance Diseases: Relevance to Type 2 Diabetes Mellitus, Non-Alcoholic Steatohepatitis, and Alzheimer's Disease. *J Alzheimers Dis* 17(4):827-44.

Tota S, Kamat PK, Shukla R, and Nath C (2011) Improvement of Brain Energy Metabolism and Cholinergic Functions Contributes to the Beneficial Effects of Silibinin against Streptozotocin Induced Memory Impairment. *Behav Brain Res* 221(1):207–15.

Van Dam D and De Deyn PP (2006) Drug Discovery in Dementia: The Role of Rodent Models. *Nat Rev Drug Discov* 5(11):956-70

Waite JJ and Chen AD (2001) Differential Changes in Rat Cholinergic Parameters Subsequent to Immunotoxic Lesion of the Basal Forebrain Nuclei. *Brain Res* 918(1-2):113-20.

Wang W, Zhao F, Ma X, Perry G, and Zhu X (2020) Mitochondria Dysfunction in the Pathogenesis of Alzheimer's Disease: Recent Advances. *Mol Neurodegener* 15(1):30.

White H and Venkatesh B (2011) Introduction Clinical Review: Ketones and Brain Injury. *Crit Care* 15:219

Wood AJJ and Cummings JL (2004) Drug Therapy Alzheimer's Disease. *N Engl J Med* 351:56–67.

Yuliani T, Lobentanzer S, Klein J (2020) Central cholinergic function and metabolic changes in streptozotocin-induced rat brain injury. *J Neurochem*. doi:10.1111/jnc.15155

Zafeer MF, Firdaus F, Anis E, and Hossain MM (2019) Prolong Treatment with Trans-Ferulic Acid Mitigates Bioenergetics Loss and Restores Mitochondrial Dynamics in Streptozotocin-Induced Sporadic Dementia of Alzheimer's Type. *Neurotoxicol* 73:246–57.

Zhang M, Cheng X, Dang R, Zhang W, Zhang J, and Yao Z (2018) Lactate Deficit in an Alzheimer Disease Mouse Model: The Relationship with Neuronal Damage. *J Neuropathol Exp Neurol* 77(12):1163–76.

6 List of figures

| | |
|---|----|
| Figure 1. 1. Proposed pathways leading to A β plaques and NFT formation..... | 2 |
| Figure 1. 2. Coronal section of a rat brain on hippocampus and striatum | 4 |
| Figure 1. 3. Illustration of septohippocampal connection..... | 4 |
| Figure 1. 4. Synaptic inputs to striatal cholinergic interneurons | 5 |
| Figure 1. 5. Cholinergic synapse..... | 6 |
| Figure 1. 6. Interesting features of cholinergic synapse | 7 |
| Figure 1. 7. STZ structure | 15 |
| Figure 1. 8. A coronal section of a rat brain at 0.80 posterior to bregma | 17 |
| Figure 1. 9. Proposed mechanism of icv-STZ induced brain insulin resistance..... | 20 |
| Figure 1. 10. Proposed mechanism of icv-STZ induced brain injury | 21 |
| Figure 2. 1. Flow diagram of the histology, mitochondrial respiration and cholinergic marker studies..... | 32 |
| Figure 2. 2. Flow diagram of microdialysis study | 33 |
| Figure 2. 3. Citrate synthase-catalyzed reaction coupled with DTNB (irreversible reaction).37 | |
| Figure 2. 4. Hydrolysis of the acetylthiocholine catalyzed by AChE..... | 39 |
| Figure 2. 5. Schematic illustration of a microdialysis probe | 41 |
| Figure 2. 6. Schematic illustrations of 30 kDa probe assembly..... | 43 |
| Figure 2. 7. Operation setup for probe implantation..... | 44 |
| Figure 2. 8. Probe implantation..... | 45 |
| Figure 2. 9. Illustration of probe location | 46 |
| Figure 2. 10. Experimental setup of microdialysis in rats.. .. | 47 |
| Figure 2. 11. HPLC machine for ACh and Choline determination. | 48 |
| Figure 2. 12. Reaction of analyte in the HPLC/ECD machine. | 49 |
| Figure 2. 13. Schematic reaction by CMA 600 | 50 |
| Figure 2. 14. Isoprostane standard curve. | 52 |
| Figure 3. 1. Body weight and hippocampus weight..... | 53 |
| Figure 3. 2. Coronal cryosections of the hippocampus (14 μ m) at AP -5.6 mm from bregma54 | |
| Figure 3. 3. Mitochondrial respiration in hippocampus..... | 56 |
| Figure 3. 4. Metabolite levels in hippocampal microdialysates during behavioral and cholinergic challenges..... | 59 |
| Figure 3. 5. Acetylcholine (ACh) levels in rat hippocampal microdialysates during behavioral and cholinergic challenges. | 60 |
| Figure 3. 6. Mitochondrial respiration in striatum..... | 61 |
| Figure 3. 7. Metabolite levels in striatal microdialysates during behavioral and cholinergic challenges..... | 64 |
| Figure 3. 8. Acetylcholine (ACh) levels in rat striatal microdialysates during behavioral and cholinergic challenges..... | 65 |
| Figure 3. 9. In vitro recovery of acetylcholine, choline, glucose, and lactate. | 66 |
| Figure 4. 1. Single-cell expression of cholinergic-associated transcripts and glucose transporters in neurons of hippocampus and striatum of the adult mouse..... | 79 |
| Figure 4. 2. Correlation of expression of cholinergic-associated transcripts and glucose transporters in single cells of the murine nervous system. | 83 |

7 List of tables

| | |
|---|----|
| Table 2. 1. List of equipments | 24 |
| Table 2. 2. List of chemicals and solvents | 25 |
| Table 2. 3. List of supporting materials and tools..... | 28 |
| Table 2. 4. Kits Used..... | 29 |
| Table 2. 5. Primary Antibody Used | 29 |
| Table 2. 6. Secondary Antibody Used | 29 |
| Table 2. 7. Albumin concentration for the standard curve | 38 |
| Table 2. 8. Acetylcholinesterase concentration for standard curve | 38 |
| Table 2. 9. Composition of the Krebs-Henseleit buffer..... | 40 |
| Table 2. 10. Composition of ChAT reaction medium | 40 |
| Table 2. 11. Recovery mix..... | 43 |
| Table 3. 1. Cholinergic parameters as determined in rat hippocampus three weeks after icv-STZ administration. | 57 |
| Table 3. 2. Extracellular concentrations of hippocampal metabolites as determined by microdialysis under basal conditions (not corrected for recovery)..... | 58 |
| Table 3. 3. Cholinergic parameters as determined in rat striatum three weeks after icv-STZ administration..... | 62 |
| Table 3. 4. Extracellular concentrations of striatal metabolites as determined by microdialysis under basal conditions | 63 |

8 Required Documents

8.1 Declarations

Except where stated otherwise by reference or acknowledgment, the work presented was generated by myself under the supervision of my advisor during my doctoral studies. The material listed below was obtained in the context of collaborative research:

Table 3.1. »Cholinergic parameters as determined in rat in rat hippocampus three weeks after icv-STZ administration«, Helene Lau (Institute of Pharmacology and Clinical Pharmacy, Goethe University). Her contribution: sample measurement and calculation, my own contribution: sample preparation and data analysis.

Table 3.3. »Cholinergic parameters as determined in rat striatum three weeks after icv-STZ administration«, Helene Lau (Institute of Pharmacology and Clinical Pharmacy, Goethe University). Her contribution: sample measurement and calculation, my own contribution: sample preparation and data analysis.

Figure 4.1. »Single-cell expression of cholinergic-associated transcripts and glucose transporters in neurons of hippocampus and striatum of the adult mouse«, Sebastian Lobentanzer (Institute of Pharmacology and Clinical Pharmacy, Goethe University). His contribution: data generation, analysis and visual representation of the entire figure.

Figure 4.2. »Correlation of expression of cholinergic-associated transcripts and glucose transporters in single cells of the murine nervous system«, Sebastian Lobentanzer (Institute of Pharmacology and Clinical Pharmacy, Goethe University). His contribution: data generation, analysis and visual representation of the entire figure.

The following parts of the thesis have been previously published:

- Chapter 3 has in large parts been described in Yuliani et al. (2020). This includes Figures 3.1, 3.2, 3.3, 3.4, 3.5, 3.7, and 3.8.
- Chapter 4 have been partly described in Yuliani et al. (2020). This includes parts of Figures 4.1 and 4.2.

8.2 Summary in German Language

Einleitung:

Morbus Alzheimer (MA) gilt als Hauptursache einer Demenzerkrankung. Er zeichnet sich durch die Akkumulation missgefalteter Proteine (Amyloid- β Plaques und Neurofibrillen) aus, die zum Verlust von Synapsen, Dendriten, Neuronen, Erinnerung und Kognition führt. Spät einsetzender, sporadischer MA ist die häufigste Form, gekennzeichnet durch eine unvollständig geklärte Ätiologie und fehlende krankheitsmodifizierende Therapien. Um das Krankheitsgeschehen besser zu verstehen, wurde eine alternative MA- Hypothese entwickelt: Bei MA könnte es sich um einen Diabetes auf neuronaler Ebene (Diabetes Typ III) handeln. Diese Hypothese wird durch die Fakten gestützt, dass (1) neuronaler Glukose-Hypometabolismus zu den Vorläufer-Symptome des MA zählt und (2) ein Diabetes das Risiko erhöht, an MA zu erkranken.

Zur Testung dieser Hypothese wurden Wildtyp-Ratten, die eine intracerebroventrikuläre Streptozotocin (icv-STZ) Injektion erhalten haben, als Modell verwendet. Streptozotocin (STZ) ist eine Glucosamin-Nitrosoharnstoff Verbindung, die üblicherweise peripher zur Induktion eines experimentellen Diabetes verabreicht wird. Die bereits bekannte, sich in der Peripherie entfaltende Toxizität des STZ wird nach intracerebroventrikulärer Gabe auf zentralnervöser Ebene erwartet: die Störung der Insulin-Rezeptor Signalwege ruft einen Glukose-Hypometabolismus hervor, der zu kognitiven Defiziten führt.

Zielsetzung:

Die icv-STZ Injektion birgt als Toxin-induziertes, nicht transgenes MA-Modell die Möglichkeit, MA und einen der Risikofaktoren - Diabetes Mellitus (DM) - in direkte Verbindung zu setzen. Allerdings bleibt der Mechanismus der icv-STZ Induktion von MA-Symptomen unklar. Daher wurden mittels Mikrodialyse zwei MA-Hypothesen in diesem Modell getestet: (1) Der Glukose-Hypometabolismus als alternative MA-Hypothese und (2) das cholinerge Defizit als essenzielle Charakteristik der MA-Pathologie. Zum einen wurde der Hippocampus untersucht, da die cholinerge Funktion dieser Hirnregion bei MA stark beeinträchtigt ist, sowie zusätzlich das Striatum, welches cholinerge Interneurone enthält, jedoch bei MA weniger betroffen ist.

Methoden:

In dieser Arbeit wurden männliche Wistar-Ratten mit einem Körpergewicht von 190-220 g in einem Alter von 5 Wochen verwendet. Die Ratten erhielten entweder eine icv-STZ Injektion

von 3 mg/kg KG (2x 1.5 mg/kg KG; „Hochdosis“) oder 0.6 mg/kg KG („Niedrigdosis“). Kochsalz diente als Kontrolle. Nach 21 Tagen wurden Proben gesammelt, um cholinerge und metabolische Veränderungen zu untersuchen. Dazu wurden neben der Mikrodialyse histologische und biochemische Methoden verwendet. Die Hirnschädigung wurde mittels GFAP-Färbung bestätigt, im Hippocampus durch Fluoro-Jade Färbung. Um die mitochondriale Toxizität in Hippocampus und Striatum zu bestimmen, wurde die mitochondriale Atmung in beiden Hirnregionen untersucht. Die Aktivitäten der Acetylcholinesterase (AChE), der Cholin-Acetyltransferase (ChAT) und des Cholin-Transporters (CHT-1), auch bekannt als hochaffiner Cholin-Uptake (HACU), dienten als cholinerge Marker und wurden durch spektrophotometrische und szintillatorische Messungen bestimmt.

Die Mikrodialyse wurde in wachen Tieren durchgeführt, während diese zunächst einer verhaltensbezogenen, am nächsten Tag einer pharmakologischen Stimulation ausgesetzt waren. Selbstgebaute Sonden mit einer semipermeablen Membran (Porengröße von 30 kDa) wurden entweder in den Hippocampus oder das Striatum implantiert. Zur Erfassung extrazellulärer Acetylcholin-Konzentrationen wurden die Sonden mit artifizieller Cerebrospinalflüssigkeit (aCSF), versetzt mit 0.1 μ M Neostigmin, perfundiert. Während die Sonde perfundiert wird, diffundieren kleine hydrophile Moleküle aus dem Extrazellulärraum in das Dialysat. Das Dialysat wurde in einem Intervall von 15 Minuten gesammelt und anschließend analysiert. Nach den ersten 90 Minuten (Basal-Werte) wurden die Ratten zur verhaltensbezogenen Stimulation in eine Open-Field Box (35x32x20 cm) transferiert. Nach 90 Minuten wurde die Ratte zurück in ihren ursprünglichen Käfig gesetzt und es wurde für weitere 90 Minuten Dialysat gesammelt. Am zweiten Tag wurde nach Sammeln der Basal-Werte der Perfusionsflüssigkeit für 90 Minuten 1 μ M Scopolamin zur Stimulation der Acetylcholin-Freisetzung zugesetzt. Abschließend wurde für 90 Minuten Dialysat ohne Perfusion von Scopolamin gesammelt. Die Mikrodialyse-Proben wurden wie folgt analysiert: Acetylcholin (ACh) wurde mittels HPLC-ECD gemessen. Glukose-Metaboliten (Glukose, Laktat und Pyruvat) wurden im CMA-600 Mikroanalysator vermessen. Der alternative Energie-Metabolit BHB wurde mittels GC-MS gemessen. Cholin und Glycerol als Marker für Membranschädigungen wurden ebenfalls in der HPLC-ECD bzw. im CMA-600 vermessen. Isoprostan-Konzentrationen, Marker für oxidativen Stress, wurden mit Hilfe eines kommerziell erhältlichen ELISA-Kits bestimmt.

Ergebnisse:

Ausmaß der Toxizität:

Der Verlust an Körpergewicht (hervorgerufen durch die Toxizität der icv-STZ Injektion) war an Tag 7 nur in der Hochdosis Gruppe deutlich sichtbar. Zwar war ab Tag 10 eine Erholung der Hochdosis-Gruppe zu verzeichnen, doch blieb ihr Körpergewicht bis zum Ende des Experiments deutlich unter dem der Kontroll-Gruppe (21 Tage; -17%). Die histologischen Ergebnisse aus der Hochdosisgruppe zeigten neben einer Astrogliose im dorsalen und ventralen Hippocampus eine Neurodegeneration der hippocampalen CA1 Region.

Auch im Mikrodialyse-Experiment sind *in vivo* Anzeichen einer Toxizität erkennbar. Im Zuge der Hochdosis-Gabe waren extrazelluläre Cholin-Konzentrationen im Striatum dosisabhängig erhöht. Cholin und Glycerol gelten als bekannte Marker für Membranschädigungen. Andererseits jedoch blieben die Isoprostane als Marker für oxidativen Stress unverändert.

Hinweise mitochondrialer Beeinträchtigung waren im Hippocampus erkennbar. Die respiratorische Aktivität aller mitochondrialen Komplexe war erniedrigt (ca. -14%; normalisiert auf Citratsynthase (CS) Aktivität), wobei sich statistisch signifikante Unterschiede in Komplex II und IV zeigten. Diese Erniedrigung tritt zusammen mit einer erhöhten CS-Aktivität auf, was auf Veränderungen in der mitochondrialen Biogenese hinweist. Im Striatum hingegen waren diese Unterschiede nicht sichtbar.

Metabolische Veränderungen:

Interessanterweise stützen die Ergebnisse der Mikrodialyse nicht die Hypothese des „Diabetes im Gehirn. Sowohl im Hippocampus als auch im Striatum zeigten sich die extrazellulären Glukose-Konzentrationen in den Basalwerten und unter Stimulation unverändert. Kleinere, nicht signifikante Glukose-Anstiege, wie sie in der hippocampalen CA1 Region sichtbar waren, sind wahrscheinlich auf vereinzelt Zelltod zurückzuführen. Auch extrazelluläres BHB als alternativer Energielieferant blieb unverändert.

In weiteren Gehirnregionen wurden ebenfalls Veränderungen beobachtet. Extrazelluläres Laktat im Hippocampus war in beiden Dosisgruppen nur leicht erniedrigt, veränderte sich jedoch im Zuge der verhaltensbezogenen Stimulation. Im Striatum wiederum zeigte sich ein dosisabhängiger Anstieg von Laktat und Pyruvat.

Bioinformatische Studien (Kooperation mit S. Lobentanzer) legen einen Wirkmechanismus von intracerebroventrikulär applizierten STZ nahe, der sich von dem von peripher

verabreichten STZ unterscheidet. Es erscheint wahrscheinlich, dass die neuronale STZ Aufnahme GLUT-1- und GLUT-3-vermittelt abläuft, denn diese Transporter werden in Neuronen und Astrocyten hoch exprimiert, wogegensowohl GLUT-2 als auch GLUT-4, welche für den transmembranären Transport von STZ in der Peripherie verantwortlich sind, in einem nur sehr geringen Ausmaß im Gehirn zu finden sind. Der unspezifische Zelltod, der in der CA1-Region beobachtet wurde, und die Astrozyten- Aktivierung könnten somit Grund für die Beeinträchtigung der mitochondrialen Atmung und die verringerte Glucose-Aufnahme im Hippocampus sein.

Cholinerge Veränderungen:

Ähnlich zu anderen Arbeiten konnten auch in unserer Studie eine Veränderung cholinerges Marker beobachtet werden. Die ChAT Aktivität im Hippocampus war im Zuge der icv-STZ Injektion signifikant reduziert (-30 %), während sie im Striatum unverändert blieb. Auch die Aktivität der AChE war im Hippocampus signifikant reduziert (-30 %), im Striatum hingegen leicht erhöht (+7 %). Die Aktivität des HACU zeigte keine Veränderungen im Hippocampus, im Striatum war sie in der Hochdosisgruppe signifikant erhöht (+30 %).

Bemerkenswerterweise hat die Mikrodialyse aufgezeigt, dass die cholinerge Funktion im Zuge der icv-STZ Injektion erhalten blieb. Die extrazellulären ACh Konzentrationen in Hippocampus und Striatum zeigten sich unverändert, auch während der verhaltensbezogenen und pharmakologischen Stimulationen.

Zwischen den ACh Werten und der HACU Aktivität ist eine deutliche Korrelation erkennbar. Im Hippocampus blieben extrazelluläres ACh und die HACU-Aktivität unverändert. Demgegenüber steht eine erhöhte HACU-Aktivität im Striatum, was auf eine erhöhte cholinerge Feuerungsrate hinweist und sich durch leicht erhöhte striatale ACh-Konzentrationen bekräftigen lässt. Viele andere Arbeiten haben zwar bisher ein cholinerges Defizit mit Bezug auf ChAT- und AChE-Aktivitäten in diesem Tiermodell beschrieben, jedoch haben diese Parameter nur eine schwache Korrelation zum extrazellulärem ACh. Beachtenswert sind bioinformatische Daten, die zeigen, dass AChE nicht exklusiv cholinerg exprimiert wird, wohingegen ChAT und CHT-1 (SLC5A7) einer hohen Co-Expression in cholinergen Neuronen unterliegen. Außerdem weist GLUT3 eine hohe Korrelation mit cholinergen Genen auf, GLUT2 und GLUT4 zeigen diese Korrelation nicht.

Der Hippocampus scheint anfälliger gegenüber der icv-STZ Injektion zu sein als das Striatum, was sich mit Erkenntnissen aus anderen Studien deckt. Unsere hippocampalen Daten zeigen

erniedrigte cholinerge Marker (ChAT und AChE) und verringerte mitochondriale Atmung, trotz normaler Verfügbarkeit an extrazellulärer Glucose und Cholin. Dennoch hatten diese Veränderungen keinen Einfluss auf extrazelluläre Ach-Konzentrationen, die durch die verbleibenden Nervenendigungen mit ausreichend intakter HACU Aktivität nach icv-STZ Injektion freigesetzt wurden. Dadurch, dass der Hippocampus cholinerge Innervation aus dem Septum erhält, ließe sich verringerte ChAT-Aktivität durch axonale und terminale Nervenschädigungen erklären. Wir vermuten, dass dies GLUT-3-vermittelt geschieht, da dessen Korrelation mit cholinergen Neuronen deutlich höher ist als die anderer GLUT. Im Vergleich dazu blieben die kurzen Interneurone im Striatum von der STZ-Toxizität weitestgehend verschont. Die striatalen Daten weisen auf eine erhöhte cholinerge Feuerungsrate gepaart mit erhöhter Ach-Degradation hin, was in gleichgebliebenen Ach-Konzentrationen resultiert. Außerdem blieben striatale Laktat-Freisetzung und mitochondriale Atmung unverändert. Diese Beobachtungen lassen sich durch limitierte Diffusion des STZ in cholinerge Neurone des Striatums oder (wahrscheinlicher) durch geringere Empfindlichkeit der cholinergen Interneurone gegenüber STZ erklären. Zusammenfassend weisen unsere Daten darauf hin, dass das für dieses AD-Modell beschriebene cholinerge Defizit entweder nicht vorhanden (Striatum) oder nur unvollständig ausgeprägt ist (Hippocampus). Da in der CA1-Region des Hippocampus und im Striatum vorwiegend GABAerge Interneurone und GABAerge Nervenendigungen zu finden sind, vermuten wir, dass verringerte inhibitorische Neurotransmission im Zuge der Schädigung GABAerger Neurone indirekte Auswirkungen auf die cholinerge Transmission haben könnte.

Schlussfolgerung:

STZ induziert keinen neuronalen Diabetes. Es verantwortet verschiedene unspezifische Toxizitäten wie den Verlust an Körpergewicht, hippocampale Astrogliose und Neurodegeneration, sowie Beeinträchtigungen des Energiemetabolismus. Demgegenüber scheint die cholinerge Transmission in Hippocampus und Striatum gut erhalten zu bleiben, wenn sich auch manche Biomarker unterscheiden. Insbesondere die striatalen cholinergen Neurone scheinen von der STZ-Toxizität verschont zu bleiben, wohingegen im Hippocampus geringfügige Schäden an cholinergen Endigungen auftraten. Zusammengenommen scheitert das icv-STZ Modell daran, die cholinerge Dysfunktion - einen zentralen Bestandteil der MA-Pathologie - nachzubilden. Vielmehr ist dieses Tiermodell zur Induktion hippocampaler Astrogliose mit neuronaler Schädigung der CA1-Region geeignet.

8.3 Curriculum vitae



Personal Information

Name : Tri Yuliani
Place/ Date of Birth : Yogyakarta/ 5 July 1985
Nationality : Indonesian
Marital Status : Married, 1 child

Education

September 2016–Oktober 2020 : PhD Program in Pharmacy
Research group of Prof. Dr. Jochen Klein
Institute of Pharmacology and Clinical Pharmacy
Goethe University, Frankfurt, Germany
Thesis: Cholinergic and Metabolic Consequences of
Streptozotocin-induced Brain Injury

September 2013–July 2015 : Master Program in Biomedical Science
Pharmacology, Faculty of Medicine
Universitas Indonesia, Jakarta, Indonesia
Thesis: Cardioprotective effect of quercetin in an animal
model of chronic kidney disease
GPA 3.33/4.00

August 2007–August 2008 : Professional Pharmacy Program
Pharmacy Science and Industry, Faculty of Pharmacy
Gadjah Mada University, Yogyakarta, Indonesia
GPA 3.60/4.00

August 2003–July 2007 : Bachelor's Program in Pharmacy
Pharmacy Science and Industry, Faculty of Pharmacy
Gadjah Mada University, Yogyakarta, Indonesia
GPA 3.66/4.00
Thesis: Effect of cefadroxil on glutathione s-transferase
activities in rats' kidney

Working Experience

December 2018- December 2019 : Facilitator of Journal Club
Master in Interdisciplinary Neuroscience
Goethe University, Frankfurt, Germany

Since December 2010 : Researcher at Pharmacology Laboratory
Research Center for Chemistry,
Indonesian Institute of Sciences (LIPI), Serpong, Indonesia

August 2008 –October 2009 : In process control supervisor
Non-antibiotics Pharmaceutical Plant
PT Sanbe Farma, Bandung, Indonesia

8.4 Publications

Parts of the present dissertation have already been published

1. **Yuliani T**, Lobentanzer S, Klein J. Central cholinergic function and metabolic changes in streptozotocin-induced rat brain injury. J Neurochem. doi:10.1111/jnc.15155.